SASOR 2014

5th Southern African Conference on Rheology

2 - 3 September 2014

Conference Proceedings

Edited by

Sonia Fidder-Woudberg

SASOR SOUTHERN AFRICAN SOCIETY OF RHEOLOGY

www.sasor.co.za

5th Southern African Conference on Rheology

SASOR 2014

Stellenbosch
South Africa
2-3 September 2014

Programme & Abstracts

SASOR SOUTHERN AFRICAN SOCIETY OF RHEOLOGY

Gold Sponsor	AEL Mining Services	TA Instruments ALS ADVANCED LABORATORY SOLUTIONS
Silver Sponsor	Anton Paar	

Organising Committee

Prof Rainer Haldenwang
Prof Veruscha Fester
Mr Peter Goosen
Dr Sonia Fidder-Woudberg

Technical Committee

Prof Irina Masalova
Dr Sonia Fidder-Woudberg
Prof Rainer Haldenwang

Although utmost care was taken when this book of abstracts was created, the organising committee cannot be held responsible for any misprints or omissions.

Welcome

Welcome to the 5th Southern African Conference on Rheology, SASOR 2014. We held our first conference in 2006. Our second conference in 2008 came soon after the International Committee on Rheology's meeting in Monterey in August 2008, where we were elected to full membership of this international body. This represents full recognition of our young society, and we have been assigned to the European sector of the ICR. Our third conference SASOR 2010 was well attended by the international rheological community with speakers from France, Italy, Sweden and the USA. SASOR 2012 boasted with international speakers from USA, Germany, Switzerland and Australia and local representatives from all universities in the Western Cape as well as the University of Pretoria and from industry. We had the same number of local speakers from industry and academia as our international speakers, showing that the interest in rheology is growing in South Africa.

This year, however, we are very pleased to have mainly postgraduate students presenting in addition to the invited speakers and those from industry.

SASOR 2014 will consist of plenary lectures and oral presentations. The really valuable discussions, debate and interactions are in reality up to you – so please participate as freely as you are able. We hope that you will find the conference stimulating.

We wish to express our gratitude to the individuals and organizations that have contributed to the success of the conference.

Dr Piet Halliday
SASOR 2014 Chairman

Programme

Tuesday 2 September 2014		Page
08:30	**Registration : Coffee/Tea**	
09:15	**Opening: President of SASOR**	
	Chairperson: *Rainer Haldenwang*	
09h30	**Plenary: Prof L Choplin** **Process Viscosity: Couette and Poiseuille Analogies** *Program Officer "Industrial Chairs", ANR, Paris, Director of International and Industrial Partnerships ENSIC, Industrial Chair in Chem. Eng. of Complex Media (GEMICO) University of Lorraine , France*	6
10:35	**Effect of surfactant structure on interfacial film and stability of highly concentrated emulsions with supersaturated dispersed phase** N Sanatkaran, I Masalova *Flow Process & Rheology Centre, Faculty of Engineering, Cape Peninsula University of Technology*	7
11:00	**Promotion: Gold Sponsor: Advanced Laboratory Solutions (ALS)**	
11:10	**Coffee/Tea**	
	Chairperson: *Sonia Fidder-Woudberg*	
11:30	**Keynote: Dr P A Rühs** **Interfacial rheology of bacterial adhesion layers at air/water and oil/water interfaces** *Department of Health, Science and Technology, ETH Zürich, Zürich, Switzerland*	13
12:35	**Using fumed silica nano particles in combination with SMO conventional surfactant to stabilize w/o highly concentrated emulsion: Effect of surfactant/particle ratio on rheological properties and emulsion stability** N Tshilumbu, I Masalova *Flow Process & Rheology Centre, Faculty of Engineering, Cape Peninsula University of Technology*	15
13:00	**Promotion: Gold Sponsor: AEL Mining Services**	
13:10	**Lunch**	
	Chairperson: *Veruscha Fester*	
14:00	**Plenary: Dr S S Ray** **Melt-state rheology: An important tool to establish structure-property relationship in clay-containing nanocomposites** *DST/CSIR National Centre for Nanostructured Materials, Council for Scientific and Industrial Research, Pretoria 0001, South Africa*	21
15:05	**Influence of oil type on stability and rheological properties of highly concentrated emulsions** E Mamedov, I Masalova *Flow Process & Rheology Centre, Faculty of Engineering, Cape Peninsula University of Technology*	22
15:30	**Promotion: Silver Sponsor: Anton Paar**	
15:40	**Coffee/Tea**	
15:40	**SASOR AGM**	
18:30	**Conference Dinner at Barrique**	

	Wednesday 3 September 2014	Page
09:00	Registration : Coffee/Tea	
	Chairperson: *Peter Goosen*	
09h30	**Plenary: Dr Angus Paterson** **Rheology and practical slurry pipeline flow in the mining industry** *Paterson & Cooke Consulting Engineers (Pty) Ltd, Cape Town, South Africa*	28
10:35	**The influence of rheology in pipe flow predictions** E M van den Heever, A P N Sutherland *Department of Civil Engineering and Surveying, Cape Peninsula University of Technology, Cape Town*	31
11:05	**Coffee/Tea**	
	Chairperson: *Irina Masalova*	
11:25	**Shear stress at the pipe invert as an indication of stationary vs sliding bed in laminar slurry flow** P Goosen *Paterson & Cooke, Sunrise Park, Prestige Drive, Ndabeni Cape Town, South Africa*	36
11:50	**A fully integrated and commercial in-line fluid characterization system for industrial applications** R Kotzé*, J Wiklund°, R Haldenwang* **Cape Peninsula University of Technology, PO Box 652, Cape Town, 8000,* °*SIK – The Swedish Institute for Food and Biotechnoogy, PO Box 5401, Gothenburg*	40
12:15	**An investigation of the nature of the effects causing mechanical sensitizer pumping properties variation** E Kharatyan, P Halliday, L Wilson *AEL Mining Services, AEL Research and Development Department, Ardeer Road, Pinelands Office Park, Building N7 Pinelands, Modderfontein*	44
12:40	**Lunch**	
13:40	**The effect of different PPC binders, partially replaced by fly ash and slag on the properties of self-compacting concrete** O Almuwbber, R Haldenwang, I Masalova *Department of Civil Engineering and Survey, Cape Peninsula University of Technology, Cape Town*	47
14:05	**Effect of different cements and superplasticisers on rheology of cement paste** W Mbasha, R Haldenwang, I Masalova *Department of Civil Engineering and Survey, Cape Peninsula University of Technology, Cape Town*	52
14:30	**Conference Closing**	

PROCESS VISCOSITY: COUETTE AND POISEUILLE ANALOGIES

L. Choplin

University of Lorraine, 1 rue Grandville, BP 20451, F-54001 Nancy Cedex, France.
E-mail: lionel.choplin@univ-lorraine.fr.

ABSTRACT

The viscosity determination of Non-Newtonian complex liquids is in general not an easy task due to the faxt that, in most practical situations, the flow field is far from being rheologically homogeneous. As a consequence, experimentally accessible experimental data (flow rate, pressure drop, angular velocity, torque,...) require a complex treatment in order to allow the determination of an acceptable viscous rheogram of the fluid under consideration. Couette and Poiseuille analogies use a simplified analysis of (even strongly) heterogeneous situations of flow, allowing a very good viscosity determination (maximum error around 8%). This methodology also allows the development of in line / on line viscometers.

EFFECT OF SURFACTANT STRUCTURE ON INTERFACIAL FILM AND STABILITY OF HIGHLY CONCENTRATED EMULSIONS WITH SUPERSATURATED DISPERSED PHASE

N. Sanatkaran, I. Masalova

Department of Civil Engineering, Faculty of Engineering, Cape Peninsula University of Technology,
PO Box 652, Cape Town 8000, Republic of South Africa
E-mail: sanatkaran@gmail.com

INTRODUCTION

Highly concentrated water-in-oil emulsions (HCE) with metastable dispersed phase consist of a high volume ratio (~85%) of super saturated inorganic salts solution in the form of droplets in an immiscible oil medium which is stabilized by an emulsifier. The stability of these types of emulsions in bulk phase are related to the crystallization of inorganic salts, which are promoted by a prolonged shelf life and under high shear conditions (1, 2). Poly(isobutenyl) succinic anhydride-based surfactants (PIBSA) are used in general to stabilize these types of emulsions providing optimal shelf life stability due to the formation of a huge number of micelles which creates a steric barrier between the inter-droplet layer (3). But instability was observed during pumping applications, owing to the heavy molecular weight of the surfactant which does not quickly cover the new droplet surfaces created under shear.

The most promising method seems to be addition of a binary surfactant mixture to the emulsion formulation in order to have better stability both in shelf and under high shear (4, 5). Surfactant mixtures are used in many emulsion formulations mostly because of superior properties of mixtures when compared to individual surfactants (6-11). The molecular structure of these surfactants have an effect on the interaction between the two surfactants at the interfacial layer around droplets, which results in different processing, interfacial and rheological properties of the final emulsion (12, 13). Many studies have been conducted on understanding this effect, however, there is a lack of systematic investigation of the effect of surfactant mixtures on HCEs with a supersaturated dispersed phase.

The aim of the current study is to investigate the effect of addition of binary surfactant systems including oil/oil and oil/water soluble surfactants on the stability of HCEs in terms of crystallization of the supersaturated dispersed phase. A group of oil and water soluble surfactants with different hydrophobic tail structures under trade names of Spans and Tweens, respectively, were chosen as co-surfactants in combination with a PIBSA-based polymeric surfactant (oil soluble). To have a clearer insight on the surfactant properties, interfacial tension measurements were performed at the water-oil interface in the presence of surfactant mixtures and the interaction between the surfactants at the interface were applied according to the regular theory by (14). In addition, the influence of the chemical structure of co-surfactants on the strength and rigidity of the emulsions characterized by the yield stress and the storage modulus, respectively, were studied.

MATERIAL AND METHODS

PIBSA-based surfactant (PIBSA-Mea) and oil were supplied by Lake International Technologies (South Africa). The oil contains paraffins (>99.9%) and aromatics (less than 0.1%), with the density equal to 794 kg/m3 at 20°C. Ammonium nitrate (AN) as an inorganic salt wsa purchased from Merck. Sorbitan monolaurate (Span20), sorbitan monostearate (Span60), Polyoxyethylene sorbitan monolaurate (Tween20) and polyoxyethylene sorbitan monostearate (Tween60) were obtained from Merck. Sorbitan monopalmit (Span40) and polyoxyethylene sorbitan monopalmitate (Tween40) were purchased from Aldrich and Sigma, respectively. Figure 1 shows the structure of co-surfactants.

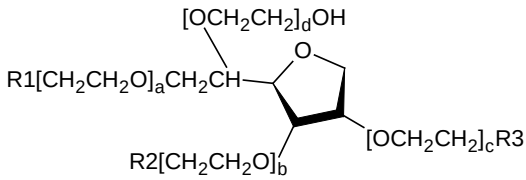

Surfactant	R1	R2	R3	M_w
Span 20	OOC(C11H23)	OH	OH	346
Span 40	OOC(C15H31)	OH	OH	403
Span 60	OOC(C17H35)	OH	OH	431
Tween 20	OOC(C11H23)	OH	OH	1228
Tween 60	OOC(C15H31)	OH	OH	1277
Tween 60	OOC(C17H35)	OH	OH	1312

Figure 1. The structures of Spans (a+b+c+d=0) and Tweens (a+b+c+d=20).

The prepared emulsions consisted of 92.4% water phase in oil phase, and were mixed using a standard Hobart N50 Mixer at 80°C and were refined until a certain droplet size (d_{32}=10μm) was achieved, measured using a Malvern Mastersizer 2000. The

water phase comprised of supersaturated 80 wt % AN which could be stable for a short time. Surfactants used in all compositions were mixed at a 10:1 ratio of PIBSA/co-surfactants.

Interfacial tension, σ, was measured using a Krűss K100 Tensiometer based on the Wilhelmy method. Oil phases with different concentrations of individual PIBSA-Mea, co-surfactants and mixtures, with the same ratio as in the emulsions (10:1) in contact with 60 wt % solution of AN as the aqueous phase was used for interfacial tension tests at 25 °C.

All measurements of rheological properties were conducted using a Paar Physica MCR-301 rotational rheometer (cone and plate geometry, angle between cone and plate was 1 grad). Amplitude sweeps in the strain amplitude range from 0.01 to 200% at a constant frequency of 1 Hz and flow curves in the shear rate range from 10^{-4} to 200 s^{-1} were performed.

To simulate high shear conditions, a home-made pumping system was used, which consisted of a cylindrical chamber which extruded a sample under 4 bars of pressure from one cylinder through an orifice with a diameter of 4 mm into another.

THEORY

CMCs (critical micelle concentrations) were found from the cross point of the lines of the part in which the interfacial tension is changed with the surfactant concentration and the part in which the interfacial tension remains relatively constant due to formation of micelles in the oil. The Gibbs adsorption isotherm was used to calculate the average minimum area per molecule (A_{CMC}) (15):

$$\Gamma = -\frac{1}{RT}\frac{d\sigma}{d\ln C}\ , \qquad (1)$$

$$A_{CMC} = \frac{1}{\Gamma N}\ , \qquad (2)$$

where Γ is the surface excess concentration, R the gas constant, T the absolute temperature and N the Avogadro number.

The molecular interaction between two surfactants at the interfacial layer was quantified by the β parameter (6). As indicated in equation (3), the β parameter shows a comparison between the molecular interaction of a surfactant mixture and the self-interactions of individual surfactants before mixing (7) defined as:

$$\beta = \frac{W_{12} - (W_{11} + W_{22})}{2} RT\ , \qquad (3)$$

where W_{AA} ,W_{BB} and W_{AB} are the molar self-interaction energy of the first surfactant, second surfactant and the molar interaction energy between the mixed surfactants, respectively. The positive value of β represents a weaker attraction or stronger repulsion between two surfactant molecules compared to the self-interactions of individual surfactants, called antagonism. A negative value of β shows a stronger attraction or weaker repulsion between mixed surfactants compared to self-interaction of individuals, called synergism. A number of theories have been formulated to describe the synergism between surfactant mixtures (16-18). A regular non-ideal model developed by Rosen (14) was found as a successful model to calculate the interaction parameter which is presented in equations (4) and (5).

$$\frac{X_1^2 \ln(\alpha C_{12} / X_1 C_1)}{(1-X_1)^2 \ln[(1-\alpha)C_{12}/(1-X_1)C_2]} = 1\ , \qquad (4)$$

where C_1, C_2 are the concentrations of the individual surfactants 1 and 2, respectively; C_{12} is the concentrations of the binary surfactant mixture required for a certain interfacial tension before the CMC point (Figure 2). α is the molar fraction of surfactant 1 in the mixture. Hereafter, the interaction parameter, β will be:

$$\beta = \frac{\ln(\alpha C_{12} / X_1 C_1)}{(1-X_1)^2}\ , \qquad (5)$$

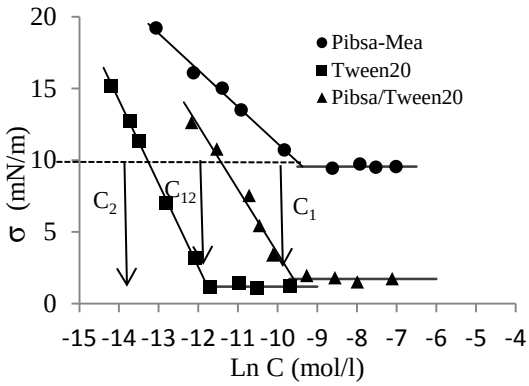

Figure 2. Determination of the interaction parameter.

It was shown in all cases, that the kinetics of the emulsifying process (Figure 3) can be fitted by the exponential equation of the following type ((4)):

$$D(t) = D_\infty + (D_0 - D_\infty)e^{-t/\theta}\ , \qquad (6)$$

where D(t), D_0 and D_∞ are the current, initial and final average diameters of the droplets, respectively, and t is time. The D_∞ values correspond to the situation when the droplet size did not change noticeably for a long enough time.

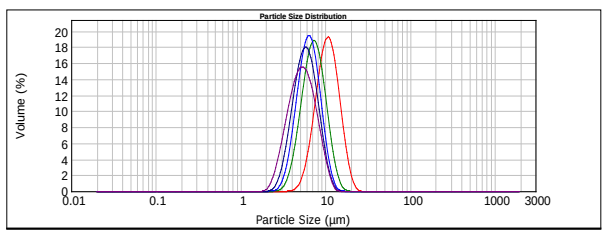

Figure 3. A typical histogram of drop size distribution of the emulsions at different refining time.

RESULTS AND DISCUSSION

Interfacial Properties

The results are presented for PIBSA, PIBSA/Span and PIBSA/Tween mixtures in Table 1. CMC decreased slightly for the longer alkyl tail length of co-surfactants. It has been shown that the higher degree of hydrophobicity (e.g, hydrophobic chain length) has a major effect on lowering the CMC value (19-21).

In the case of PIBSA/Tweens, some effects opposite to PIBSA/Span mixtures can be seen with regards to the degree of synergism. In general, two factors controlling the mixing effect and interaction between non-ionic groups can occur: steric repulsion and electrostatic interaction which both depend on the size of the head groups (6) and Van-der-Walls interaction between hydrophobic tails which becomes stronger for longer hydrophobic tails (22). After mixing, low molecular Spans molecules occupies the free spaces between bulky polymeric molecules of PIBSA and creates a condensed layer at the interface, resulting in negative values for β while this penetration becomes more difficult for longer tail Spans, resulting in a lower synergism.

Table 1. Interfacial properties of PIBSA-Mea/co-surfactant mixtures.

Material	CMCx10^5 [mol/l]	A_{min} [A°^{2}]	X_1	β
PIBSA-Mea/ Span 20	22.9	109.9	0.48	-3.0
PIBSA-Mea/ Span 40	29.5	134.1	0.45	-2.6
PIBSA-Mea/ Span 60	33.9	133.1	0.41	-1.5
PIBSA-Mea/ Tween 20	6.7	92.5	0.45	-3.3
PIBSA-Mea/ Tween 40	3.6	87.8	0.45	-5.6
PIBSA-Mea/ Tween 60	3.9	86.4	0.46	-5.8

For PIBSA/Tweens, longer alkyl tail length led to a higher synergism. The reason could be when PIBSA - Mea and Tweens are used together, the ethoxylated parts of Tweens are squeezed to sub-phase and those parts of the Tween's hydrocarbon tails that are located in the oil phase penetrate between the adsorbed PIBSA molecules. Thus, the distance between neighbouring hydrophobic tails is reduced increasing the probability of attraction between surfactant chains and thus higher synergism (23).

Emulsification

The aim was to prepare HCEs with an average droplet size of 10 µm. The kinetics of the droplet refinement was followed using the Malvern mastersizer as it shown in Figure 4. Obtained data was fitted using Eq.6 and characteristic refinement time (θ) for all samples was listed in Table 2.

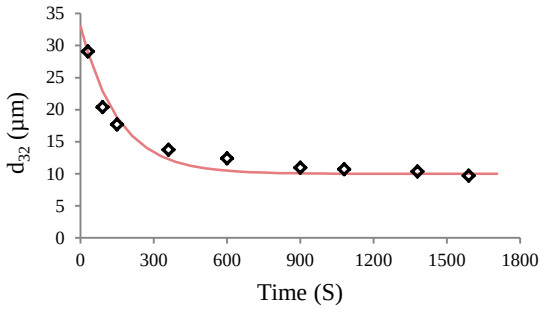

Figure 4. Droplet size evolution as a function of refining time for the PIBSA/Span 60 emulsion (dots) fitted by model (line).

These results demonstrate that both co-surfactants strongly affect the rate of refining and a decrease was observed in comparison with the pure PIBSA-Mea, however the influence of Tweens on refining is much higher than Spans. Emulsification consists of two steps: droplet break-up and re-coalescence of smaller droplets. Higher adsorption efficiency of Tween molecules compared to Spans increased the break-up rate while stronger synergism between PIBSA and Tweens prevented re-coalescence of freshly formed droplets.

Table 2. Characteristic time of refinement for different surfactant systems.

Surfactant system	θ [s]
PIBSA (pure)	290
PIBSA-Mea/Span 20	115
PIBSA-Mea/Span 40	140
PIBSA-Mea/Span 60	155
PIBSA-Mea/Tween 20	85
PIBSA-Mea/Tween 40	80
PIBSA-Mea/ Tween 60	75

Rheological Properties

From the flow curve measurements, yield stress (τ_y) and from the amplitude sweep, storage modulus (G') was determined and summarized in Table 3.

Increasing the tail length of co-surfactants for both Spans and Tweens led to the growth of characteristic parameters, τ_y and G'. However, in all cases maximum yield stress and storage modulus were observed for pure PIBSA-Mea. In addition, a close correlation between the strength of the interface structure (yield stress) and its rigidity (storage modulus) was obtained, as shown in Figure 5. Therefore, both structure strength and its rigidity are obliged to the same physical source- intermolecular interaction between the surfactants.

Table 3. Experimental τ_y and G' values for the emulsions under study.

Surfactant mixture	G' [Pa]	τ_y [Pa]
PIBSA-Mea	990	16.7
PIBSA-Mea/Span 40	729	14.3
PIBSA-Mea/Span 60	831	15.3
PIBSA-Mea/Tween 20	405	8.6
PIBSA-Mea/Tween 40	427	10.9
PIBSA-Mea/ Tween 60	456	11
PIBSA-Mea/Span 40	729	14.3

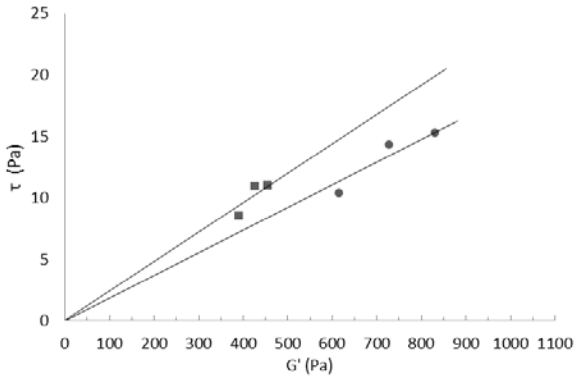

Figure 5. Correlations between rheological parameters, τ_y and G', PIBSA -Mea/Spans (circles) and PIBSA-Mea/Tweens (squares).

Correlations between the interaction parameter (β) and the rheological parameters (τ_y and G') are shown in Figure 6. It can be seen that a lower τ_y and G' resulted from the systems with a higher degree of synergism and it is more pronounced for the PIBSA/Span group. This can be explained by a higher possibility of micelles formation for the PIBSA/Tween group, which led to a weaker network and also reduced the rheological properties of the emulsion (24).

Stability

The stability of highly concentrated emulsions with the metastable dispersed phase is associated with crystallisation of the aqueous phase (Figure 7). Below the crystallization temperature (60°C in this study) and under high shear conditions, crystal nucleation of the salt solution is a major concern (1, 25).

Stability in shelf- The stability of HCEs in this study was followed using an optical microscope while samples were kept under the same environmental conditions. The starting day of crystallization of the un-pumped emulsions are presented in Figure 8. From the graph, the stability trend of the HCE samples prepared, using a mixture of surfactants, was found to be relatively close to the line obtained from their interaction parameter.

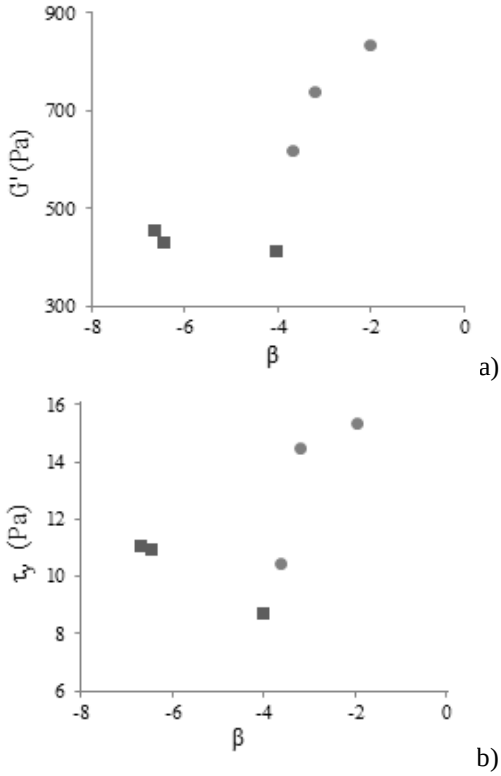

Figure 6. Correlation between the interaction parameter (β) and storage modulus (a); yield stress (b) for PIBSA-Mea/Span (circle) and PIBSA -Mea/Tween (square) samples.

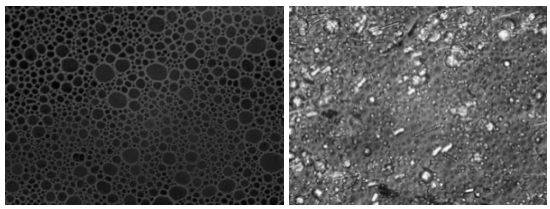

Figure 7. Microscopic image of the fresh emulsion (left) and the crystallized emulsion (right).

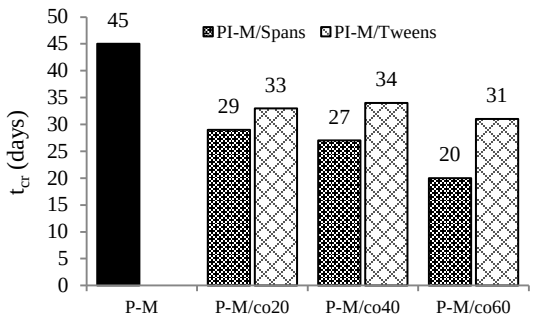

Figure 8. Starting of crystallization for the un-pumped emulsions (P-M represents PIBSA-Mea and P-M/co represents the mixtures of PIBSA-Mea/different co-surfactants include Spans and Tweens).

Stability under shear- To investigate the effect of the surfactant mixtures on pumpability of the emulsions, all samples were pumped for 3, 5, 7 and 10 pumping cycles using the pumping system described in the methodology section. The dependence of the droplet diameter on the number of passes through the orifice hole is described by the same exponential equation (equation (6)), by replacing t with the pumping cycles and θ will be the final average

diameter of droplet (d_{32}). The averge droplet size for the pumped emulsions prepared with all PIBSA/Spans mixtures decreased from 10 to 4.0 μm and with PIBSA/Tween mixtures decreased to 4.6 μm, on average. A decrease in the droplet size lowers the pumpability due to an increase in the viscosity of the emulsion (26), indicating that a better pumpability can be achieved by adding water soluble surfactant (Tweens) to the system.

CONCLUSION

The effect of interfacial behaviour of different mixtures of oil/oil and oil/water soluble surfactants on the stability, pumbability and rheological properties of highly concentrated emulsions with a varyied co-surfactant structure was investigated. A direct correlation between the synergism of non-ionic co-surfactant (Spans and Tweens) and a polymeric surfactant poly(isobutylene) succinic anhydride derivative was observed. The degree of synergism was affected by the chemistry of the head group and alkyl tail length of co-surfactants. Stability and pumbability increased when water soluble surfactants were used, while the refinement time and rheological parameters were lower as compared to Spans providing emulsions quite acceptable for different technological applications (long shelf life, significant pumping characteristic storage, etc).

REFERENCES

1. Masalova, I., Malkin, A.Y., Ferg, E., Kharatiyan, E., Taylor, M., Haldenwang R. (2006) Evolution of rheological properties of highly concentrated emulsions with aging - Emulsion-to-suspension transition. *J. Rheol.*, 50: 435-451.
2. Masalova, I., Malkin, A.Y. (2007) Rheology of highly concentrated emulsions - Concentration and droplet size dependencies. Appl. Rheol., 17: 42250-42259.
3. Reynolds, P.A., Gilbert, E.P., Henderson, M.J. and White, J.W. (2009) Structure of High Internal Phase Aqueous-in-Oil Emulsions and Related Inverse Micelle Solutions. 3. Variation of Surfactant. *J. Phys. Chem. B.*, 113: 12231-12242.
4. Mudeme, S., Masalova, I., Haldenwang, R. (2010) Kinetics of emulsification and rheological properties of highly concentrated explosive emulsions. *Chem. Eng. Process*., 49: 468-475.
5. Chattopadhyay, A.K., (1996) *Emulsion explosive*. ICI Canada Inc.: 5500062 patent, United States.
6. Zhou, Q., M.J. Rosen (2003) Molecular Interactions of Surfactants in Mixed Monolayers at the Air/Aqueous Solution Interface and in Mixed Micelles in Aqueous Media: The Regular Solution Approach. *Langmuir*, 19: 4555-4562.
7. Rubingh, D. (1979) *Mixed Micelle Solutions, in Solution Chemistry of Surfactants*, K.L. Mittal, Editor., New York: Springer.
8. Jost, F., Leiter, H., Schwuger, M.J. (1988) Synergisms in binary surfactant mixtures. *Colloid & Polymer Sci.*, 266: 554-561.
9. Huber, K. (1991) Interactions in mixed interfaces of binary surfactant solutions. *J. Colloid Interface Sci.*, 147: 321-332.
10. Huibers, P.D.T., Shah, D.O. (1997) Evidence for Synergism in Nonionic Surfactant Mixtures: Enhancement of Solubilization in Water-in-Oil Microemulsions. *Langmuir*, 13: 5762-5765.
11. Kang, W., Xu, B., Wang, Y., Li, Y., Shan, X., An, F. and Liu J. (2011) Stability mechanism of W/O crude oil emulsion stabilized by polymer and surfactant. *Colloids Surf., A*, 384: 555-560.
12. Campana, M., Webster, J.R.P., Gutberlet, T. Wojciechowski, K., Zarbakhsh, A. (2013) Surfactant mixtures at the oil–water interface. *J. Colloid Interface Sci.*, 398: 126-133.
13. Tshilumbu, N.N., Ferg, E.E., Masalova, I. (2010) Instability of highly concentrated emulsions with oversaturated dispersed phase. Role of a surfactant. *Colloid J.*, 72: 569-573.
14. Myers, D. (2005) *Fluid Surfaces and Interfaces, in Surfactant Science and Technology*., New York: John Wiley & Sons, Inc.
15. Lucassen-Reynders, E.H. (1973) Interactions in mixed monolayers. I. Assessment of interaction between surfactants.. *J. Colloid Interface Sci.*, 42: 554-562.
16. Frumkin, A.N. (1925) Electrocapillary curve of higher aliphatic acids and the state equation of the surface layer. *Z. Phys. Chem.*, 116: 466-488.
17. Motomura, K., Yamanaka, M., Aratono, M. (1984) Thermodynamic consideration of the mixed micelle of surfactants. *Colloid. Polym. Sci.*, 262: 948-955.
18. Rosen, M.J., Kunjappu, J.T. (2012) *Surfactants and Interfacial Phenomen.* New York: Wiley.
19. Peltonen, L., Hirvonen, J., Yliruusi, J. (2001) The Behavior of Sorbitan Surfactants at the Water–Oil Interface: Straight-Chained Hydrocarbons from Pentane to Dodecane as an Oil Phase. *J. Colloid Interface Sci.*, 240: 272-276.
20. Varadaraj, R., . Bock, J., Valint, P., Zushma, S. and Thomas, R. (1991) Fundamental interfacial properties of alkyl-branched sulfate and ethoxy sulfate surfactants derived from Guerbet alcohols. 1. Surface and instantaneous interfacial tensions. *J. Phys. Chem.*, 95: 1671-1676.
21. Rakshit, A.K., Zografi, G., Jalal, I.M., Gunstone, F.D. (1981) Monolayer properties of fatty acids: II. Surface vapor pressure and the free energy of compression *J. Colloid Interface Sci.*, 80: 466-473.
22. Pilpel, N., Rabbani, M.E. (1988) Interfacial films in the stabilization of sunflower oil in water

emulsions with nonionics. *J. Colloid Interface Sci.*, 122: 266-273.

23. Boyd, J., Parkinson, C., Sherman, P. (1972) Factors affecting emulsion stability, and the HLB concept. *J. Colloid Interface Sci.*, 41: 359-370.
24. Masalova, I., Foudazi, R., Malkin, A.Y. (2011) The rheology of highly concentrated emulsions stabilized with different surfactants. *Colloids Surf., A*, 375: 76-86.
25. Masalova, I., Malkin, A.Y. (2007) A new mechanism of aging of highly concentrated emulsions: Correlation between crystallization and plasticity. *Colloid J.*, 69: 198-202.
26. Malkin, A., Masalova, I., Slatter, P., Wilson, K. (2004) Effect of droplet size on the rheological properties of highly-concentrated w/o emulsions. *Rheol. Acta*, 43: 584-591.

INTERFACIAL RHEOLOGY OF BACTERIAL ADHESION LAYERS AT AIR/WATER AND OIL/WATER INTERFACES

P.A. Rühs[1], L. Böni[1], L. Böcker[1], T. De Wouters[1], C. Jans[1], E.J. Windhab[1], R.F. Inglis[2], P. Fischer[1]

[1] Department of Health, Science and Technology, ETH Zürich, Zürich, Switzerland
[2] Department of Environmental Sciences, ETH Zürich, Switzerland and Department of Environmental Microbiology, EAWAG, Dübendorf, Switzerland

INTRODUCTION

Bacteria adhesion layers are highly complex biological assemblies composed of bacterial cells embedded in an extracellular polymeric matrix. Such biofilms are ubiquitous and, on one hand may cause severe environmental and health problems but on the other hand protect and support the gut flora during digestion. Therefore it is intriguing to understand the influence factors on the formation and the destruction of bacteria biofilms [1, 2, 3, 4].

MATERIAL AND METHODS

Model bacteria capable of forming biofilms at the water-air and water-oil interfaces were chosen such as *Eschericha coli*, *Bacillus subtilis*, *Pseudomonas fluorescens*, *Pseudomonas putida*, and *Salmonella typhimurium*. They were either cultured in growth media (biofilm experiments) or suspended in buffer solutions (adhesion experiments) [2, 3].
Several biofilm measuring techniques have decisive disadvantages as they either measure biofilm strength indirectly or the measurements are invasive. In this contribution, we study the initial kinetics of bacterial attachment as well as the transient layer formation of model bacteria at both the air/water and oil/water interface through non-invasive interfacial rheology and tensiometry (see Figure 1). Electrophoretic mobility measurements and bacterial adhesion to hydrocarbons (BATH) tests were performed to characterize selected bacteria. To validate interfacial rheology and tensiometry measurements, we monitored biofilm formation utilizing both confocal laser scanning microscopy and light microscopy. To observe the effect of changing subphase conditions, a subphase controlled interfacial rheological setup was used [5]. Additionally, bioadhesion assays against specifically modified surfaces were performed.

RESULTS AND DISCUSSION

In the first step of biofilm formation, bacteria attach to hydrophobic interfaces. These measurements were performed under non-growing conditions with interfacial rheology (see Figure 2) and tensiometry at the water-oil interface.

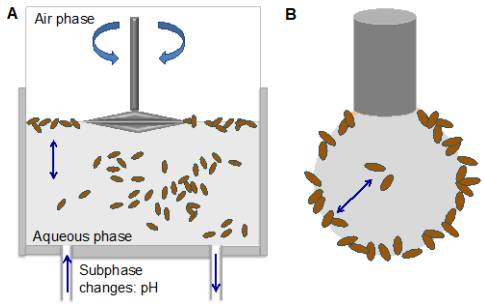

Figure 1. Schematic overview of subphase controlled interfacial rheological setup used for the bacterial biofilm elasticity measurements (**A**) and of a pendant drop tensiometer with a biofilm (**B**).

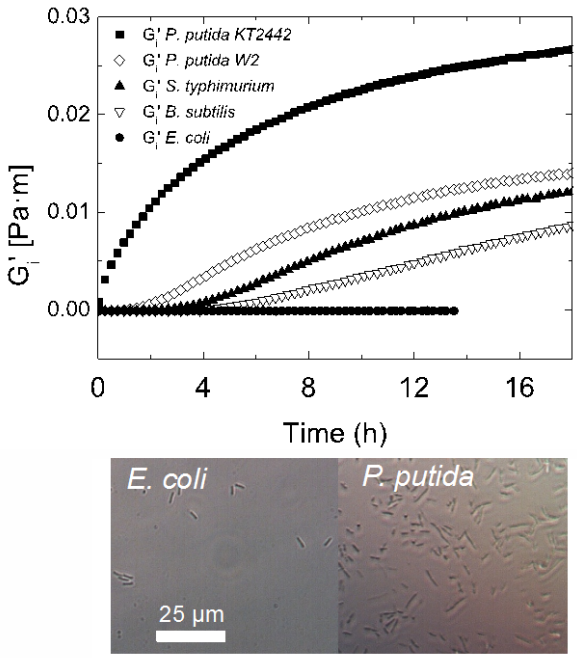

Figure 2. Interfacial elasticity measurements of bacteria at the oil-water interface. Microscopic images of *E. coli* and *P. putida* at the water-oil interface.

Bacteria, with very little hydrophobicity (e.g. *Escherichia coli*) formed very weak adsorption layers whereas bacteria with a high hydrophobicity (e.g. *Pseudomonas putida KT2442)* formed strong adsorption layers against oil.
This weak adhesion also leads to weaker biofilms formed at the water-oil interface (see Figure 3) under growing conditions.

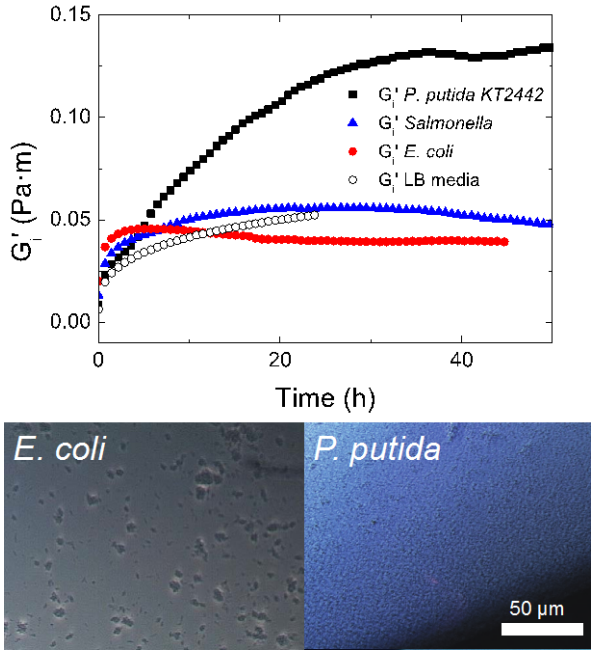

Figure 3. Transient interfacial elasticity of bacteria growing at the water-oil interface. Microscopic images of the water-oil interface of *E. coli* and *P. putida*.

Under growing conditions, the several stages of the biofilm lifecycle of different bacteria were observed (see Figure 4 A and B) at the water-air interface.

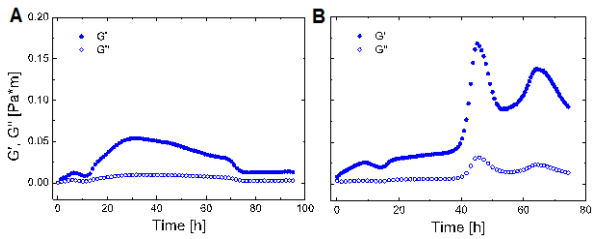

Figure 4. The elastic and viscous moduli are plotted as a function of time for (**A**) *P. fluorescens* and (**B**) *E. coli* of biofilms growing at the water-air interface.

To observe the long-term effect of biofilm formation, long time experiments were performed. In Figure 4, the biofilm formation of *P. putida KT2442*, a bacterium used in bioremediation, is shown at the water-oil interface after 48 hours and after 2 - 3 weeks.

CONCLUSION

By combining different techniques, we were able to observe the interfacial tension and elasticity development over time, from the first bacterial attachment up to biofilm formation at water-air and water-oil interfaces. Through the observation of characteristic dynamic elasticity profiles of each bacterium and in combination with pendant drop tensiometry we were able to gain further insights into the still poorly understood mechanical properties of biofilms. Interfacial rheology proved to be an effective method to measure biofilm formation online at the water-air and water-oil interface as the influence of temperature, media type, bacterial strain, pH and surfactant concentration could be observed successfully during biofilm formation [2, 3].

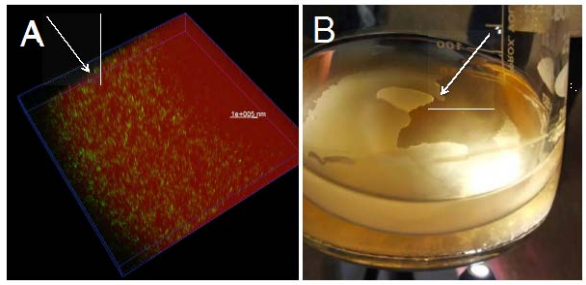

Figure 5. (**A**) Confocal Laser Scanning Microscopy image of *P. putida* KT2442 at the water-oil interface. (**B**) The biofilm formed after 2 - 3 weeks is shown. The arrows indicate the position of the interface.

ACKNOWLEDGEMENTS

We would like to express our thanks to the Laboratory of Biotechnology at ETH Zurich and in particular Leo Meile for their support and helpful discussions. P.R. acknowledges financial support by ETH Zürich (Project ETHIIRA TH 32-1: Amyloid Protein Fibers at Surfaces and Interfaces).

REFERENCES

1. Hall-Stoodley, L., Costerton, J. W., and Stoodley, P. (2004) *Nature Reviews Microbiology*, 2: 95–108.
2. Rühs, P.A., Böni, L., Fuller, G.G., Inglis, R.F., Fischer P. (2013) *PLOS One*, 8: e78524.
3. Rühs, P.A., Böcker, L., Inglis, R.F., Fischer, P., (2014) *Colloids and Surfaces B: Biointerfaces*, 117: 174-184.
4. Wu, C., Lim, J.Y., Fuller, G.G., Cegelski, L. (2012) *Biophysical Journal*, 103: 464-471.
5. Rühs, P.A., Scheuble, N., Windhab, E.J., Mezzenga R., and Fischer P. (2012) *Langmuir*, 28: 12536-12543.

USING FUMED SILICA NANOPARTICLES IN COMBINATION WITH SMO CONVENTIONAL SURFACTANT TO STABILIZE W/O HIGHLY CONCENTRATED EMULSION: EFFECT OF SURFACTANT/PARTICLE RATIO ON RHEOLOGICAL PROPERTIES AND EMULSION STABILITY

N. Tshilumbu, I. Masalova

Material Science and Technology (MST), Cape Peninsula University of Technology,
PO Box 652, Cape Town, South Africa, Email: Tshilumbun@cput.ac.za

INTRODUCTION

Highly concentrated emulsions (HCE) represent a rather special class of colloids. As with any other emulsion, they are a mixture of two incompatible liquids usually stabilized with a surfactant. But in contrast to standard emulsions, the concentration of the dispersed phase in highly concentrated emulsions exceeds the limit of the closest packing of regular spheres (app. 0.74), which is possible due to the "compressed" state of droplets that have a polyhedral shape. The subject of this investigation is water-in-oil super-concentrated emulsions (90vol.%) with a dispersed phase kept in a thermodynamically unstable super-cooled state (over-saturated aqueous salt solution). These kinds of emulsions are inclined to crystallization inside the super-cooled droplets during storage [1, 6] or when subjected to shearing conditions [6]. It is known that the requirements for a surfactant to stabilize such emulsions under shear are often contrary to those required for stabilization during storage. These conflicting requirements can be satisfied by using combinations of different surfactants, in particular mixtures of polymeric and low-molecular-weight compounds. However, due to increasingly demanding legal and consumer requirements, the limitations on classical emulsions have increased [5]. With this in mind, using a combination of standard low-molecular-weight compounds and nanoparticles of different hydrophobicity appears to be an attractive alternative method of creating a mixed emulsifier.

The goal of this study was to combine fumed silica nanoparticles with such a standard low-molecular weight surfactant as sorbitan monooleate (SMO) to examine their synergetic (or antagonistic) action in stabilizing highly concentrated W/O emulsions with the over-cooled internal phase. We studied the effect of varying surfactant/particle ratio on rheological properties and stability during crystallization at rest (during storage) of HCE which is important for technological applications.

Theory: rheological models for HCE or particle dispersions:

- Princen and Kiss model for HCE:

$$\tau = \tau_{yo} + 64(\varphi - 0.73)\frac{\sigma}{d_{32}}Ca^{1/2} \quad (1)$$

where τ_{y0} is the yield stress; φ is the dispersed phase volume fraction; σ is the interfacial tension; d_{32} is the area-volume mean diameter and *Ca* is the capillary number.

- Windhab model for highly concentrated particle dispersions:

$$\tau = \tau_{y0} + \eta_\infty \dot{\gamma} + (\tau_{y1} - \tau_{y0})[1 - \exp(-\dot{\gamma}/\dot{\gamma}^*)] \quad (4)$$

The Windhab model includes the directly measured yield stress, τ_{y0}, and the high shear viscosity, η_∞. It also considers the crossover point (hump), τ_{y1}, observed at the intermediate shear rate $\dot{\gamma}^*$. τ_{y1} has been introduced in this model as a secondary yield stress.

- Foudazi-Masalova model for HCE:

$$\tau = \tau_{y0} + K\gamma^{0.5} + (\tau_{y1} - \tau_{y0})[1 - \exp(-\dot{\gamma}/\dot{\gamma}^*)] \quad (5)$$

where τ_{y1} is an asymptotic value of the yield stress value that corresponds to the transition (hump) in the flow behaviour at shear rate and K is an empirical constant.

MATERIALS AND METHODS

Continuous phase: A series of five fumed nanosilica dispersed in hydrocarbon oil were used for this study; 6wt% of each fumed nanosilica was mixed with SMO in the concentration range of 1 to 10 wt%. The hydrophobicity index (HI) of particles used in this investigation were in the ranges: 0.60-1.34 and HI > 3.

Dispersed phase: A super-cooled aqueous solution of inorganic salts. Water comprises < 20% by mass of the solution. So the salt concentration exceeds 80wt%; Φ = 90vol%.

Emulsion preparation: The emulsification process was conducted in 2.5 kg batches by a Hobart N50 mixer (Manufactured and supplied by the Hobart Corporation, USA) .

Droplet size distribution: The droplet size distribution was measured using the Malvern Mastersize 2000 technique.

Bottle test: A rapid indication on oil aggregation properties of particle dispersions in oil was given by the bottle test method by monitoring the extent of flow five minutes after the bottle has been fully inverted.

Microscopy: the observations were carried out on the samples under the investigation with an optical microscope ('Leica') equipped with a digital camera, at a magnification of x500.

Rheological characterisation: All rheological measurements were carried out by using a rotational dynamic rheometer MCR 300 (Paar Physica).

RESULTS AND DISCUSSIONS

Bottle test for particle dispersions in oil

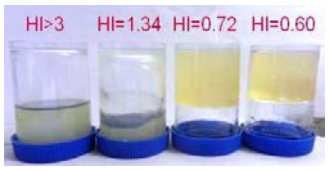

Figure1: Typical pphotograph of 6wt % particles dispersion in oil 5 min after inverting the vessels.

Macroscopic considerations show that fumed silica particles behave as thickening agents of paraffin oil. For more hydrophilic particles (HI = 0.60 -0.72) the bottles fully inverted showed no flow (Figure 1). This is a consequence of the mechanism of formation of the structure via hydrogen bond [10], and this possibility decreases with the increase in hydrophobicity on nanoparticles [9].

Addition of an increasing amount of SMO destroys the 3D network structure: by adsorbing at the fumed silica nanoparticle surface, SMO molecules and positive charges created by reverse micelles' dissociation [11] reduces their gelling ability as evidenced in Figure 2. The surface charge is expected to increase as the particle HI decreases in line with density of OH-groups available on the particle surface.

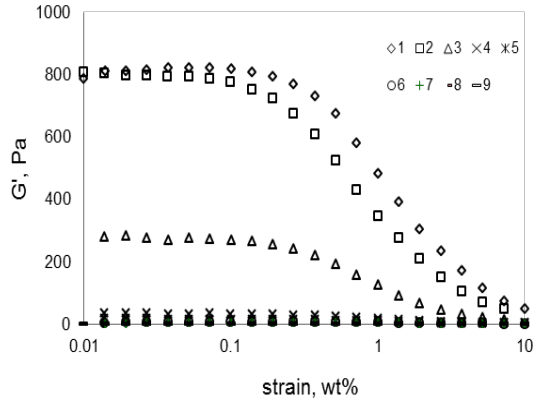

Figure 2. Typical amplitude dependence of the elastic shear modulus for 6 wt% nanosilica dispersion (HI=0.60) in oil as a function of SMO concentration of 0 wt% (1), 1wt% (2), 2 wt% (3), 3wt% (4), 3.5wt% (5), 4wt% (6), 5wt% (7), 6wt% (8) and 7wt% SMO (9).

The evolution of the particle flocculation in the samples was observed after 24 hours. The vessels were then inverted and sedimentation after a further 5 minutes was noted (Figure 3).

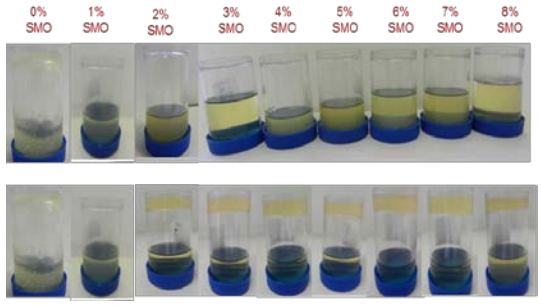

Figure 3. Typical photograph showing the ageing of oil phases samples containing 6wt% fumed silica (HI=1.34) in a mixture with different concentrations of SMO (0 – 8%); upper layer: fresh samples and bottom layer: aged samples after t = 24 hours, 5 min after inverting the vessels.

Figure 3 shows that in contrast to particle dispersions without SMO (far left in Figure 4), ageing of the mixtures of nanosilica and SMO leads to a dramatic change in the particle stability of the dispersions. It can be seen that at about 2wt% SMO the initial stable dispersion begins to sediment. The sedimentation is complete after 24 h, and particles separate from the bulk oil (see second row in Figure 3). It is likely that the flocculation observed here is due to depletion of reverse micelles between particles on close approach.

Samples of the aged dispersions were taken for rheological analysis after particle aggregates (flocs) have been separated from the bulk liquid phase. The zero modulus was obtained from the linear region of the storage modulus by extrapolation of the curve to zero deformation and plotted as a function of SMO concentration (Figure 4).

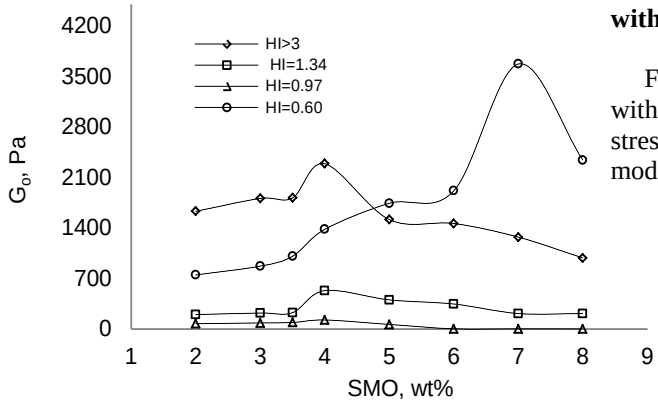

Figure 4. Effect of SMO/silica mass ratio on the shear modulus of flocs after 24 hours of storage.

It can be seen that regardless of particle HI, the strength of particle network shows a maximum at a specific SMO/particle ratio. This maximum occurs at 4 ± 0.5wt% and 6 ± 1 wt% SMO for more hydrophobic (HI ≥ 0.97) or more hydrophilic (HI < 0.97) particles respectively.

Emulsification: characteristic refinement time

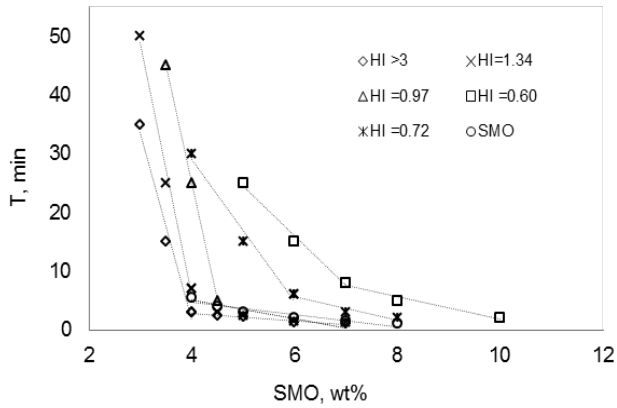

Figure 5. Emulsion characteristic refinement time, used a measure of stability under shearing in the emulsification process for emulsion stabilized by SMO/silica mixture.

It is clear from Figure 5 that both particles with HI < 0.97 and particles with HI ≥ 0.97 show a deflection point/transitional point at 6 ± 1 wt% and 4 ± 0.5 wt% respectively. Below the deflection point/transitional point, there is a rapid decrease in the characteristic refinement time with an increasing slope as the particle hydrophobicity index increases. This seems to be related to both increase of the diffusion rate of SMO and a decrease in Debye length of electrostatic forces [12], caused by a concomitant increase of reverse micelles. In this sense more particles and/or surfactants can quickly adsorb onto the newly created surfaces and stabilize the emulsion against crystallization or coalescence. By contrast, above the deflection point/transitional point, there is a slow decrease in the refinement time which then follows closely the data for emulsions without silica present. In other words, in this region SMO dominates over particles.

Rheological properties of emulsions stabilized with mixed Nanosilica/SMO emulsifier

Flow curves obtained for emulsions stabilized with mixed emulsifier show a pronounced yield stress and a hump in the flow curve in the range of moderate shear rates (0.4 – 0.6 s^{-1}) (Figure 6).

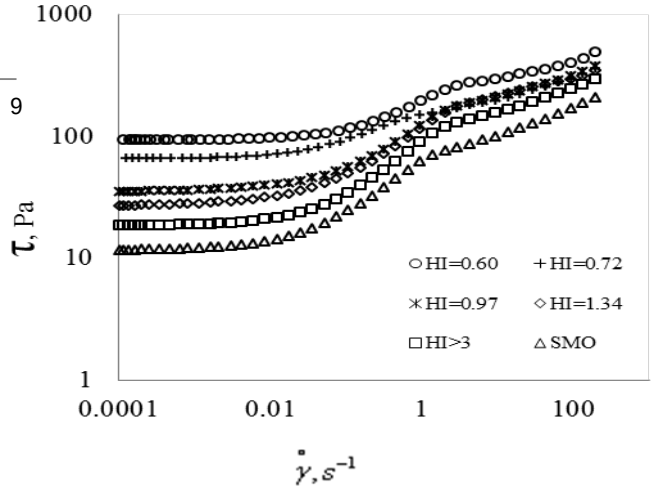

Figure 6. Typical flow curves of emulsions prepared with 5wt% SMO and 6wt% particles of different HI.

The Foudazi-Masalova model recently developed for surfactant-stabilized highly concentrated emulsions (HCE) was found to describe successfully the rheological behaviour of emulsions in the presence of a mixture of surfactant and fumed nanosilica (Figure 7).

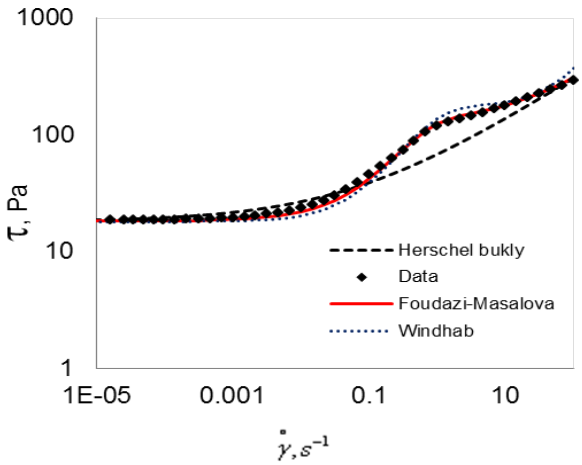

Figure 7. Typical best fittings of Herschel-Bulkley, Windhab and Foudazi-Masalova's models on flow curves of particles/SMO stabilized emulsions.

Structure formation in HCE in the presence of mixtures of SMO and different HI was confirmed by the results of measurements of the elastic modulus.
In Figure 8 the effect of varying the surfactant-to-particle mass ratio on the plateau modulus is shown.

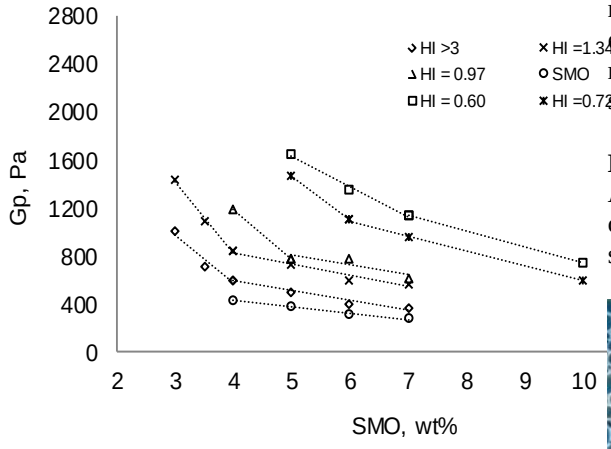

Figure 8. Effect of varying the SMO/silica ratio (3 – 10wt% of SMO and 6wt% of silica) on the plateau modulus of HCE.

From Figure 8 three clear observations can be made. Firstly, emulsions stabilised only by SMO have a relatively low shear modulus regardless of SMO concentration, but adding nanosilica particles increases the shear modulus. The magnitude of the increase in shear modulus is significantly more with reducing particle HI (decreasing hydrophobicity). Secondly, shear modulus reduces with increasing SMO concentration. Thirdly, as with refinement time, the correlation shows a deflection /transitional point at a surfactant concentration of 4 ± 0.5 wt% (for particles with HI < 0.97) or 6 ±1 wt% (for particles with HI ≥ 0.97) which, as before, mark the transition points between regions of particle or SMO domination.

As evidenced by the qualitative bottle test and the rheology of the fresh oil dispersions with different concentrations of SMO (3-7 wt%), the nanosilica network in the interfacial layers between droplets is broken. The formation of a network of silica particles in the bulk phase is therefore not the (only) mechanism controlling the strength of the emulsion structure. It is clear that scaling of the storage modulus by Laplace pressure does not result in superimposition of values corresponding to different compositions.

It seems reasonable to assume that the decrease in shear modulus with increasing HI or SMO concentration is caused mainly by a reduction of the inter-particle repulsive forces at the interface and in the thin film between droplets which is caused by the increased concentration of reverse micelles. It is clear from Figure 8 that low HI values result in a high elastic modulus over the entire SMO concentration range, since a high surface charge is expected with fewer reverse micelles remaining in the oil phase because of the extensive adsorption of SMO molecules onto the particles' surfaces. The higher the electrostatic repulsion between particles adsorbed at the interface, the more ordered the generated structure [14] and the greater the stored energy [2-3, 8]. The higher the concentration of reverse micelles (higher HI), the greater the possibility of charged micelles. This will decrease the Debye length of the electrostatic forces, and hence the electrostatic repulsion. Lower electrostatic repulsion means less stored energy [2-3, 8].

Emulsion stability with time

Ageing of the emulsion was associated with the crystallisation process of the dispersed phase as shown in Figure 9.

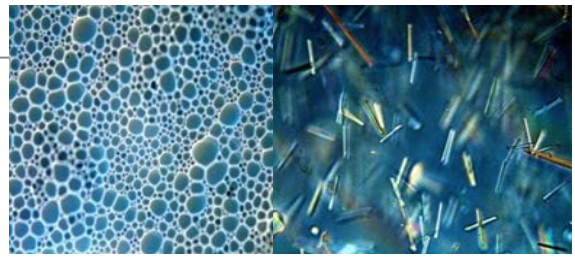

Figure 9. Microscopic images of a fresh emulsion (a) and a crystallized emulsion (b).

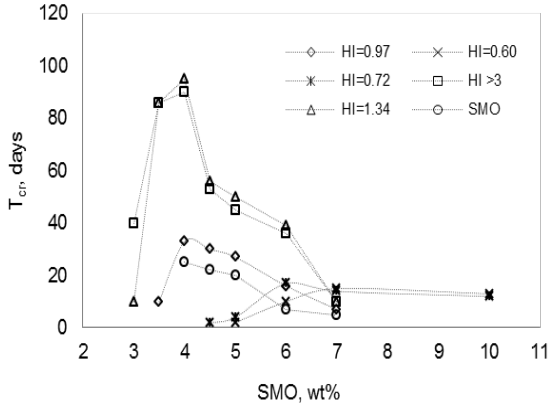

Figure 10. Effect of varying the SMO/silica mass ratio on the starting crystallization point (shelf life) of HCE with an overcooled dispersed phase.

The emulsion stability in terms of time to the start of crystallization shows a maximum (marked or a slight) at 4 ± 0.5 wt% SMO for the more hydrophobic particles (HI ≥ 0.97) and at 6 ± 1wt% SMO for the less hydrophobic and extremely hydrophilic particles (HI < 0.97). Again, this transitional point marks the boundary between particle or SMO dominated regions. Below the transitional point the time to onset of crystallization increases rapidly with SMO concentration (left part of the dependence in Figure 10). For non-surface active particles (particles with HI>3) this is caused by the surface of aqueous droplets being coated with an increasing amount of surfactant, which builds a close packed monolayer. Hydrogen bonding between OH groups from the SMO and ions from the dissolved salts delay the initiation of crystallization [13]. On the other hand, for surface active particles (0.97 ≤ HI ≤ 1.34) there was evidence from the rheology tests of increased particle network strength. This indicates reduced repulsive forces between the particles (reduction in Debye length of the electrostatic repulsion), caused by increased reverse micelle concentration. This assertion was further corroborated by the drastic reduction in both elastic modulus and emulsion refinement time. It is

concluded that the significant improvement in the time to the start of crystallization is a result of the surfaces of the aqueous droplets being coated with an increasing amount of surfactant and fumed nanosilica particles [12], This builds a close packing of fumed nanosilica [14] in which the hydrogen bonding between the OH groups of the fumed nanosilica and SMO, and ions from the dissolved salts, delay the initiation of crystallization. This is in agreement with the fact that comparison between Figure 4 and Figure 10 reveal that the most stable emulsions are prepared from the most unstable dispersions.

Increasing the amount of surfactant above SMO/particle ratio corresponding to the transitional point dramatically reduces the time to the start of crystallization, eventually to that for surfactant alone, as seen in Figure 9. Similarly to emulsions stabilized solely by SMO; this behavior could be caused by coating of aqueous droplets with surfactant multilayers [7]. This results in crystallization being induced from the interface [15].

CONCLUSIONS

A detailed investigation into the stabilization of highly concentrated water-in-oil emulsions with an overcooled dispersed phase stabilized by a mixture of fumed nanosilica particles and, SMO has been made. The influence of the surfactant to particle ratio on emulsion refinement time, rheology and emulsion stability against the crystallization of salt inside the emulsion droplet has proved important. Regardless of the particle hydrophobicity, the relationship between the emulsion's refinement time and SMO/particle ratio shows a transitional point in the stabilization mechanism of the emulsion. The silica content dominates over SMO below this critical point whereas SMO dominates above this point over particles. The mixing of SMO and silica nanoparticles significantly increased rheological properties responsible for solid-like behaviour of emulsions (the yield stress and plateau modulus) compared to the SMO only system. The effect was found to be more pronounced with a reduction of HI. The Foudazi-Masalova model recently developed for surfactant-stabilized HCE was found to describe the rheological behaviour of emulsions successfully in the presence of a mixture of surfactant and fumed nanosilica. The relationship between the shear modulus and SMO-to-particle ratio shows a transitional point related to the same SMO/particle ratio found with the refinement time. Interestingly, for each HI, the emulsions are most stable against crystallization of the dispersed phase on shelf (long-term storage) when prepared with a SMO/particle ratio exactly equal to the transitional point. By determining the zero modulus of particle dispersions in oil, we show that the most stable emulsions are formed from dispersions which show a maximum particle flocculation, induced by SMO reverse micelles, in line with the transitional point. Particle network could resist the spreading of the crystallization of salts from nucleated droplets to their dormant neighbours, hence stabilize the emulsion.

REFERENCES

1. Masalova, I., Malkin, A. Ya (2007) A new mechanism of aging of highly concentrated emulsions: Correlation between crystallization and plasticity. *Colloid J.*, 69 (2): 198-202.
2. Foudazi, R., Masalova, I., Malkin, A Ya (2010) Effect of interdroplet interaction on elasticity of highly concentrated emulsions. *Appl. Rheol*., 20: 45096-45106.
3. Masalova, I., Foudazi, R., Malkin, A. Ya (2011) The rheology of highly concentrated emulsions stabilized with different surfactants. *Colloids Surf. A Physicochem. Eng. Aspects*, 375: 76-86.
4. Masalova, I., Malkin, A. Ya, Ferg, E., Taylor, M., Kharatiyan, E., Haldenwang, R. (2006) Evolution of rheological properties of highly concentrated emulsions with aging — Emulsion-to-suspension transition. *J. Rheol.,* 50 (4):435–451.
5. Dutschk,V., Stöckelhuber, W., Albrecht, V., Geißler, U., Simon,F., Petzold, G., Bellmann, C. (2007) Differently modified synthetic alumina particles as stabilizer of W/O emulsions: surface properties and dispersing mechanisms, in: *Proceedings PARTEC, March* 27–29, Nuremberg.
6. Chattopadyay, A.K. (1966) US Patent, 5,500,062.
7. Drelich, A., Gomez, F., Clausse, D., Pezron, I. (2010) Evolution of water-in-oil emulsions stabilized with solid particles. Influence of added emulsifier *Colloids Surf. A*, 365: 171.
8. Derkach S.R. (2009) Rheology of emulsions. *Adv. Colloid Interface Sci.*, 151, 1-23.
9. Simovic, S., Prestidge C.A. (2007) Nanoparticle layers controlling drug release from emulsions, *Eur. J. Pharm. Biopharm*, 67: 39-47.
10. Barthel, H. (1995) Surface interactions of dimethylsiloxy group-modified fumed silica. *Colloids Surf. A*, 101: 217.
11. Dukhin A.S., Goetz P.J. (2006) How non-ionic "electrically neutral" surfactants enhanceelectrical conductivity and ion stability in non-polar liquids. *J.Electroanal.Chem*., 588: 44-55.
12. Lucassen-Reynders, E.H., Van den Tempel, M. (1963) Stabilization of water-in-oil emulsions by solid particles, *J. Phys. Chem.*, 67: 731-734.
13. Ashok, K..A., Neilson, G.W. (1991) Structure of a 50 mol kg^{-1} aqueous solution of ammonium nitrate at 373 K by the isotopic difference method of neutron diffraction. *J. Chem. Soc. Faraday Trans.* 87: 279–286.

14. Horozov, T.S., Aveyard, R., Binks, B.P., Clint, J.H. (2005) Structure and Stability of Silica Particle Monolayers at Horizontal and Vertical Octane−Water Interfaces. *Langmuir*, 21: 7405-7412.

15. Taborek, P. (1985) Nucleation in emulsified supercooled water, *Physical review B*, 32: 9.

MELT-STATE RHEOLOGY: AN IMPORTANT TOOL TO ESTABLISH STRUCTURE-PROPERTY RELATIONSHIP IN CLAY-CONTAINING NANOCOMPOSITES

S.S. Ray

DST/CSIR National Centre for Nanostructured Materials, Council for Scientific and Industrial Research, Pretoria 0001, South Africa
E-mail: rsuprakas@csir.co.za

ABSTRACT

Since the end of the last decade, much research and development effort has emerged in addressing hybrid organic-inorganic systems; particular attention has been given to those systems in which nanofillers are dispersed in polymer matrices. This class of materials is called polymer nanocomposites and shows unique value-added properties that are completely absent in neat matrices and conventional composites. Researchers believe that the interaction between filler and matrix at the nanoscale is the basis for new and novel properties of the nanocomposites, as opposed to conventional composites. Over the past few years, various types of nanofillers have been used for the preparation of composites with almost all types of polymer matrices. However, clay-containing polymer nanocomposites (PNCs) have attracted great interest in today's materials research because these substances can significantly enhance nanocomposite properties, especially when compared with those of a neat polymer. These improvements may include high moduli, increased strength, flexibility and heat resistance, decreased gas permeability and flammability, increased rate of crystallization, and enhanced rheological properties.

Understanding the rheological properties of PNCs under molten state conditions is crucial for obtaining fundamental knowledge about the processability and the structure-property relationship of these materials. In the case of PNCs, the melt rheological behaviors are strongly influenced by their nanostructure. In this presentation, we attempt to summarize the recent progress in the melt-state rheological properties of various types of PNCs and the relationship of these properties with their structure. Both the linear and non-linear rheological properties have been summarized with a specific focus on the effects of applied shear stress, both steady and dynamic, on the orientation of silicate platelets inside the polymer melts.

INFLUENCE OF OIL TYPE ON STABILITY AND RHEOLOGICAL PROPERTIES OF HIGHLY CONCENTRATED EMULSIONS

E. Mamedov, I. Masalova

Department of Civil Engineering, Faculty of Engineering, Cape Peninsula University of Technology,
PO Box 652, Cape Town 8000, Republic of South Africa
E-mail: 212291718@mycput.ac.za

INTRODUCTION

The subject of this study is highly concentrated W/O emulsions (HCE) with super-cooled dispersed phase. Such emulsions comprise a rather special class of colloids. In contrast to standard emulsions and suspensions, the concentration of the dispersed phase in highly concentrated emulsions exceeds the limit of the closest packing of regular spheres (app. 74%). This is possible due to the "compressed" state of droplets which have a polyhedron shape. The aqueous phase is an oversaturated (over-cooled) inorganic salt solution at room temperature, comprising less than 20% water by mass.

Generally emulsions are recognized as thermodynamically unstable systems that tend to break down with time due to gravitational separation, flocculation, creaming, coalescence or Ostwald ripening [1-6]. Relative instability of the emulsions with super-cooled dispersed phase is due to the fact that these systems comprise of a thermodynamically unstable dispersion of metastable inorganic salt solution in an oil continuous phase. If the emulsion remains stable, super-cooled droplets are prevented from crystallizing or solidifying. If the emulsion weakens or becomes unstable, crystallization of the droplets takes place generally resulting in change of properties [7-10]. It has been demonstrated by [11] that in these types of emulsions - the dominating mechanism of destabilization with time is crystallization of the supersaturated dispersed phase or emulsion – suspo-emulsion transition. The same study demonstrated minimal to no coalescence taking place within the system with ageing and therefore coalescence will not be considered a destabilizing mechanism for the system in this study.

Stability is one of the most crucial characteristics that affects the final quality of any product existing in the form of emulsion or comprising emulsion as one of its components [11-15]. A number of factors affecting emulsion stability have been under investigation in the past years which include: the nature of the surfactant used to stabilize the emulsion [14-16], dispersed phase fraction [17], mechanical properties of manufactured emulsion [12, 18, 19] and aqueous phase composition [1-6].

The goal of this study is to investigate the influence of different types of industrial grade oil comprising the continuous phase of emulsions on the stability of such emulsions with time (ageing) and under high shear (pumping). Ten types of industrial grade oil subdivided into three categories based on their viscosity were used. Oils in each category have the same viscosity parameters but different relative polarity and hence interfacial tension parameters. This approach allowed investigation of the influence of both viscosity and relative polarity of industrial grade oil on the stability of high internal phase concentration W/O emulsions. For a better understanding of the research question emulsions stabilized by two most widely used industrial types of emulsifiers were investigated: emulsions stabilized by non-ionic surfactant sorbitan monooleate (SMO); and emulsions stabilized by polymeric surfactant poly(isobutylene) succinic anhydride based surfactant (PIBSA-Mea). These surfactants differ both structurally and in mechanism of stabilization. As part of the study, the rheological parameters of the bulk emulsion prepared using the industrial grade oils as well as the interfacial properties of these oils were analyzed.

MATERIAL AND METHODS

The oils under investigation were industrial grade hydrocarbon oils: Shellsol (Shell Chemicals), Ash-H 057 (PetroSA), Ash-H 064 (PetroSA), Parproll 2325 (ENGEN), Wittol (ENGEN), Mosspar-H (PetroSA), Ash-1925 (PetroSA), Ash-H 3 (PetroSA), Fluidox (Lake) and Sunflower Oil. Detailed oil specifications can be found on manufacturers web-pages. Based on the specification, no difference exists between Ash-H 057, Ash-H 064 and Ash-H 3 oils being three production batches of the same oil from the same production line. However interfacial tension measurements performed in 60% aqueous solution of ammonium nitrate revealed a significant difference in relative polarity of these three batches with Ash-H 057 being the most polar oil followed by Ash-H 064 which in turn is more polar than Ash-H 3 oil. From this finding, the decision was made to treat the three batches as different type of oils. Industrial grade emulsifiers – SMO and PIBSA-Mea were used as supplied. 5% and 8% by mass of SMO and PIBSA-Mea respectively were dissolved in different types of oil and such solutions were utilized as the continuous

phase in the various emulsions. 80% by mass supersaturated aqueous solution of inorganic oxidiser salt ammonium nitrate (AN) was used as the emulsion dispersed phase. The above materials were used in order to manufacture highly concentrated W/O emulsions with continuous phase fraction not exceeding 6.5% of the emulsion by mass.

The Hobart N50 mixer was used to manufacture all the samples under study. A more detailed description of emulsion manufacturing can be found elsewhere [11, 12, 15].

Measurements of the dispersed phase droplet sizes were done with the Mastersizer 2000 device (Malvern Instruments Co.). The average value d_{32} was used as a measure of droplet size in the investigation. The measurement of accuracy was 99 %. The droplet size was kept identical at 10 μm for all the samples investigated.

Interfacial tension measurements between the oil phase containing surfactant and aqueous phases with the 60% by mass ammonium nitrate were performed at a planar aqueous-oil boundary with the use of a Krüss K100 tensiometer.

The rheological measurements were carried out with the use of a rotational dynamic rheometer MCR 300 (Paar Physica) with the "bob-in-cup" measuring unit having a sandblasted bob surface. The bob diameter was 27 mm and the gap distance between the cup and the bob was 1 mm. Steady state measuring flow curves and oscillatory measurements for measuring strain amplitude dependencies of the storage components of dynamic modules were chosen for the investigation. Oscillatory measurements for measuring strain amplitude dependencies of the (storage and loss) components of dynamic modules; the frequency (1 Hz) was kept constant in the amplitude sweep test. The strain was controlled between 0.01% and 200%. The shear rate region used in the flow test ranged from 200 s^{-1} to 0.00001 s^{-1}. All rheological measurements were conducted at 30±0.1°C.

The optical analysis was conducted with the use of a 'Leica' optical microscope equipped with a digital camera, at a magnification of 40 times (x40).

RESULTS AND DISCUSSION

Characterisation of Oils

In order to understand the difference between the different types of oil, the interfacial tension at the planar aqueous-oil interface was measured for a series of oils under investigation.

Since the system used for interfacial tension measurements comprises of the polar aqueous phase (60% AN solution) as one of its components, it follows that the lower water-oil interfacial tension in the system will correspond to the higher relative polarity of oil and vice versa [20].

To further characterise the oils, rheological analysis of the pure oils was performed in order to determine the oil viscosity. Based on the obtained viscosity results, oils under investigation were then further grouped by similar viscosity regions. The result is three classes (Group A, Group B and Group C) of oils with their respective viscosity and interfacial tension values presented in Table 1. Oils within each class are arranged in the order of decreasing relative polarity. Such a grouping allowed for further ease of investigation of effects of both polarity and viscosity on the stability of highly concentrated emulsions with super-cooled dispersed phase.

Table 1. Classification of pure oils under investigation based on viscosity values.

Oil Type	**μ (cP)**	**σ (mN/m)**
Group A: Viscosity < 2 cP		
Shellsol	1.9	2.4
Fluidox	1.7	23.9
Ash-1925	1.4	36.2
Group B: Viscosity 2.5-3.5 cP		
Ash-H 057	2.6	3.0
Ash-H 064	3.4	19.3
Mosspar-H	3.1	24.0
Ash-H 3	3.2	30.1
Group C: Viscosity > 25 cP		
Parprol	51.6	8.0
Sunflower	53.2	10.7
Wittol	27.0	24.0

Characterisation of Emulsions

The time required to form the emulsion with a droplet size (d_{32}) equal to 10 μm (refinement time) as well as the rheological properties of emulsions, were determined and compared. The stability of the emulsions was monitored by following the emulsion droplets crystallization.

Refinement time (t_{ref}) for each emulsion prepared was recorded and results are presented in the Table 2 and Table 3 for SMO and PIBSA-Mea, respectively.

Table 2. Refinement time of the emulsions containing 5% SMO as surfactant within the continuous phase.

Oil Type	**t_{ref} (min)**
Group A	
Shellsol	5.0
Fluidox	5.0
Ash-1925	5.0
Group B	
Ash-H 057	3.0
Ash-H 064	3.0
Mosspar-H	3.0
Ash-H 3	3.5
Group C	
Parprol	0.5
Wittol	2.5

Emulsions prepared using SMO in Sunflower oil as well as emulsions prepared using PIBSA-Mea in Mosspar-H, Ash-H 3 and Wittol oils displayed high instability. Crystallisation of these emulsions occurred at the homogenisation stage of emulsion manufacturing

Table 3. Refinement time of the emulsions containing 8% PIBSA-Mea as surfactant within the continuous phase.

Oil Type	**t_{ref} (min)**
Group A	
Shellsol	43.0
Fluidox	37.0
Ash-1925	40.0
Group B	
Ash-H 057	35.0
Ash-H 064	30.0
Group C	
Parprol	5.0
Sunflower	2.0

rendering any further investigation of these emulsions impossible along with data collection.

Rheological measurements were performed for each successively formed emulsion for both storage modulus (G') and yield stress (τ_y) and are presented in Table 4 and Table 5 along with amplitude sweep and flow graphs in Figure 1 and Figure 2 for SMO and PIBSA-Mea, respectively. Other parameters such as emulsion volume fraction, droplet size and droplet size distribution were fixed throughout the experiment across all the analysed samples.

Table 4. Rheological parameters for the bulk emulsions containing 5% SMO as surfactant within the continuous phase.

Oil Type	**G' (Pa)**	**τ_y (Pa)**
Group A		
Shellsol	491.0	7.4
Fluidox	509.0	10.9
Ash-1925	600.0	11.8
Group B		
Ash-H 057	403.0	7.7
Ash-H 064	414.0	9.9
Mosspar-H	427.0	11.0
Ash-H 3	439.0	11.2

Emulsions prepared using SMO in high viscous (group C) oils displayed high instability and crystallisation during the emulsification or cooling stages of the manufactured emulsion. Whilst it was possible to measure and analyse the refinement time parameter any further investigation of rheological and crystallization properties became impossible.

Analysis of the rheological properties obtained indicates the dependency of the rheology of the bulk emulsion on oil relative polarity.

a.

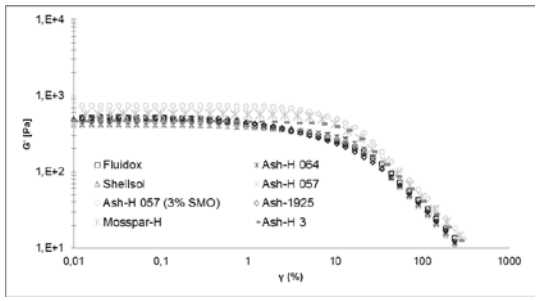

b.

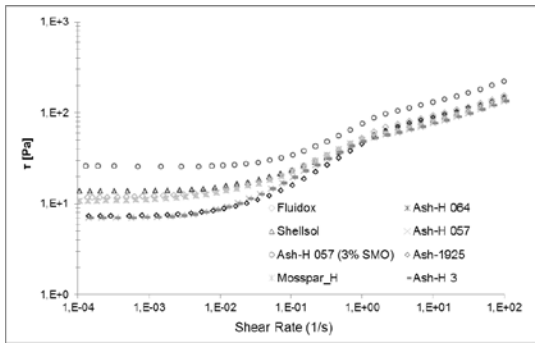

Figure 1. Amplitude Sweep (a) and Flow Curve (b) plots for the samples manufactured with the use of SMO surfactant

Table 5. Rheological parameters for the bulk emulsions containing 8% PIBSA-Mea as surfactant within the continuous phase.

Oil Type	**G' (Pa)**	**τ_y (Pa)**
Group A		
Shellsol	1540.0	30.3
Fluidox	1640.0	39.8
Ash-1925	1730.0	42.7
Group B		
Ash-H 057	1010.0	14.5
Ash-H 064	1220.0	22.7
Group C		
Parprol	1170.0	20.0
Sunflower	1400.0	32.5

A decrease of the yield stress and storage modulus with increase in oil polarity is observed for both emulsions manufactured using SMO and PIBSA-Mea as stabiliser. Hence the oil polarity influences the elasticity of highly concentrated emulsions.

a.

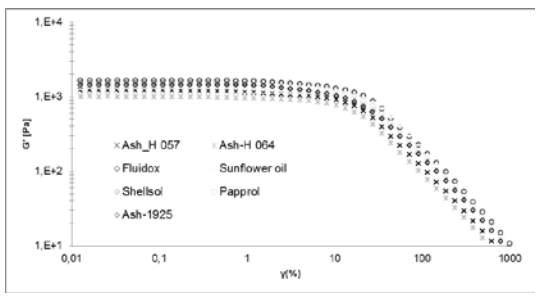

b.

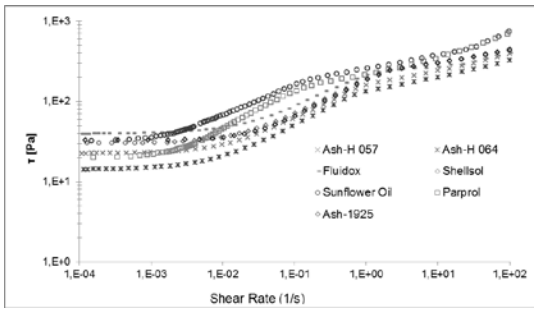

Figure 2: Amplitude Sweep (a) and Flow Curve (b) plots for the samples manufactured with the use of PIBSA-Mea surfactant

This effect was stronger for the set of samples manufactured using the less viscous oils and is especially evident in the samples stabilised by the PIBSA-Mea surfactant. This effect can be related to the decrease in the surfactant micelle content due to an increase in critical micelle concentration (CMC) as the relative oil polarity increases [21-25].

Investigation of ageing for the samples manufactured using low viscosity oils (group A and B) and SMO revealed several important key points regarding the stability with ageing and these are illustrated in Figure 3.

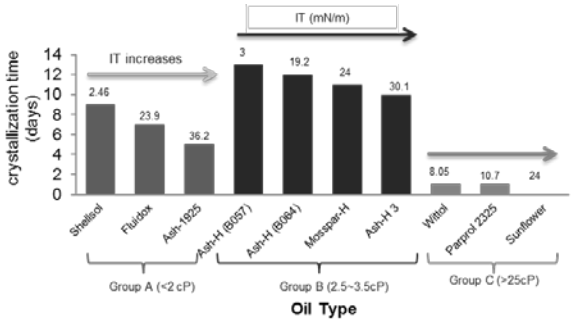

Figure 3. Comparative chart - representation of starting time for crystallisation in the samples prepared with the use of various oils under investigation in combination with SMO surfactant.

It can be seen that use of oils of group B with a viscosity between 2.5 to 3.5 cP results in samples with the highest stability to crystallization with time.

The second important finding for the samples manufactured with the low viscosity oils is the relation between stability and relative oil polarity. In samples manufactured with the use of both oils, group A and B, the stability to crystallisation with time decreases with decreasing relative oil polarity. SMO molecules tend to develop the multilayer structure at the interface, which becomes gradually opaque with time [14, 26] which can initiate crystallization at the interfacial layer. For high polar oils (with low interfacial tension) the multilayer structure is not developing at aqueous-oil interface, delaying the crystallization of droplets.

Investigation of ageing for the PIBSA-Mea samples revealed a very straight-forward relation between viscosity and relative polarity of the oils with emulsion stability to crystallization with time. More stable samples were obtained from the formulations adopting low polar and high viscous oils, indicating that the relative polarity and viscosity of the oils are directly proportional to the stability of these emulsions. However it has been observed that the viscosity parameter affects the shelf life stability to a higher extent than the relative oil polarity. Results of the investigation of ageing for the samples manufactured using low viscosity oils (group A and B) and PIBSA-Mea are summarised in Figure 4.

The highest stability to crystallisation with time has been demonstrated by the samples manufactured using group C highly viscous oils with PIBSA-Mea. For the PIBSA based surfactants it was found that the stability of the emulsions is strongly affected by the amount of

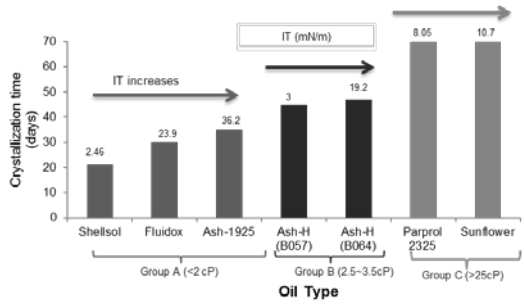

Figure 4. Comparative chart representation of starting time for crystallisation in samples prepared with the use of various oils under investigation in combination with PIBSA-Mea surfactant.

surfactant micelles in the bulk of emulsion which create a strong steric barrier, hence, preventing the spreading of crystallization within the bulk of the emulsion [27]. High polar oils could destroy these micelles. In addition, oils with lower viscosity can wash micelles out at the inter-droplet layer.

CONCLUSION

A study has been performed on the effect of relative oil polarity and viscosity on stability to crystallisation with time, shelf life, of highly concentrated W/O emulsions. It has been found that the overall shelf life stability of these emulsions is significantly affected by both the viscosity and polarity of the oil used as part of the continuous phase. Based on the obtained results it is concluded that even though properties of the oils under discussion do affect the stability of emulsions, these effects may differ for different surfactant types used in the emulsion formulation. In this particular study for emulsions stabilised by the means of SMO surfactant it was found that only a very specific region of the oil viscosity (2.5– 3.5 cP) exists in which it is possible to form the most stable emulsions and the stability increases with the oil polarity. This optimal condition may prevent SMO molecules to form a multilayer structure at the interface as a point of crystallization. On the other hand, for samples stabilised using PIBSA-Mea surfactant it was evident that the higher the oil viscosity and the lower the oil polarity, the final product is more stable to crystallisation with time by enhancing the micelles

formation in the inter-droplet layer and hence, creating a strong steric barrier.

REFERENCES

1. Becher, P. (1985). Encyclopedia of emulsion technology, Vol. 2, Applications, Derek, New York.

2. Hunter, R.J. (1986) Fundamentals of Colloid Science: Vol. 1, Oxford Science.

3. Becher, P. (1988) Encyclopedia of emulsion technology, Vol. 3, Basic Theory, Measurements and Applications, Derek, New York.
4. Schramm, L.L. (1992) Emulsions: Fundamentals and Application, Am. Chem. Soc.
5. Hunter, R.J. (1993) Introduction to Modern Colloid Science, Oxford Univ. Press.

6. McClements, D.J. (1999) Food Emulsions: Principles, Practice and Technologies, CRC Press.

7. Cooper, J., Baker, A.S. (1989) Emulsion explosive composition, US Patent 4822433.

8. McKenzie, L.F. and Lawrence, D.L. (1990) Emulsion explosives containing a polymeric emulsifier, US Patent 4931110.

9. McKenzie, L. F. (1991) Stabilized emulsion explosive and method, US Patent 5086867.

10. Boer, W. G. (2003). Composition and emulsifier, US Patent 6630596.

11. Masalova, I., Malkin, A.Y., Ferg, E., Kharatiyan, E., Taylor, M., Haldenwang, R. (2006) Evolution of rheological properties of highly-concentrated emulsions with ageing – emulsion-to-suspension transition, J. Rheol., 50 (4): 435.

12. Masalova, I., Malkin, A.Y. (2007) A New Mechanism of Aging of Highly Concentrated Emulsions: Correlation between Crystallization and Plasticity, Colloid Journal, 69 (2): 220.

13. Kim J., Lee D., Shum H.C., Weitz, D.A. (2008) Advanced Materials, 20: 323.

14. Drelich, A., Gomez, F., Clausse, D., Pezron, I. (2010) Evolution of water-in-oil emulsions stabilized with solid particles: Influence of added emulsifier, Colloids and Surfaces A, 365: 171-177.

15. Tshilumbu, N.N., Ferg, E.E., Masalova, I. (2010) Instability of Highly Concentrated Emulsions with Oversaturated Dispersed Phase. Role of a Surfactant, Colloid Journal, 72 (4): 569.

16. Binks, B.P. (2002) Current Opinion in Colloid and Interface Sci., 7: 21.

17. Binks, B.P., Rodrigues, J.A. (2005) Inversion of Emulsions Stabilized Solely by Ionazable Nanoparticles, Angew. Chem. Int. Ed., 44: 441.

18. Bobra, M., Fingas, M., Tennyson, E. (1992) When oil spills emulsify, Chemtech, 22: 236-241.

19. Fingas, M., Fieldhouse, B., Bier, I., Condor, D. (1993) Tennyson E., in Proceedings of the Workshop on Emulsions, Marine Spill Response Corporation: 7, 9, 73.

20. Wagner, C. Z. (1961) Theory of the Aging of Precipitates by Dissolution-Reprecipitation (Ostwald Ripening), Journal of Electrochemistry, 65: 581

21. Krishnakumar, S., Somasundaran, P. (1994) Role of Surfactant-Adsorbent Acidity and Solvent Polarity in Adsorption-Desorption of Surfactants from Nonaqueous Media, Langmuir, 10: 2786-2789.

22. Chatterjee, M., Naskar, M.K., Siladitya B., Ganguli D. J. (2000) Sol-emulsion-gel synthesis of alumina nanospheroids, Transactions of the Indian Ceramic Society, 59(3): 54-57, 63.

23. Muto, S., Meguro, K. (1973) Catalysis in Micellar and Macromolecular Systems, Bull. Chem. Soc. Japan, 46: 1316.

24. Santhanalakshmi, J., Imaya, S.I. (1997) Solvent Effects on Reverse Micellisation of Tween 80 and Span 80 in Pure and Mixed Organic Solvents, Proc. Indian Acad. Sci. (Chem. Sci.), 109 (1): 27-38.

25. Masalova, I., Foudazi, R., Malkin, A.Y. (2010) The rheology of highly concentrated emulsions stabilized with different surfactants, Colloids and Surfaces A: Physicochem. Eng. Aspects, 375: 76-86.

26. Kovalchuk, K. and Masalova, I. (2012) Factors influencing the crystallisation of highly concentrated water-in-oil emulsions: A DSC study. South African Journal of Science, 108: 3-4.

27. Reynolds, P.A., Gilbert E.P., Henderson M.J., White J.W. (2009) Structure of High Internal Phase Aqueous-in-Oil Emulsions and Related Inverse Micelle Solutions. 3. Variation of Surfactant, The Journal of Physical Chemistry B, 113(36): 12231-12242.

RHEOLOGY AND PRACTICAL SLURRY PIPELINE FLOW IN THE MINING INDUSTRY

A.J.C. Paterson

Paterson & Cooke Consulting Engineers (Pty) Ltd, Cape Town, South Africa
E-mail: AngusP@PatersonCooke.com

INTRODUCTION

Rheology is a term that is widely used in the minerals processing industry, however it is not always used in the correct and appropriate context and does not always apply to all slurries. Rheology is the study of the flow of matter and this broad definition covers the flow and response of liquids and suspensions to an applied force.

In the mineral processing industry it is common to refer to the "rheology of the material". This has merit when dealing with a purely homogeneous suspension or polymer where we understand that it refers to viscoelastic properties that can be measured and completely describe the behaviour of the material. However when a material contains a wide range of discrete mineral particles it is rarely truly homogeneous and so the behaviour cannot be properly defined and is at best approximated.

Rheology, as a descriptor or property of a fluid, has through common usage become a term that encapsulates the sum total of the "flow properties" of a fluid that may or may not exhibit viscoelastic behaviour.

This paper discusses slurry pipeline applications in the mineral processing industry and presents examples of why it is important to understand the differences in the flow behaviour of fluids in pipelines that may not necessarily be influenced by the viscous properties of the fluid alone.

DEFINITIONS

In the context of this paper, slurry is a two phase mixture of solid particles and water that do not react with each other. Slurry can contain particles that range from micron size clay size particles to large boulder size particles. Particle size influences the nature of the material, the finer the particles the more homogenous the mixture appears, and the coarser the particles the more rapidly they settle.

Figure 1 shows a well graded size distribution and for such materials a fraction of the particles below a certain size will settle very slowly and combine with the liquid to form an apparently homogeneous suspension, or "vehicle" that acts as a conveying medium for the coarser particles. If we consider a slurry comprising only the vehicle fraction, in this case all particles below 45 micron, then the mixture will likely exhibit some viscous properties at high solids concentrations and may be *non-Newtonian*. A slurry of just the coarse plus 45 micron fraction will always show clear solid-liquid separation and will behave as a *heterogeneous* mixture. A mixture comprising the full range of fine and coarse particles is termed mixed-*regime* slurry and requires an understanding of the flow behaviour of the vehicle as well as the coarse fraction.

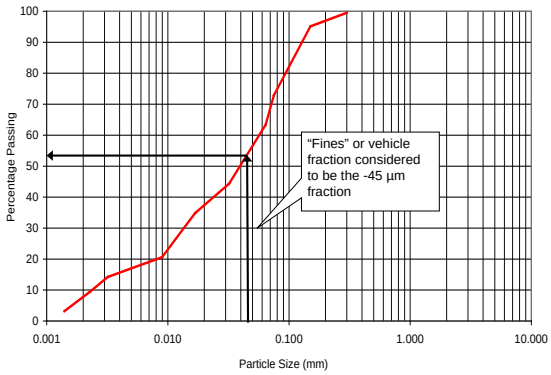

Figure 1. Particle size distribution

CHANGES IN MINING TECHNOLOGY

Mines essentially liberate precious metals from the host ore through the beneficiation process. This requires that the ore is finely ground to produce a solid-water mixture, or slurry, that is then treated in the metallurgical facility that generates two principal streams, a relatively low volume concentrate slurry that is enriched and used as feedstock to a smelter to produce the metal, and a high volume waste gangue (or "tailings") material that is disposed in surface impoundments or underground as backfill. In order to improve recovery many processes are now generating a finer material through increased milling.

Environmental best practice also dictates that water consumption is minimised and promotes the re-cycling of water as far as possible. This means that the waste stream must be de-watered at the beneficiation plant and so together with the finer milling, the waste material becomes increasingly viscous and influences the pipeline flow behaviour.

PIPELINE FLOW

When dealing with the pipeline flow of slurries the flow behaviour is a function of many variables, most importantly particle size distribution and solids concentration. These dictate whether the slurry is treated as a heterogeneous, non-Newtonian, or mixed-regime slurry.

Heterogeneous slurries

Slurries that are purely heterogeneous are dominated by the settling characteristics of the particles and the pipe flow regime is always turbulent. These slurries do not have any meaningful viscous properties and so the term "rheology" cannot be used when studying heterogeneous flow. Examples include sand dredged material and low concentration cyclone underflow materials.

Non-Newtonian slurries

Non-Newtonian slurries have several of the following characteristics; a non-linear rheogram, a rheogram that does not pass through the origin, or a rheogram that is dependent on shear history. This also implies that there is no settling or segregation between the solid and liquid phases. In practice this rarely occurs as all solids will slowly settle given sufficient time, however for pipeline flow estimates a rheogram that meets these criteria provides sufficient laminar flow data that can be used to estimate the pipeline flow behaviour.

The "rheology" of these materials is important to quantify as non-Newtonian mixtures that are essentially non-settling when quiescent need to be treated with care when considering pipeline flow. When sheared during laminar pipeline flow the coarser particles do not remain in suspension and deposit on the pipeline invert and there is no mechanism to re-suspend the particles into the main body of flow. For low yield stress materials it is preferable to transport these slurries in the turbulent flow regime, as shown in Figure 2. Unfortunately this is not always feasible as the yield stress may be such that the laminar to turbulent transition velocity is high, making pipeline flow impractical. In such instances where it is necessary to transport in laminar flow, a regime may develop that is known as stratified laminar flow. This occurs when coarser particles on the pipe invert are transported as a sliding bed and the flow regime above these particles remains laminar. Pressure losses in this condition are generally higher as there is a reduced flow area. If there is an insufficient pressure gradient in the pipeline the coarse particles will not be transported on the invert and the pipeline may eventually block. Several cases exist where long overland pipeline systems have blocked as a result of laminar flow deposition.

For extremely viscous slurries it is possible to design a pipeline to operate at very low velocities. This requires high pipeline pressure gradients that provide sufficient force across the settled bed portion of the pipeline so that the particles move as a sliding bed. Slurries such as concrete, shotcrete or paste backfill are pumped at low velocities and require substantial pump discharge pressures. In these instances the "rheology" of the material must be known, in particular the yield stress.

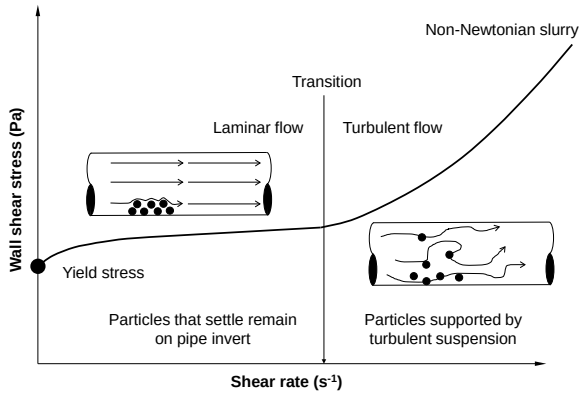

Figure 2. Non-Newtonian slurry pipeline flow

The yield stress is an important parameter for pipeline flow as it is the shear stress that needs to be overcome to initiate flow in the pipeline. As solids concentration increases the yield stress of the mixture tends to increase exponentially and this has a direct influence on the pumping costs. For many waste disposal pumping systems this proves to be a major obstacle for mines as the cost of disposing of highly concentrated "paste" tailings or backfill is often prohibitive, however in arid areas where water is scarce, these costs can be justified.

There are several instances of high concentration mine waste disposal systems and one of the most notable best practice examples is at De Beers Combined Treatment Plant in Kimberley, South Africa. This system dewaters the waste material at the process plant and pumps the thickened slurry several kilometres to the disposal site. The material forms a stable conical landform deposit that is different from the conventional waste disposal sites, and water consumption is extremely low. In this case the thickened slurry contains a high clay fraction as well as a coarser "grit" fraction. As the clay is so viscous the flow regime in the pipeline is laminar, however there is segregation along the pipeline as the grit material settles and is transported on the invert.

Non-Newtonian slurries are generally always fine and can be quantified by the "rheology" of the total mixture. In some cases they can be transported in the turbulent pipe flow regime and may also be pumped at low velocities in laminar flow provided that certain conditions can be met.

Mixed-regime slurries

Mixed-regime slurries exhibit characteristics of both settling and non-settling slurry behaviour. These are the most commonly encountered slurry types and include mine waste tailings at medium and high solids concentrations.

The flow behaviour of these slurries is governed by the total solids concentration and the properties of

the coarse settling particles as well as the viscous nature of the fine, non-settling particles. In Figure 1 the fine fraction is estimated arbitrarily at 45 micron and the analysis considers the two size fractions as follows:

- The coarse fraction is characterised by the particle properties such as particle size, shape, density and freely-settled bed packing concentration.
- The vehicle is characterised by its "rheology" that is measured using a viscometer.

To analyse the pipeline flow behaviour of these slurries the particle size distribution is split into the fine and coarse fractions and the relative contributions of each fraction to the total wall shear stress are calculated.

An important criterion is to ensure that the selected operating velocity is above the stationary deposit velocity that can be calculated by considering the relationship between particle size and the laminar sub-layer at the pipeline wall. Once particles are contained within the laminar sub-layer the turbulence required to support them is absent and so they form a bed on the pipeline invert. This requires an understanding of the viscosity of the fine vehicle fraction as well as the coarse particle packing within the settled bed on the pipe invert.

Figure 3 presents typical measured data showing the change in deposition velocity as pipe diameter and solids concentration varies.

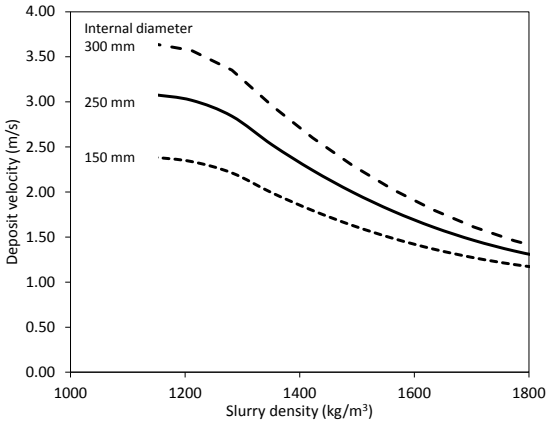

Figure 3. Deposit velocity as a function of pipeline diameter and mixture density

At low solids concentration there is a strong relationship between diameter and deposit velocity as the viscous contribution of the vehicle is small. As concentration increases so the deposit velocity becomes increasingly independent of pipeline diameter and is a function of overall mixture density as the effective vehicle viscosity increases as the fine solids concentration increases.

Concentrate and ore pipelines

Long distance concentrate and ore pipelines are well established as economical alternatives to conventional bulk materials handling. The key to reducing the operating costs in terms of power consumption and pipeline wear rates is to transport the slurry at as low a velocity as possible. These products behave as mixed-regime slurries and require a careful assessment of the contributions of the fine viscous fraction and coarse material to the overall pressure loss. If the material is too fine and viscous, pressure gradients can be high even at low velocities. If there are too few fines the deposit velocity will increase. The optimum particle size distribution for pipeline transport is such an important economic criterion that the milling process is selected to provide a tightly controlled particle size grading. Typically long distance pipelines operate at velocities below 2 m/s and particle sizes are usually less than 100 microns. Any changes in particle size, and in particular the "rheology" of the fine fraction can severely affect the performance of these systems.

Conclusions

The flow behaviour of many types of slurries is affected by the viscous properties of the fine particle size fraction. However in many instances the fine fraction is negligible and so the flow behaviour cannot be defined in terms of the "rheology" of the mixture. These include heterogeneous slurries and low concentration mixed-regime slurries.

For highly concentrated suspensions rheology is important when the term is understood to cover all the viscoelastic properties of the material. When transporting thickened paste like materials the flow behaviour is dominated by properties such as the yield stress versus solids concentration relationship and provided the pressure losses are sufficiently high these materials can be transported in laminar flow.

The flow behaviour of mixed-regime slurries, such as concentrate and ore pipelines, is influenced by both the viscous nature of the vehicle and the properties of the coarse suspended portion. There is an optimum combination of particle size and viscosity that results in a low deposit velocity and pipeline pressure gradient without being too viscous.

Rheology, when used in the context of describing a property of the fluid, is a useful term, however it does not necessarily apply to the pipeline flow of all mineral slurries and should be used with caution.

THE INFLUENCE OF RHEOLOGY IN PIPE FLOW PREDICTIONS

E.M. van den Heever, A.P.N. Sutherland

Department of Civil Engineering and Surveying, Cape Peninsula University of Technology, Cape Town, 8000. E-mail: vandenheevere@cput.ac.za

INTRODUCTION

Pipe tests with three types of non-Newtonian, time-independant, homogeneous fluids were conducted in pipe diameters of Ø40 to Ø200 mm, in laminar and turbulent flow. The fluids were characterised using the power law, Bingham plastic and Herschel-Bulkley, Casson and Hallbom rheological models. For each of these rheologies transitional velocity and turbulent flow predictions were done using techniques commonly reported in the literature, with the aim of evaluating the influence of rheology in reproducing experimental laminar flow, and on transitional velocity and turbulent flow predictions. The gist of the study and a few representative results are presented below.

THEORY AND LITERATURE

Rheology and laminar flow

In the absence of slip and end effects the volumetric flow rate in pipe flow is given by equation (1) [1]:

$$Q = \frac{\pi R^3}{\tau_w^3}\int_0^{\tau_w} \tau_{rz}^2 f(\tau_{rz})\, d\tau_{rz} \; ; \; \tau_w = D\Delta p/4L \qquad (1)$$

In this study five rheological models were considered, as given in equations (2) to (6).

$$\tau = K(\dot{\gamma})^n \qquad \text{Power law} \qquad (2)$$

$$\tau = \tau_y + \eta_p(\dot{\gamma}) \qquad \text{BP} \qquad (3)$$

$$\tau = \tau_y + K(\dot{\gamma})^n \qquad \text{HB} \qquad (4)$$

$$\tau^{0.5} = \tau_C^{0.5} + (\eta_C \dot{\gamma})^{0.5} \qquad \text{Casson} \qquad (5)$$

$$\tau_w{}^k = \tau_0{}^k + (\mu_\infty)^k (\dot{\gamma})^k \qquad \text{Hallbom} \qquad (6)$$

Integrating equation (1) after substituting the appropriate rheological model (equations (2) to (5)) gives the relevant flow rate equations, which are written in terms of ($8V/D$) and τ_w. For example, substituting equation (2) into equation (1) gives [1]:

$$\frac{8V}{D} = 4\left(\frac{\tau_w}{K}\right)^{\frac{1}{n}}\left(\frac{n}{3n+1}\right) . \qquad (7)$$

The equations for ($8V/D$) corresponding to the other rheological models are given in [2], [3]. For the Hallbom model equation (1) cannot be integrated analytically for arbitrary k, and an approximation is required [4]. In laminar flow these expressions for ($8V/D$) can be used directly to calculate V if τ_w is known, or iterated to get τ_w (and so pressure drop: equation (1) for a given V [1], [5].

Transitional flow

Several critical Reynolds number criteria have been proposed in the literature to estimate the end of laminar flow of homogeneous non-Newtonian fluids in pipes. Hallbom [4] and Peixinho et al [6] indicate that transition from laminar to turbulent flow occurs over a velocity range, from the point at which eddies begin to form (instability point transition) to the higher velocity at which the rate of change in pressure gradient increases significantly. Güzel et al [7] and Frigaard and Nouar [8] suggest that the the inability to differentiate between the two transition points is a weakness with the single critical Reynolds number criteria and is a reason for the continuing discrepancy between predicted and experimental transitional velocities.

Notwithstanding these observations, only existing "single point" criteria were considered. These were the Newtonian approximation and Slatter method [9], Metzner & Reed [10], Ryan & Johnson [11], Hedström intersection [12] (using [16]), Slatter & Wasp [13] and the Wilson & Thomas [14] methods. Predictions were done using each of the rheologies given in equations (2) to (5) in each method for each material. The rheology given by Eq. 6 was used only in the prediction techniques proposed by Hallbom [4]. Full details are summarised in [2].

Turbulent flow

Most of the equations available to predict the turbulent flow of time-independent, non-Newtonian fluids are based on experimental findings combined with dimensional analysis [1]. According to Slatter [9] non-Newtonian turbulent flow models can be categorised as analytical, purely empirical or somewhere in-between. The models considered in this study were: Newtonian and Slatter [9], Torrance [15], Wilson and Thomas [16], Hallbom [4] (analytical); Bowen scale-up [17] (empirical); Dodge & Metzner [18] (semi-empirical). Hallbom's methods are essentially the Wilson & Thomas method or the Nikuradse equation, but using parameters derived from equation (6). Details of these techniques are summarised in [2], but the relevant equations for the

more commonly known Dodge & Metzner, Wilson & Thomas and Slatter methods are included below.

Dodge & Metzner

Dodge & Metzner [18] conducted pipe flow tests with power law fluids in the ranges $2900 \leq Re_{MR} \leq 36000$ and $0.36 \leq n' \leq 1$, from which they developed equation (8)

$$\frac{1}{\sqrt{f}} = \frac{4}{n'^{0.75}} log\left(Re_{MR} f^{\frac{(2-n')}{2}} \right) - \frac{0.4}{n'^{0.2}} . \quad (8)$$

When applying equation (8), care must be taken to not exceed these limits, in which case it can be used with confidence [19]. Equation (8) also applies for Bingham plastic, Herschel-Bulkley and Casson fluids as long as n' and K' (see [2], [3] for details) are obtained from the laminar τ_w versus 8V/D curve at the τ_w value of the turbulent flow [20], [18], [1]. In practice such data can be very difficult to achieve.

Wilson & Thomas

Wilson & Thomas [16] derived a turbulent flow model which gives the mean turbulent velocity as:

$$\frac{V}{U_*} = 2.5 ln\left(\frac{D\rho U_*}{\mu'} \right) + \left[11.6(\alpha - 1) - 2.5 ln(\alpha) - \Omega \right] \quad (9)$$

where α is given by equations (10) to (13).

$$\alpha = 2/(1+n) \quad \text{Power law} \quad (10)$$

$$\alpha = 1 + (\tau_y / \tau_w) \quad \text{BP} \quad (11)$$

$$\alpha = \left(\frac{2}{1+n} \right) \left(1 + n(\tau_y / \tau_w \right) \quad \text{HB} \quad (12)$$

$$\alpha = 1 + \left(\frac{2}{3} \right) \left(\frac{\tau_C}{\tau_w} \right)^{0.5} + \left(\frac{1}{3} \right) \left(\frac{\tau_C}{\tau_w} \right) \quad \text{Casson} \quad (13)$$

and Ω by equation (14):

$$\Omega = -2.5 \ln\left[1 - \left(\frac{\tau_y}{\tau_w} \right) \right] - 2.5 \left(\frac{\tau_y}{\tau_w} \right) \left[1 + 0.5 \left(\frac{\tau_y}{\tau_w} \right) \right] \quad (14)$$

Slatter

Slatter [9] developed a non-continuum theory for the turbulent flow of non-Newtonian slurries, assuming a roughness effect caused by solid particles in the slurry and a Newtonian approach. He defined a roughness Reynolds number Re_r based on the material d_{85} size. In this theory, for smooth wall turbulent flow ($Re_r \leq 3.32$) the average turbulent velocity is:

$$V = U_* \left[2.5 ln\left(\frac{R}{d_{85}} \right) + 2.5 ln Re_r + 1.75 \right] \quad (15)$$

For rough wall turbulent flow ($Re_r > 3.32$) the average turbulent velocity is:

$$V = U_* \left[2.5 ln\left(\frac{R}{d_{85}} \right) + 4.75 \right] . \quad (16)$$

For Herschel-Bulkley fluids Re_r is given by

$$Re_r = 8\rho U_*^2 \Big/ \left(\tau_y + K \left(\frac{8U_*}{d_{85}} \right)^n \right) . \quad (17)$$

In equation (17) $n = 1$, $K = \eta_p$ for Bingham plastic material and $\tau_y = 0$ for power law material. For Casson material Re_r is given by equation (18):

$$Re_r = 8\rho U_*^2 \Big/ \left((\tau_c)^{0.5} + \left[\eta_c \left(\frac{8U_*}{d_{85}} \right) \right]^{0.5} \right)^2 . \quad (18)$$

The turbulent flow models use the rheological model evaluated at the turbulent flow wall shear stresses, but the assumption that it still holds at these higher wall shear stresses may not be be true. Strictly, the rheological model should be based on laminar Q versus $D\Delta P/L$ data up to the turbulent wall shear stress for which turbulent flow predictions are required [20], [18], [1]. Figure 1 shows an example of extending the different rheology models to high turbulent shear stresses. It is clear that for a given value of τ_w apparent viscosities μ' will vary greatly, so different predictions can be expected.

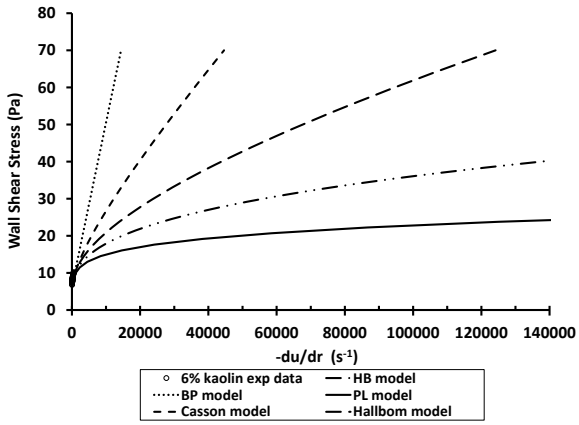

Figure 1. Extention of rheological models to maximum measured turbulent shear stress for 6% kaolin.

MATERIALS, EQUIPMENT AND DATA TREATMENT

Primary data (Q and $\Delta P/L$) were acquired for various concentrations of three types of non-Newtonian fluids, namely shear thinning (CMC: 3 to 8%), Bingham plastic (bentonite: 6 to 9%) and viscoplastic (kaolin: 6 to 15%). The experiments were done in the pipe test loops of the FPRC, CPUT [2]. Test pipe diameters ranged from Ø40 to Ø200 mm and nominal wall shear rates from a (practical) minimum of approximately 40 s^{-1} to the maximum attainable value in each test pipe (the maximum achieved was about 1000 s^{-1}).

Each rheological model was fitted to each set of laminar data and the suitability of each to characterise the material was ranked according to the unweighted RMSE. For transitional flow a single critical velocity was calculated for each pipe diameter using each technique and rheological model. Experimental transition velocities (V_c) were determined from the last observed laminar $(8V/D)_{exp}$ point and plotted against D. For turbulent flow, $(8V/D)_{calc}$ values were predicted for each experimental wall shear stress value, using each turbulent technique and the appropriate rheological model, plotted on diagrams of τ_w versus 8V/D and compared with the experimental data.

RESULTS

The study [2] generated a very large volume of results, but only a few representative results are given here. Figure 2 shows the laminar data and rheological model fits for a 6% kaolin suspension. Co-linearity of the laminar data from all pipe sizes is evident (within experimental error), and was observed similarly for all the pipe tests. For the ($8V/D$) range considered, in laminar flow there is little difference between the different model fits, as reported also in [5], [21] and [22]. Consequently the choice of rheological model has little influence on predicted pressure gradients in laminar flow.

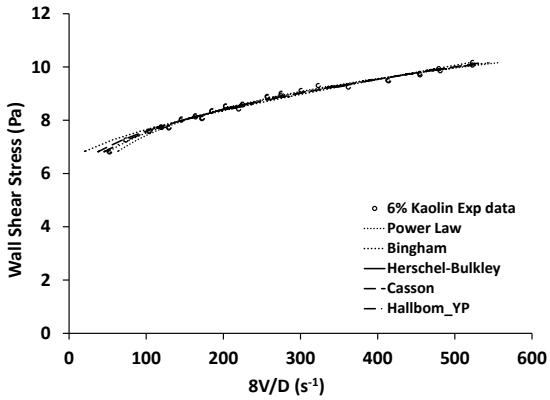

Model	Rheological Constants			RMSE
	τ_y	K	n	
Herschel-Bulkley	3.9	0.50230	0.361	13.9
Bingham Plastic	6.3	0.00443	-	19.6
Power Law	-	2.79710	0.182	14.8
	τ_C	η_C		
Casson	5.2	0.00083	-	14.9
	τ_0	μ_∞	k	
Hallbom_YP	4.4	0.00010	0.310	14.1
Hallbom_BP	6.3	0.00443	1	19.6
Hallbom_Casson	5.2	0.00083	0.5	14.9

Figure 2. Rheological model fits - 6% kaolin.

Figure 3 shows transitional velocity predictions using the the different rheologies in the Slatter [9] method. Whilst the trend of each prediction with increasing D is similar, it is clear that the rheology has a large influence on the magnitude of the calculated critical velocity.

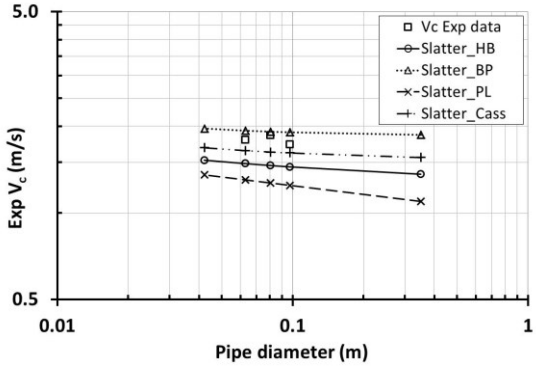

Diameter	Critical velocity (Exp) m/s	Vc Error values - SLATTER Re3			
		HB m/s	BP m/s	PL m/s	CASSON m/s
350mm		1.363	1.868	1.097	1.558
100mm	1.728	1.446	1.907	1.247	1.616
		-16.3%	10.3%	-27.8%	-6.5%
80mm	1.864	1.462	1.917	1.271	1.628
		-21.5%	2.9%	-31.8%	-12.6%
63mm	1.794	1.484	1.932	1.302	1.647
		-17.3%	7.7%	-27.4%	-8.2%
40mm		1.525	1.965	1.356	1.684
	Ave	-18.4%	7.0%	-29.0%	-9.1%

Figure 3. Transitional velocity predictions: all rheologies in Slatter technique – 6% kaolin.

Figure 4 gives the predicted critical velocities for this 6% kaolin in Ø63, Ø80 and Ø100mm pipes from all the methods using all of the rheology models. The wide discrepancy between the methods and the large errors for many of the predictions are obvious. Similar results were obtained for all the materials tested.

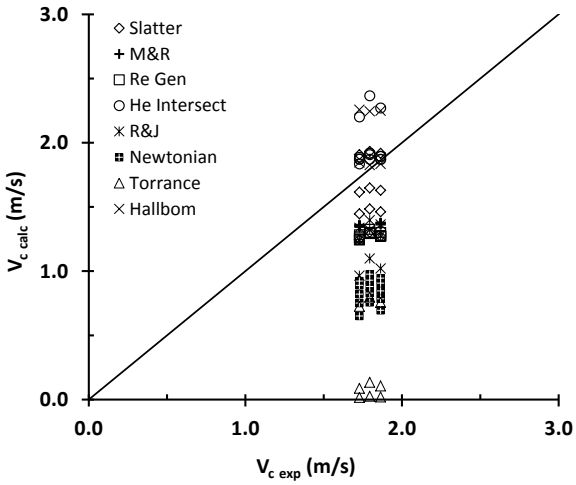

Figure 4. Transitional velocity predictions: all techniques using all rheologies - 6% kaolin in Ø63, Ø80 and Ø100mm pipes.

Figure 5 shows experimental and predicted turbulent flow curves for a 6% kaolin suspension using the Wilson & Thomas [16], Dodge & Metzner [18] and Slatter [9] methods with Herschel-Bulkley rheology. The Dodge & Metzner and Wilson & Thomas methods increasingly over-predict V with increasing D and wall shear stress. The Slatter technique agreed well with experimental results, especially in the lower turbulent shear stress range, and

did not display any obvious diameter effect. It tended to under-predict *V* with increasing wall shear stress.

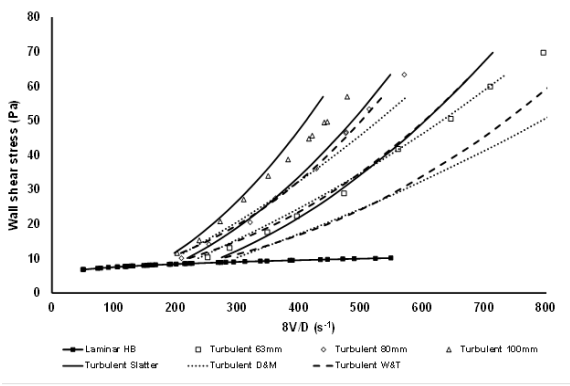

(8V/D) % Error values - Herschel-Bulkley			
Pipe diameter	W&T	D&M	SLATTER
63mm	15.4%	18.0%	6.4%
80mm	11.2%	12.0%	3.1%
100mm	7.8%	6.8%	3.2%
Ave	**11.5%**	**12.3%**	**4.2%**

Figure 5. Turbulent flow predictions using the Herschel-Bulkley model for pipe diameters Ø63, Ø80 and Ø100 mm - 6% kaolin.

Figure 6 repeats the data of Figure 5, but in this case the predictions were done using Casson rheology. As is evident these turbulent predictions are significantly better than those using the Herschel-Bulkley model.

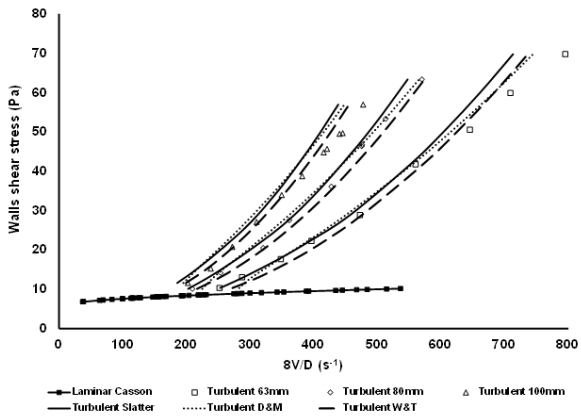

(8V/D) % Error values - Casson			
Pipe diameter	W&T	D&M	SLATTER
63mm	7.8%	6.1%	0.8%
80mm	3.0%	5.1%	3.8%
100mm	1.5%	6.2%	7.3%
Ave	**4.1%**	**5.8%**	**3.9%**

Figure 6. Turbulent flow predictions using the Casson model for pipe diameters Ø63, Ø80 and Ø100 mm - 6% kaolin.

NOMENCLATURE

BP	Bingham plastic
HB	Herschel-Bulkley

Latin symbols

D	Internal pipe diameter (m)
f	Friction factor (-)
K	Fluid consistency coefficient (Pa.s^n)
k	Scaling factor for yield plastic fluids (-)
L	Length of pipe or test section (m)
n	Flow behaviour index (-)
Q	Volumetric flow rate (m^3/s)
R	Pipe internal radius (m)
Re	Reynolds number (-)
u	Localised linear velocity at (r) value (m/s)
U_*	Shear velocity (m/s)
V	Velocity, mean velocity (m/s)

Greek symbols

α	Area ratio (-)
$\dot{\gamma}$	Shear rate (1/s)
ΔP	Differential pressure between 2 measuring points (Pa)
η_C	Casson plastic viscosity (Pa.s)
η_p	Bingham plastic viscosity (Pa.s)
μ'	Apparent viscosity = $\tau_w / \dot{\gamma}$ (Pa.s)
μ_∞	Infinite shear rate viscosity for yield plastic fluids (Pa.s)
ρ	Fluid density (kg/m^3)
τ	Shear stress (Pa)
Ω	Velocity profile blunting factor

Subscripts

C	Casson
c or crit	Critical
MR	Metzner-Reed
r	radial coordinate, roughness
w	Wall
y, 0	Yield
z	axial coordinate, in flow direction
85	85th percentile passing

CONCLUSIONS

For the fluids and (*8V/D*) range (~40 to 1000 s^{-1}) of this study, little difference existed in laminar flow pressure gradients calculated using the different rheological models. The rheological model which best reproduced laminar flow was the one that most correctly fitted the laminar flow data for a particular fluid. It was found though that the Casson model can confidently be used for any of the fluid types covered by this study.

Transitional and turbulent flow predictions too were generally better when using the rheological model most appropriate to the fluid type. It is important therefore to take care to correctly characterise fluids. Use of a different rheological model can significantly affect predictions (sometimes for the better), especially for viscoplastic fluids. The Casson model was mostly found to result in acceptably accurate predictions for all methods across all flow regimes, fluids and pipe sizes tested. This confirmed the view of Wilson & Addie [23] that the Casson model should not be overlooked.

REFERENCES

1. Chhabra, R.P. & Richardson, J.F. (2008) *Non-Newtonian flow and applied rheology*. Oxford: Butterworth-Heinemann.

2. Van den Heever, E.M. (2014) Rheological model influence on pipe flow predictions for homogeneous non-Newtonian fluids. Unpublished MTech dissertation, Cape Peninsula University of Technology, Cape Town

3. Van den Heever, E.M., Sutherland, A.P.N., Haldenwang, R. (2014) The influence of the rheological model used in pipe flow prediction techniques for homogeneous non-Newtonian fluids. Accepted for publication in ASCE Journal of Hydraulic Eng.

4. Hallbom, D.J. (2008) Pipe flow of homogeneous slurry. Unpublished PhD dissertation, University of British Columbia, Vancouver.

5. Heywood, N.I., Cheng, D.C.-H. (1984) Comparison of methods for predicting headloss in turbulent pipe-flow of non-Newtonian fluids. *Trans. Inst. M C*. 6 (1): 33-44..

6. Peixinho, J., Nouar, C., Desaubry, C., Theron, B. (2005) Laminar transitional and turbulent flow of yield stress fluid in a pipe. *Journal of Non-Newtonian Fluid Mechanics*, 128: 172-184.

7. Güzel, B., Burghelea, T., Frigaard, I.A., Martinez, D.M. (2009) Observation of laminar-turbulent transition of a yield stress fluid in Hagen-Poiseuille flow. *Journal of Fluid Mechanics*, 627: 97-128.

8. Frigaard, I.A., Nouar, C. (2003) On three dimensional linear stability of Poiseuille flow of Bingham fluids. *Physics of Fluids*, 15 (10): 2843-2851.

9. Slatter, P.T. (1994) Transitional and turbulent flow of non-Newtonian slurries. Unpublished PhD dissertation, University of Cape Town, Cape Town.

10. Metzner, A.B., Reed, J.C. (1955) Flow of Non-Newtonian fluids – correlations of the laminar, turbulent and transition flow regions. *A.I.Ch.E. Journal*, 1: 434-440.

11. Ryan, N.W., Johnson, M.M. (1959) Transition from laminar to turbulent flow in pipes. *A.I.Ch. E. Journal*, 5: 433-435.

12. Hedström, B.O.A. (1952) Flow of plastic materials in pipes. *Industrial Engineering and Chemistry*, 44 (3): 652-656.

13. Slatter, P.T., Wasp, E.J. (2000) The Laminar/ Turbulent transition in Large pipes. *10th international Conference on Transport and Sedimentation of Solid Particles*, Wroclaw, 4-7 September 2000: 389-399.

14. Wilson, K.C., Thomas, A.D. (2006) Analytic model of laminar-turbulent transition for Bingham plastics, *Canadian Journal of Chemical Engineering*, 84 (5): 520-526.

15. Torrance, B.McK. (1963) Friction Factors for Turbulent non-Newtonian Fluid Flow in Circular pipes. *The South African Mechanical Engineer*, 13 (4): 89-92, November.

16. Wilson, K., Thomas, A.D. (1985) A new analysis of the turbulent flow of non-Newtonian fluids. *The Canadian Journal of Chemical Engineering*, 63: 539-546.

17. Bowen, R.L. (1961) Designing Turbulent Flow Systems. *Chemical Engineering*, 68 (14): 143-150.

18. Dodge, D.W., Metzner, A.B. (1959) Turbulent flow of non-Newtonian systems. *AIChE Journal*, 5 (2): 198-204.

19. Brown, N.P., Heywood, N.I. (1991) *Slurry Handling: Design of Solid-Liquid systems*. Elsevier Science Publishers, England.

20. Skelland, A.H.P. (1967) *Non-Newtonian flow and heat transfer*, John Wiley and Sons Inc., New York.

21. Malkin, A., Masalova, I., Pavlovski, D., Slatter, P. (2004) Is the choice of flow curve fitting equation crucial for the estimation of pumping characteristics? *Applied Rheology*, 14 (2): 89-95.

22. Mullineux, G., Simmons, M. (2008) Influence of rheological model on the processing of yoghurt. *Journal of Food Engineering*, 84 (2): 250-257.

23. Wilson, K.C., Addie, G.R. (2002) Pipe-flow experiments with a sand-clay mixture. *15th International conference on the Hydraulic transport of Solids in Pipes*, Banff: 865-878.

YIELD STRESS AT THE PIPE INVERT AS A INDICATION OF STATIONARY VS SLIDING BED IN LAMINAR SLURRY FLOW

Peter Goosen*

*Paterson & Cooke, Sunrise Park, Prestige Drive, Ndabeni Cape Town, South Africa
E-mail: PeterG@PatersonCooke.com

INTRODUCTION

The term "slurry" in the mining and mineral processing industry refers to a solid / liquid mixture, with the solid phase being suspended in the liquid phase. The suspension of solids in the liquid (typically water or process liquor) generally facilitates some or other mineral recovery process (for example milling, sizing, leaching, flotation, etc). The way to move this mixture from one location or unit process to another is by pipeline, either pumped or flowing under gravity.

The characteristics of a slurry are predominantly dictated by the solids particle properties, which would include density, particle size, particle shape, and in the case of minerals such as clays, surface charge. In the case of slurries with a significant content of "fine" particles, the suspension of fine particles in the liquid phase effectively forms a pseudo-fluid, with modified density and viscous properties, generally exhibiting non-Newtonian behaviour. Typically, a particle size of 45 microns can be used to differentiate between "fine" and "coarse" (although there is no clear or absolute distinction). The coarse particles can then be considered to be carried in this non-Newtonian carrier fluid.

THE STATIONARY DEPOSIT VELOCITY

Slurry pipeline systems are most frequently designed to operate in the turbulent flow regime. Under turbulent flow conditions the turbulence maintains the solid phase in suspension, and thus moving through the pipeline. A certain minimum pipeline velocity is required to provide sufficient turbulent mixing intensity and momentum transfer to the solids to ensure reliable transport. Operation of a slurry pipeline at velocities below this minimum "deposition velocity" (even if the flow regime remains turbulent) results in the coarse solids falling out of suspension and accumulating in the pipeline to form a stationary "settled bed" of solids.

This deposition velocity is a function of solids properties, fluid properties and pipe diameter. The variation of deposition velocity with these parameters has been studied extensively and many formulations giving satisfactory predictions are found in the literature. Early work (from the 1950's onwards), focused on sand or gravel slurries in a Newtonian carrier fluid (water), for example, the work by Wilson [1]. More recently (1980's onwards) more attention was given to slurries in a non-Newtonian carrier fluid, for example the work by researchers at the Saskatchewan Research Council [2].

THE CHALLENGE OF LAMINAR FLOW

A challenge which is more and more frequently being encountered in the design of slurry pipeline systems in the mining and mineral processing industry is: Designing for slurries with a broad particle size distribution, non-Newtonian carrier fluid and in particular, pipelines operating in the **laminar flow regime**. The increasingly frequent occurrence of such systems is driven by a variety of factors, including developments in solid-liquid separation technology (primarily thickener design), developments in flocculants, economic and environmental pressures for increased water recovery from tailings streams, increased application of high-density or "paste" tailings disposal facilities, and increased application of paste mine backfill.

Since under laminar flow conditions there is no turbulence to maintain solids in suspension, another mechanism must be acting to result in the transport of the coarse solids fraction in these slurries. The initial thinking was that the slurry yield stress would be able to support the larger particles and prevent them from settling. This support of coarse particles in a yield stress fluid under **static** conditions can be easily observed (for example in a flask in the laboratory), and confirmed by simple analysis of forces acting on the particle [3]. However, it was later discovered that when the fluid is sheared (as would happen under pipe

flow conditions) the support offered by the yield stress is lost. This was discovered by some slurry pipeline system designers at significant cost (for example: The 262 km long, 530 mm diameter Belovo-Novosibirsk "stabilised" coal slurry pipeline as described by Aude et al [4].

In the light of laboratory scale tests and observations, it is understandable that this error could be made. In relatively small diameter test pipelines (in the order of 50 mm to 200 mm internal diameter) it is observed that the coarse particle fraction with a yield stress carrier fluid can be transported under laminar flow conditions, and at low pipeline velocities. There is thus an apparent discrepancy between what is observed at laboratory scale and in full scale (for example 530 mm for the above mentioned coal slurry pipeline). It is now fairly generally agreed, as described by Cooke [5] that this discrepancy is related to the pipeline friction pressure gradient. The thinking is as follows:

- In the smaller diameter (laboratory) test pipe, the coarse solids fraction does settle to the bottom of the pipe while the slurry is flowing. The resulting "bed" of settled solids then slides along the bottom of the pipe en bloc, being "pushed along" by the pressure gradient (pressure differential) acting on the settled bed cross-section. The sliding of the settled bed indicates that the driving force due to the pressure gradient has overcome the resisting force due to friction between the settled bed and the pipe wall.

- In the larger diameter (production) pipe, the pipeline pressure gradient is generally significantly lower than in the laboratory scale, since the pressure gradient is approximately inversely proportional the to pipe diameter. The friction force acting between the settled bed and the pipe wall is however approximately proportional to pipe diameter (based on geometric scaling).

- Considering scaling from laboratory scale to full-size, the force balance on the settled bed is changed, with the resisting force increasing approximately in proportion to the pipe diameter, and the driving force remaining approximately constant. This can explain the observed coarse solids transport at laboratory scale, but non-transport of coarse solids (and thus accumulation and potentially blockage) at production scale.

However, applying the assessment described above, predicts a significantly higher pressure gradient requirement for coarse solids transport than is observed in practice (both laboratory scale and full-scale). This paper now proposes a modification to the analysis:

PROPOSED ANALYSIS FOR BINGHAM PLASTIC SLURRIES

The modification of the force balance analysis now proposed is: **The force resisting sliding of the settled solids bed is evaluated by considering a yield stress acting between the settled bed and the pipe wall (as opposed to a solids – solids friction force as considered previously).** The outcome of the analysis is a prediction of whether the settled bed of solids formed under laminar pipe flow conditions will be stationary, or will be transported (sliding along the pipe invert).

With reference to Figure 1, the geometry of the pipeline flow with settled bed of solids can be defined in terms of the half-angle beta as indicated:

A_1 = cross-sectional area of flow area above the settled bed
A_2 = cross-sectional area of settled bed
L_1 = length of pipe perimeter bounding flow Area 1
L_2 = length of pipe perimeter bounding flow Area 2
L_{12} = cord length of the interface between Area 1 & Area 2

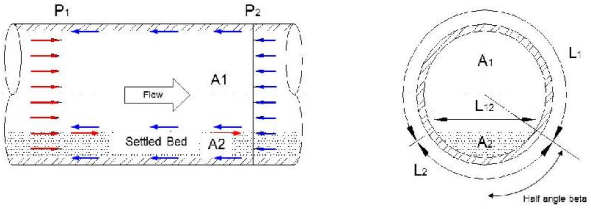

Figure 1: Definition Sketch for Force-Balance Analysis

To start the analysis for a particular flow rate being considered, Q_m, the settled bed is assumed to be stationary. We check by means of the analysis (set out below) whether this assumption is confirmed (a stationary bed condition), or shown to be an incorrect assumption (thus a sliding bed condition).

1) With the bed assumed to be stationary, all fluid and solids flow is occurring in Layer 1 above the bed. The depth of the bed is assumed to be established such that there is an equilibrium condition, with the flow velocity in area A_1 (above the bed) being just above the laminar / turbulent velocity (so that there is in fact turbulence here to achieve solids suspension and transport).

2) Conveniently, for a slurry with Bingham plastic fluid behaviour, the laminar / turbulent transition velocity, V_{trans}, can be estimated using the correlation of Slatter and Wasp, [6]:

$$V_{trans} = 26\sqrt{\frac{\tau_y}{\rho_m}}, \qquad (1)$$

where: τ_y = yield stress
ρ_m = slurry density.

2) The geometry (as per Figure 1) can now be determined if we use V_{trans} to approximate the velocity in area A_1:

$$A_1 = \frac{Q_m}{V_{trans}} \qquad (2)$$

$$A_2 = A - A_1 \qquad (3)$$

The pipeline pressure gradient is calculated (approximated) using the Buckingham equation, or by applying a turbulent flow model such as that developed by Wilson and Thomas [7], applying the relevant slurry properties with the following inputs:

- Considering the flow velocity in the upper layer = V_{trans}.
- An equivalent diameter for flow area A_1, given by:

$$D_{equ} = \frac{4 \times \text{flow area}}{\text{perimeter}} = \frac{4\,A_1}{L_1 + L_{12}} \qquad (4)$$

The wall shear stress, τ_1, acting around the perimeter of the upper layer, A_1, and the shear stress at the interface between the two layers, τ_{12}, (assumed to have the same value at the pipe wall and at the surface of the bed) is related to the pipeline pressure gradient. Using the relationship for pipeline (circular) geometry and the equivalent diameter calculated for flow area A_1:

$$\tau_1 = \frac{D_{equ}}{4} \times \frac{\Delta P}{\Delta L} = \tau_{12} \qquad (5)$$

The driving force acting on the bed due to the pressure gradient is calculated from the pressure gradient acting over the cross-sectional area of the bed, A_2 and the shear stress acting at the interface between the two layers, τ_{12}.

The **maximum** value of the force resisting the bed sliding is calculated from the yield stress, **evaluated for the slurry at the settled bed concentration**, acting over the bed / pipe interface area, L_2.

The driving and resisting forces are now compared, with the following possible outcomes:

- Driving force < maximum resisting force: The bed is stationary (as per the assumption for this analysis).
- Driving force > maximum resisting force: The bed will be sliding.

The analysis is repeated over a range of flow rates to identify the flow rate at which the transition from sliding to stationary bed occurs.

COMPARISON WITH OBSERVATIONS

The observations of stationary versus sliding bed of settled solids are presented in Figure 1 and Figure 2 in the form of a plot of pipeline velocity (vertical axis) versus slurry concentration (horizontal axis). Each plotted data point ("observed stationary deposition velocity data") indicates the velocity at which a stationary bed of solids is first noted on the invert of the pipe. These data have been visually observed in a recirculating test pipe loop with transparent observation pipe section. The slurry used in the tests is a gold tailings slurry, with a mean particle size of 40 microns, and top-size particles in the order of 300 microns.

The analysis shows a predicted switch from stationary settled bed in the laminar regime, to sliding settled bed (in the laminar flow regime) at a slurry concentration of approximately 35%v (concentration by volume). This is represented on the charts by the thick dashed line labelled "stationary deposition velocity prediction".

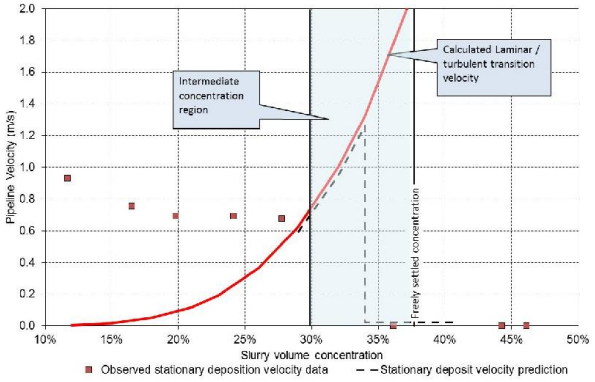

Figure 1. Stationary Deposition Velocity Prediction and Observations Comparison (100 mm Pipe Diameter)

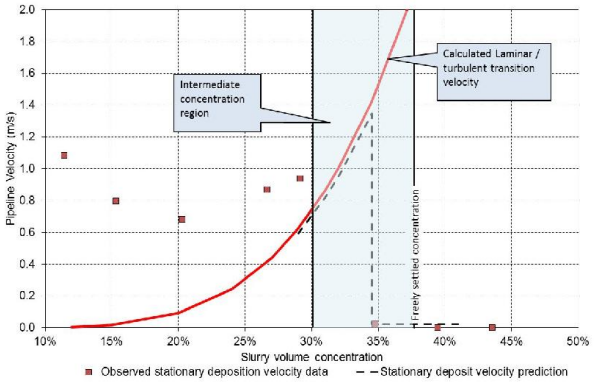

Figure 2. Stationary Deposition Velocity Prediction and Observations Comparison (152 mm Pipe Diameter)

Referring to the data presented in the two figures above:

- Figure 1 (100 mm pipe): The three data points at concentration > 35%v show operation in the laminar flow regime without a stationary bed (agreeing with the prediction).
- Figure 2 (152 mm pipe): Again, three data points at concentration > 35%v show operation in the laminar flow regime without a stationary bed (agreeing with the prediction).

CONCLUSIONS

The paper has presented an analysis of a settled solids bed in laminar slurry pipeline flow. The novel aspect of the analysis is the consideration of a yield stress acting at the interface between the settled bed and the pipe wall, as opposed to a shear stress due to solids friction.

Comparison of the analysis results against observed test data appears to support the proposed method, although more data is required in order to gain more confidence in the analysis.

REFERENCES

1. Wilson, K.C., 1976. A Unified Physically-Based Analysis of Solid-Liquid Pipeline Flow, Proc. 4th Int. Conf. on the Hydraulic Transport of Solids: Hydrotransport 4, pp. A1-1 to A1-16, Alberta, Canada.
2. Sanders, R.S., R. Sun, R.G. Gillies, M.J. McKibben, C. Litzenberger and C.A. Shook, 2004. Deposition Velocities for Particles of Intermediate Size in Turbulent Flow, Proc. 16th Int. Conf. on the Hydraulic Transport of Solids: Hydrotransport 16, Vol. II, pp. 417-428, Santiago, Chile.
3. Thomas, A.D., 1979. Pipelining of Coarse Coal as a Stabilized Slurry – Another Viewpoint, Proc. 4th Annual Conf. on Slurry Transportation, pp. 196-205, Las Vegas, USA.
4. Aude, T.C., R.H. Derammelaere and E.J. Wasp (1996) "Instability of Laminar Flow in Long Distance Pipelines and Solutions", Proc. Coal Utilisation & Fuel Systems 21st Int. Tech. Conf, Clearwater, Florida, USA.
5. Cooke, R., 2002. Laminar Flow Settling: The Potential for Unexpected Problems, Proc. 15th Int. Conf. on the Hydraulic Transport of Solids: Hydrotransport 15, Banff, Canada.
6. Slatter, P.T. and E.J. Wasp, 2000. The Laminar / Turbulent Transition in Large Pipes, Proc. 10th Int. Conf. on Transport and Sedimentation of Solid Particles, pp. 389-399, Wroclaw, Poland.
7. Wilson, K.C. and Thomas, A.D., 1985. A New Analysis of the Turbulent Flow of Non-Newtonian Liquids, Canadian Journal of Chemical Engineering, Vol. 63, Aug 1985, pp. 539-546.

A FULLY INTEGRATED AND COMMERCIAL IN-LINE FLUID CHARACTERIZATION SYSTEM FOR INDUSTRIAL APPLICATIONS

R. Kotzé*, J. Wiklund°, R. Haldenwang*

*Cape Peninsula University of Technology, PO Box 652, Cape Town, 8000,
°SIK – The Swedish Institute for Food and Biotechnoogy, PO Box 5401, Gothenburg
E-mail: kotzer@cput.ac.za

ABSTRACT

A new fully integrated ultrasound based in-line fluid characterization system "Flow-Viz™" has been developed especially for opaque, non-Newtonian industrial fluids. The new embedded and commercially available system is designed to meet industrial requirements. The system enables true non-invasive, real-time Doppler measurements and is able to visualize the flow and to rheologically characterize industrial fluids continuously while providing continuous feedback to an existing process control system for enhanced efficiency and productivity. The "Flow-Viz™" system consists of an operator's panel, a multi-touch monitor and an industrial PC unit and pulser-receiver electronics. The electronics has been improved and extended by adding a second ultrasound channel, augmenting the on-board data processing for obtaining the optimal performances in high attenuating suspensions. A new Motherboard provides an additional 8-channel digital and analog input and output capabilities for simultaneous data acquisition and connection to a process control system. The new electronics is combined with a non-invasive ultrasound sensor unit, which allows measuring the flow velocity profile even through industrial high grade stainless steel pipes. This unique solution makes possible to adapt the high resolution UVP+PD technique for industrial processes performed at high temperatures and/or pressures using a wide range of different industrial fluids. The new system is now commercially available and already installed in industry, e.g. for chocolate and grouting applications and an international patent has been filed.

INTRODUCTION

The enhanced tube viscometer concept aiming to derive information on the flow behavior of industrial fluids using the UVP+PD methodology, i.e. Ultrasound Velocity Profiling (UVP) with Pressure Difference (PD) is older than 30 years [1]. Despite this, no in-line fluids characterization instrument based on Doppler velocimetry has been made commercially available meeting industrial requirements [2]. In this work we present an embedded in-line fluids characterization system, "Flow-Viz™" has been specifically designed for the in-line velocity profile measurements and rheological assessment of opaque, non-Newtonian industrial fluids. The new system is the result of the work of several research groups that have systematically improved this concept for a period of more than 14 years to ensure that the system can be used in industry for a quantitative analysis of the rheological properties of real industrial fluids, see [2-5]. New improved and extended UVP+PD electronics, based on former work [6-8] have been developed. In industrial processes it is an absolute requirement to measure non-invasively through stainless steel pipes. Despite this, no such transducer technology has been made commercially available [2,5]. To overcome this limitation, new non-invasive sensor technology has been developed, optimized and validated for SS316L stainless steel process pipes of different diameters and wall thicknesses [2,5]. The instrument has been validated to meet industrial requirements for many different applications and to deliver accurate real-time data, such as instantaneous velocity profiles and rheology of opaque industrial fluids [2-4, 7-8]. The Flow-Viz™ system is already installed in industry, e.g. for chocolate and grouting applications.

THE FLOW-VIZ™ IN-LINE FLUIDS CHARACTERIZATION SYSTEM

The system consists of three main components:

1. Operator's panel
2. Sensor unit
3. Software

Operator's panel

The operator's panel houses the newly developed digital "Flow-Viz™" hardware platform; the pulser-receiver and data acquisition (DAQ) electronics, power supply, a 19"-multi-touch monitor, a sensor connector block and an industrial PC unit. The built-in 19"- monitor offers a user-friendly interface with multi-touch gesture navigation.

Figure 1. The operator's panel featuring the electronics, main Industrial PC unit, sensor block and multi-touch monitor.

Sensor unit

The industrial grade sensor unit is installed in the process piping network and makes up the measuring section. It comprises a stainless steel cabinet protecting the heat-jacketed stainless steel pipe with diameters ranging from 10 mm ID up to 165 mm ID (or larger). The measuring section is equipped with a pair of custom developed non-invasive transducer assemblies, a differential pressure sensor with remote seals (ABB Automation Technology Products AB, Sollentuna, Sweden) and a non-invasive PT-100 sensor (Pentronic, Gunnebo, Sweden), Figure 2.

Figure 2. The industrially approved sensor unit featuring the unique custom made non-invasive transducer assembly.

To meet industrial requirements, a new non-invasive 0.7-7 MHz sensor unit technology has been developed, optimized and validated for SS316L stainless steel pipes of different diameters and wall thicknesses [2, 5]. The non-invasive sensor unit, shown in Figure 2, is the only sensor solution that allows true non- invasive velocity profile measurements in highly attenuating suspensions through stainless steel wall materials.

Software and signal processing

The system comes with a user-friendly GUI software interface optimized for the multi- touch gesture monitor. The software is used for setting the parameters (of which most are automated), controlling the data acquisition, signal-processing and for visualization and export of the data. The data is stored in an SQL database. An output screen sample is shown in Figure 3.

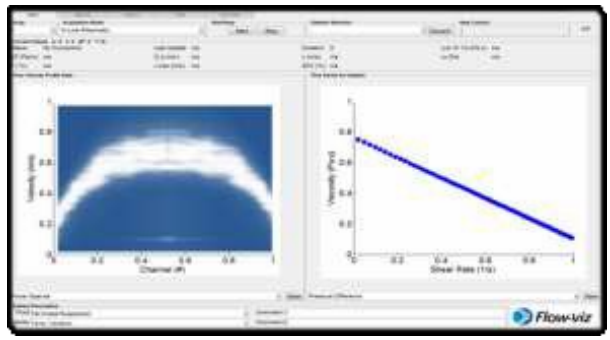

Figure 3. The GUI software interface.

The Flow-Viz™ system and software allows velocity estimation using several algorithms: FFT, time-domain, spectral, etc. that can be used simultaneously to improve the measurement accuracy under industrial process conditions. By using FFT, the velocity profile is typically estimated through a weighted mean of the Doppler power spectra from each depth. The non- invasive sensor unit and new improved electronics makes it possible to obtain the full profile over the complete pipe diameter, depending on the fluid characteristics. It also allows measurements of velocity data close to pipe walls, which is critical for accurate fluid characterization. The application of a model-fitting approach for the rheological characterization has been demonstrated to be not so robust for industrial applications due to several reasons [2-3, 8]. Therefore, an alternative method was developed in which the shear viscosities as function of shear rates are determined directly from the measured velocity profile and pressure drop data. The yield stress is automatically determined from the plug radius. The Flow-Viz™ direct non-model approach has been verified to be both more robust and accurate as it can capture e.g. a Newtonian plateau [2].

APPLICATION EXAMPLES

Ketchup

Figure 4 shows a typical example of a spectral profile of industrial fluid, ketchup, measured non-invasively through an SS316L stainless steel pipe with an inner diameter of 51mm.

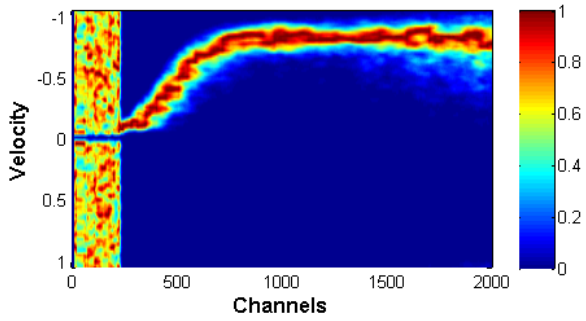

Figure 4. Spectral profile of an industrial fluid, ketchup, measured at a volumetric flow rate of 56 L/min.

The x-axis (Channels) represents measurement positions and can be converted into distance. Close to the sensor noise was measured due to no fluid flow being present within the sensor setup and pipe wall. Around channel number 220 (pipe wall position), fluid flow can be seen by observing the velocity profile gradient. The centre of the pipe (radius) is situated at channel 1200. A plug was measured, which extends all the way to the far side of the profile. Theoretically the velocities of the profile close to the opposite pipe wall should decrease; however, due to multiple ultrasonic reflections from the pipe wall an imaginary plug flow is measured. Only data between the near pipe wall and radius position is used for determining the rheology. Having access to the Doppler spectra offers several advantages. Information about the measurement confidence is directly available when viewing the spectrum. For example, signal artifacts and noise can influence Doppler measurements negatively and this can be easily revealed by plotting the Doppler spectrum. This particular Doppler spectrum shows that a good penetration depth was possible (no significant energy losses and noise present) and that no signal artifacts were present (e.g. no prominent spikes in the measured profile). Different velocity estimation algorithms can be used in order to extract the profile for determining the shear rate distribution in the pipe.

Figure 5 shows a flow curve measured using the new system (5.3 l/min, maximum shear rate 10 1/s). Good agreement was found when comparing the result obtained using the off-line rheometer (TA Instruments ARES-G2).

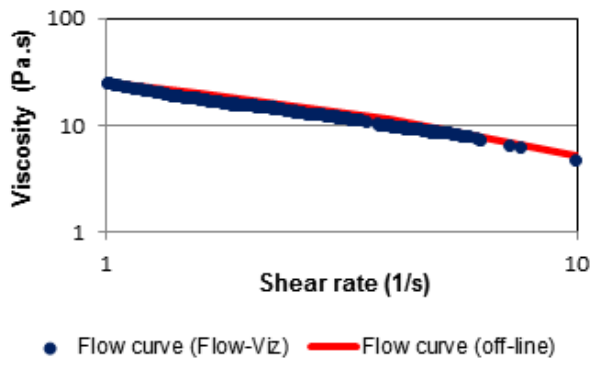

Figure 5. Flow curves measured for ketchup. The red line represents the result obtained from the off-line rheometer.

Wastewater sludge

During 2014 wastewater sludges were tested using the Flow-Viz system and comparing these with the results obtained with a tube viscometer. The portable tube viscometer consists of three tubes with diameters from 28-63 mm [10]. Figure 6 shows a velocity profile measured at solids concentration of 3.94% and a flow rate of 5.9 l/s (laminar flow) in a 51 mm high grade stainless steel pipe fitted to the tube viscometer rig.

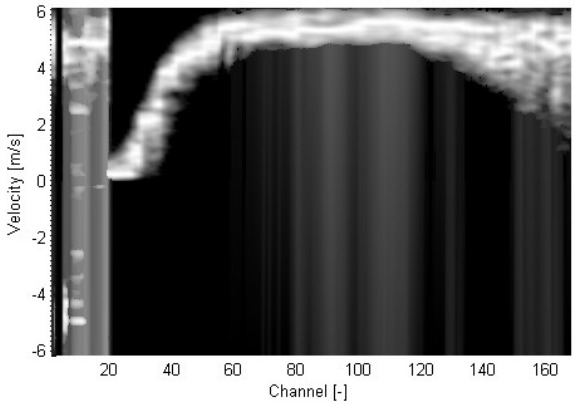

Figure 6. Velocity profile measurement in wastewater (solids concentration 3.94%) at 5.9 l/s.

The velocity profile clearly shows that a yield stress (plug-flow) is present. Figure 7 compares results obtained using the new instrument and conventional tube viscometry. The maximum difference between the values obtained by the tube viscometer and the Flow-Viz system for yield stress is 6% and for the viscosity 12% - see fitted equations, Figure 7.

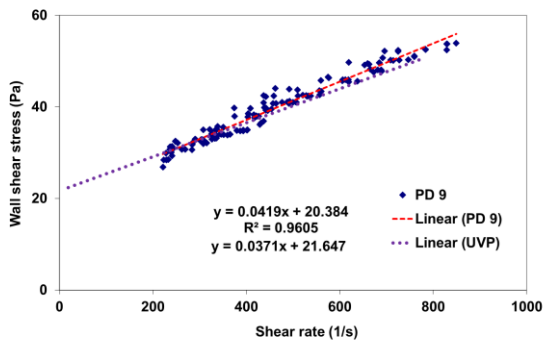

Figure 7. Potsdam secondary sludge 9 Comparison of rheology- UVP with tube viscometer

The comparison is very good especially since the tube viscometry takes 30-60 minutes to complete whereas the Flow-Viz measurement is taken over a very short time at one flow rate. The rheology done this way is therefore of much more use as it is an instantaneous flow characterisation. The feasibility of using this novel system for measuring the rheology of sludges in-line has been proven. This has huge potential for optimisation of polymer dosing if one can link the rheological parameters of the sludge to the optimum polymer concentration.

SUMMARY

A new fully integrated ultrasound based in-line fluid characterization system for industrial applications has been developed and validated under real industrial process conditions over the past 14 years. The commercial version of the Flow-Viz™ system features upgraded electronics combined with novel non-invasive sensor technology allowing true in-line flow visualization and rheological characterization of opaque, non- Newtonian industrial fluids flowing in industrial grade stainless steel pipes. An international patent has been filed and the Flow-Viz™ system has already been successfully installed in Europe and USA within large international companies. It has been successfully applied to a wide range of industrial applications, e.g. oil, petroleum, food, minerals, chocolate, explosive emulsions, pharmaceutical industry.

REFERENCES

1. Kowalewski, T.A. (1980) Velocity profiles of suspension flowing through a tube. Archiv. Mech. 32: 857-865.

2. Wiklund, J., Kotzé, R., Haldenwang, R., Stading, M. (2012) Development of an industrial UVP+PD based rheometer - optimisation of UVP system and transducer technology, Proceedings ISUD8, pp. 49-52.

3. Wiklund, J., Shahram, I., Stading, M. (2007) Methodology for in-line rheology by ultrasound Doppler velocity profiling and pressure difference techniques, Chem. Eng. Sci. 62: 4159-4500.

4. Wiklund, J., Stading, M. (2008) Application of in-line ultrasound Doppler based UVP-PD method to concentrated model and industrial suspensions, Flow Meas. Instrum. 19: 171-179.

5. Kotzé, R., Wiklund, J., Haldenwang, R. (2013) Optimisation of Pulsed Ultrasonic Velocimetry and Transducer Technology for Industrial Applications, Ultrasonics 53: 459-469.

6. Ricci, S., Boni, E., Guidi, F., Morganti, T., Tortoli, P. (2006) A programmable real-time system for development and test of new ultrasound investigation methods. IEEE Transactions on Ultrasonics, Ferroelectrics, and Frequency Control 53: 1813-1819.

7. Ricci, S., Liard, M., Birkhofer, B.H., Lootens, D., Brühwiler, A., Tortoli, P. (2012) Embedded Doppler system for industrial in- line rheometry. IEEE Transactions on Ultrasonics, Ferroelectrics, and Frequency Control 59: 1395-1401.

8. Birkhofer, B., Debacker, A., Russo, S., Ricci, S., Lootens, D. (2012) In-Line Rheometry Based on Ultrasonic Velocity Profiles: Comparison of Data Processing Methods. Appl. Rheol. 22(4): 44701-1-9.

9. Kotze, R., Ricci, S., Wiklund, J. (2014) Performance tests of a new non-invasive sensor unit and ultrasound electronics. Proceedings ISUD9.

10. Haldenwang, R., Fester, V., Sutherland, A., Holm, R., Du Toit, R. (2010) Design construction, commissioning and testing of a portable tube viscometer and pump rig. Hydrotransport 18. Rio De Janeiro, Brazil, pp. 287-298.

AN INVESTIGATION OF THE NATURE OF THE EFFECTS CAUSING MECHANICAL SENSITIZER PUMPING PROPERTIES VARIATION

E. Kharatyan, P.Halliday, L. Wilson

AEL Mining Services, AEL Research ans Development Department, Ardeer Road, Pinelands Office Park, Building N7 Pinelands, Modderfontein, E-mail: Ellina.Kharatyan@aelms.com

INTRODUCTION

Conventionally, emulsion matrices need to be sensitized to become detonable explosives. This is done either chemically or mechanically. Both methods have their advantages and disadvantages. Mechanical sensitization involves the addition of microspheres (plastic or glass) to the emulsion matrix in order to create hot spots. This type of sensitization can only be done at the emulsion explosives (EE) manufacturing sites. This means that a sensitized 1.1 type explosive material needs to be handled, transported and stored (according to strict regulations stipulated in the Explosive Act). Chemical sensitization allows for the storage, handling and transportation of only 5.1 type products (oxidizer) rather than the 1.1 type explosive, as is the case with mechanical sensitization. Chemical sensitization involves the addition of a small amount of a chemical that reacts with a component of the emulsion matrix, causing the formation of gas bubbles that act as hot spots. The disadvantage of this method is the lack of accurate density control, due to various factors affecting the reaction as well as the operator's lack of comprehensive understanding of the reaction. This could easily result in poor blast performance. Due to these disadvantages a pumpable, non-detonable (5.1 type), mechanical sensitizer was researched and developed. This product should allow for pumping at a 50:50 volume ratio with the emulsion matrix, when loading into blast holes. It is important that this "non-detonable" mechanical sensitizer can be pumped at a prescribed ratio irrespective of the ambient conditions.

It was discovered that the pumping properties of this mechanical sensitizer changed after 6 months of ageing. The nature of such changes was not understood and as such required further investigation

MATERIALS AND METHODS

Materials

A mechanical sensitizer was the main object of the investigation. It consists of an emulsion matrix with the added Expancel® plastic microspheres. The formulation must remain "non-detonable" as per UN test series (8 a-c). The water-in-oil highly concentrated emulsion was used as the emulsion matrix. Such emulsions have been described in detail elsewhere [1-5]. The dispersed phase droplets consist of an ammonium and/or metal nitrate solution. The continuous phase contains standard industrial fuels with dissolved surfactants.

The mechanical sensitizer sample manufactured at AEL Mining Services and the emulsion matrix sample, classified as bagged underground range emulsion (manufactured at the Central Bulk Emulsion Plant), were used for this investigation.

Methods

The droplet size distribution was measured using a Malvern Mastersizer 2000. The procedure is based on the sample dispersion under software control and the measurement of angle dependence of the intensity of scattering of a collimated He-Ne laser beam. The particle size distribution calculations are based on the rigorous Mie theory and using the standard software applied to the instrument. The sample was diluted in Excol D60 oil just before the measurements were carried out.

The basic rheological measurements were carried out with the use of a rotational dynamic rheometer MCR 301 (Paar Physica). The geometry of the measuring unit was "bob-in-cup" (coaxial cylinder with conical base to the bob) with a sandblasted bob surface. The bob diameter was 27 mm and the gap distance between the cup and the bob was 1 mm. One regime of deformation was used: steady state flow measuring flow curves (viscosity versus shear rate). All the rheological measurements were conducted at 15, 20, 30 and 40^{o}C.

Microscopy was performed using the OLYMPUS BX41 polarized microscope at 100x magnification (lens + camera).

RESULTS AND DISCUSSION

A mechanical sensitizer was designed to be pumped separately but simultaneously with an emulsion matrix at a 50/50 volume ratio to produce a final product with a prescribed density. Pumping of the materials at 50/50 volume ratio requires the viscosity of both components to be similar in the used pumping region. It was observed that at times this volume 50/50 ratio was not

maintained, resulting in a final product density that was not favourable. It was noted that viscosity of the sensitizer had increased. A fuel (Ash-H) was added to the sensitizer to adjust the viscosity to the target level. This was however only a temporary solution to the problem. A more effective and long term solution was required.

A few reasons were defined to explain this thickening phenomena of the mechanical sensitizer:

- The settling of the microspheres during storage
- Structure formation due to microsphere aggregation
- Crystallization of the mechanical sensitizer
- The effect of temperature on the viscosity of the mechanical sensitizer

All the above reasons were investigated.

The flow behaviour of fresh and aged mechanical sensitizer was measured (Figure 1). From Figure 1 it can be noted that both flow curves follow the same trend. Both samples can therefore be considered as being similar.

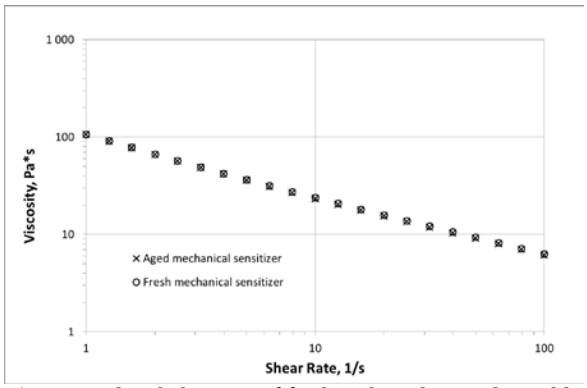

Figure 1. Flow behaviour of fresh and aged "non-detonable" pumpable mechanical sensitizer.

The plastic Expancel® microspheres can reduce the density of a liquid without a dramatic increase of viscosity when compared to glass or ceramic spheres, as described in Expancel® technical information brochure [6]. Based on the microspheres supplier's information, the microballoons are treated to avoid agglomeration or, in other words, aggregates formation. Samples of aged and diluted (with Ash-H to decrease the viscosity) mechanical sensitizer were investigated under the microscope (Figure 2).

Figure 2 clearly indicates that there is very little or no agglomeration of the microspheres. As is evident from Figure 2, the reduction in viscosity was achieved by increasing the distance between the microspheres in the mechanical sensitizer.

There are no crystals visible in the mechanical sensitizer and hence crystallization of the product can be ruled out (see Figure 2).

In order to simulate the effect of temperature on the flow properties of the "non-detonable" pumpable mechanical sensitizer, flow curves of the sensitizer were generated at different temperatures (Figure 3). This particular temperature range was chosen in order to reproduce real conditions: ambient winter/summer temperature range between 15-40^{o}C.

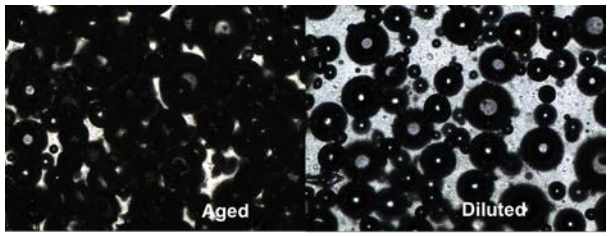

Figure 2. "Non-detonable" pumpable mechanical sensitizer samples under microscope: left –aged sample; right – diluted sample. Magnification 100x.

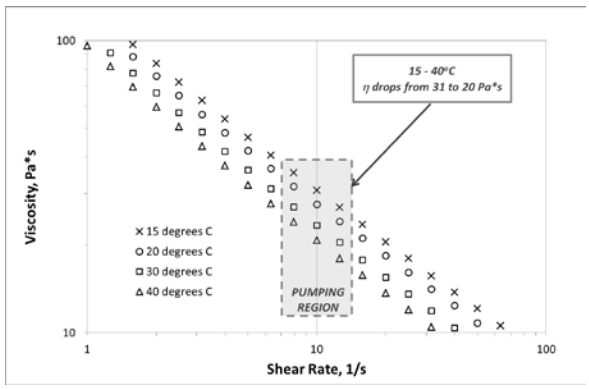

Figure 3. Effect of temperature on flow behaviour of "non-detonable" pumpable mechanical sensitizer.

The pumping region relates to a shear rate of +/- 10s^{-1}. As can be seen from Figure 3, the viscosity drops from 31 KcP to 20 KcP in the pumping region when the temperature increased from 15 to 40^{o}C.

The flow curves of the underground grade emulsion matrix (second component of the final product) as a function of temperature were also generated. In the pumping region, when the temperature ranges from 15 to 40^{o}C , the viscosity of the emulsion matrix changes from 19 to 21 kcP (see Figure 4). This change can be considered as negligible.

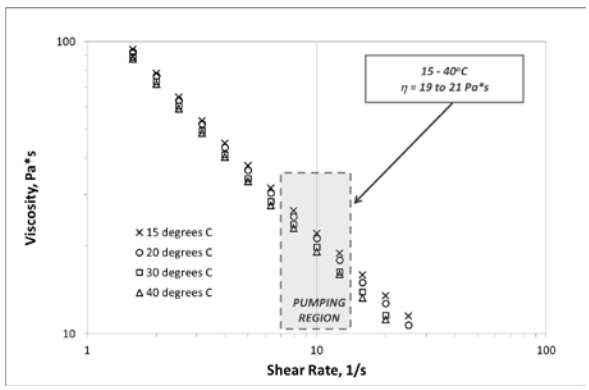

Figure 4. Effect of temperature on flow behaviour of emulsion matrix.

As was mentioned previously, in order to pump the mechanical sensitizer and the emulsion matrix at the same volume rate, the viscosity of both components needs to be similar in pumping region used. Flow curves of the diluted mechanical sensitizer, and the emulsion matrix were compared (Figure 5).

In the pumping region, the viscosity of the emulsion matrix and the mechanical sensitizer are similar at 40^{o}C. Therefore, it is optimal to pump the

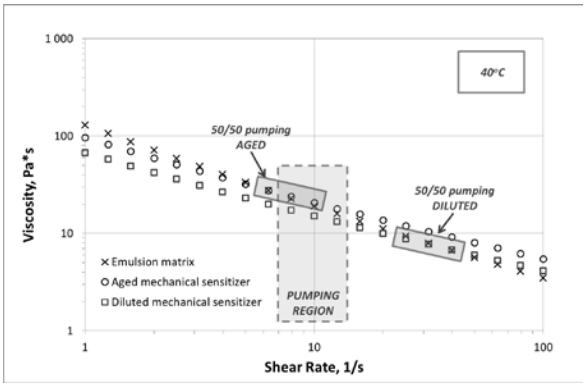

Figure 5. Comparison of viscosities of the emulsion matrix and the "non-detonable" mechanical sensitizer at 40°C (summer ambient conditions): crosses –emulsion matrix; circles – aged "non-detonable" mechanical sensitizer; squares – diluted "non-detonable" mechanical sensitizer.

mechanical sensitizer at the same volumetric flow rate as the emulsion matrix at 40°C. Whereas when the sensitizer is diluted with Ash-H, these conditions are not optimal. The diluted sensitizer has a viscosity similar (viscosities cross point) to that of the emulsion matrix at higher shear rates or at a higher pump speed/pressure.

When the flow behaviour of these materials are compared at 15°C (see Figure 6), it can be noted that the diluted mechanical sensitizer is optimally pumped at 50/50 volume ratio with emulsion at this particular temperature. However, the optimal viscosity region of the aged mechanical sensitizer is shifted to a lower shear rate region or to a lower pump speed/pressure, at this temperature.

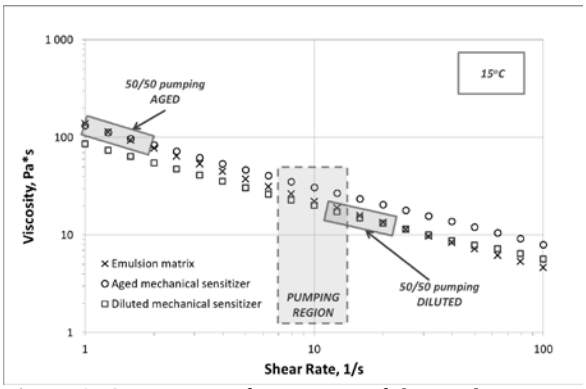

Figure 6. Comparison of viscosities of the emulsion matrix and mechanical sensitizer at 15°C (Winter conditions at South Africa): crosses –emulsion matrix; circles –aged "non-detonable" mechanical sensitizer; squares – diluted "non-detonable" mechanical sensitizer.

Based on the above results it can be suggested that the pump speed/pressure should be able to be adjusted to a wide range of speeds/pressures in order to be able to pump the mechanical sensitiser and emulsion matrix at the same volumetric flow rate at different ambient temperatures. This was however not achieved with the currrent sensitizer formulation. Therefore, a modified mechanical sensitizer formulation was required. The viscosity dependance on temperature of the new mechanical sensitizer needs to be minimized.

The Research and Development Department of AEL Mining Services was able to design a new

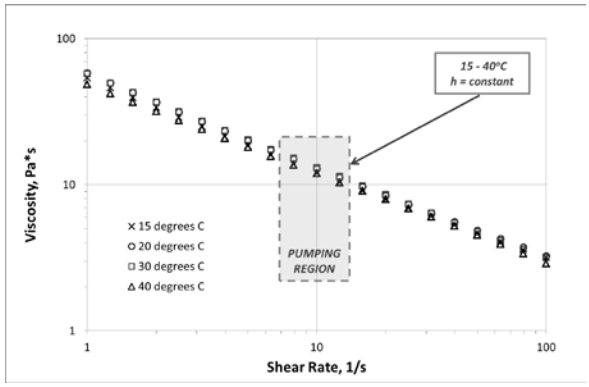

Figure 7. Effect of temperature on flow behaviour of modified "non-detonable" mechanical sensitizer.

formulation of a mechanical sensitizer. It was proved that the temperature had little or no effect on the flow properties of the modified sensitizer in the pumping region (Figure 7).

CONCLUSIONS

The flow properties behaviour of aged mechanical sensitiser is associated with the temperature dependence on viscosity. The mechanical sensitiser composition has a significant effect on optimizing the pumping requirements.

ACKNOWLEDGEMENT

The authors would like to gratefully acknowledge AEL Mining Services, the company which provided the financial support and permission to publish the results of these studies.

REFERENCES

1. Masalova, I., Malkin, Ya, A. (2008) Colloid J. 70 (3): 362-371.
2. Foudazi, R., Masalov, I., Malkin, Ya, A. (2010) Colloid J., 72 (1): 74-92.
3. Masalova, I., Foudazi, R., Malkin, Ya, A. (2011) Colloids and Surfaces A: Physicochem. Eng. Aspects, 375: 76–86.
4. Malkin, A. Ya, Masalova, I., Slatter, P., Wilson, K. (2004) Rheol. Acta, 43 (6): 584-591.
5. Masalova, I., Taylor, M., Kharatiyan, E., Malkin, Ya, A. (2005) J. Rheol., 49 (4): 839-849.
6. "Properties of dry expanded Expancel® Microspheres" technical information brochure

THE EFFECT OF DIFFERENT PPC BINDERS, PARTIALLY REPLACED BY FLY ASH AND SLAG ON THE PROPERTIES OF SELF-COMPACTING CONCRETE

O. Almuwbber, R. Haldenwang, I. Masalova

Deptartment of Civil Engineering and Survey, Cape Peninsula University of Technology
Email: omarlby17@yahoo.com

ABSTRACT

The effect of different CEM1 52N cements produced at different factories on Self-Compacting Concrete (SCC) is currenty not well understood. The effect of four cements tested and two superplasticisers (SPs) partially replaced with two types of fly ash and slag on an SCC mix were studied. Mix design and tests were done according to the European Specification and Guidelines for Self Compacting Concrete (2005). The SPs reacted differently with addition of the SPs and partial replacement of fly ash and slag. Although the differences can be distinguished from the SCC tests it is not yet understood what causes these differences.

INTRODUCTION.

SCC is a special type of concrete that can settle into heavily reinforced, deep and narrow sections by its own weight, can consolidate itself without necessitating internal or external vibration and can keep its cohesion (stability) without leading to segregation and bleeding [1]. SCC was developed in the 1980's in Japan and has since become widely used all over the world. It has been hailed as a really novel development. The development in superplasticizer technology has greatly contributed to the formation and improvement of SCC [2–4]. Super-plasticisers are essential in SCC mixes and in order to avoid separation of large particles in SCC, pozzolanic admixtures or fillers are used to increase the viscosity [5]. SCC demands a large amount of powder content compared to conventional vibrated concrete to produce a homogeneous and cohesive mix [6]. It was reported that SCC often contains powder in the order of 450–600 kg/m^3 of concrete [7]. Due to its rheological requirements, fillers (both reactive and inert) are commonly used in SCC to improve and maintain the workability, to regulate the cement content and to reduce the heat of hydration. Part of this powder content can be effectively replaced by mineral admixtures like fly ash and slag.

Even though SCC consists basically of the same components as normal vibrated concrete, there are distinct differences in the concrete composition in order to achieve the desired ''self-compacting properties''.

On the one hand, SCC has to reach a high segregation resistance and on the other hand a high deformability. Therefore, the content of ultra fine materials in SCC is essentially higher [8].

One of the disadvantages of SCC is its cost, associated with the use of chemical admixtures and use of high volumes of cement. One alternative to reduce the cost of SCC is the use of mineral admixtures such as fly ash and slag.

The use of fly ash and slag provides benefits in the production of SCC such as reduction in the water requirements with increased workability and increased strength at later ages of curing, which cannot be achieved through the use of additional cement.

It is also known that fly ash and slag increase the workability, durability and long-term properties of SCC [9].

MATERIAL AND EXPERIMENTAL STUDY

Materials

Four types of Ordinary Portland cement were used in this study and produced in different PPC factories according to the European Standards EN-197/1 and labelled as CEM I 52.5 N. The maximum size of coarse aggregate was selected as 13 mm in order to avoid any blocking effect. The fine aggregate was Malmesbury sand which is a river sand with a good grading. Cyclone dust was used as a viscosity modifiyng filler in the mix. The mix design was for a 28 day 50 MPa compressive strength, according to European Standards EN-196/1.

Tables 1-3 depict the chemical and physical properties of the cements and SPs used in this study.

Mix proportions

One control and several mixes with mineral admixtures were prepared and tested to quantify the properties of SCC. In some of the mixes, cement was replaced with two types of fly ash and one type of slag at the same contents of 10%, 20%,

Table 1. Chemical Properties of cements

Chemical components	Destination of the cement samples			
	C1	C2	C3	C4
SiO_2 (%)	20.15	20.7	19.4	21.7
Al_2O_3 (%)	3.82	4.37	3.59	4.95
Fe_2O_3 (%)	3.22	2.45	2.93	2.99
Mn_2O_3 (%)	0.09	0.81	0.75	0.49
TiO_2(%)	0.22	0.33	0.32	0.42
CaO(%)	63.37	63.7	61.7	60.9
MgO(%)	1.13	3.58	4.26	2.17
P_2O_5(%)	0.14	0.08	0.02	0.1
Wet SO_3(%)	2.1	2.27	2.13	3.4
Wet Cl(%)	0.004	0.01	0.01	0.004
K_2O(%)	0.62	0.52	0.29	0.34
Na_2O(%)	0.99	0.16	0.14	0.18
LOI(%)	3	1.57	5.13	2.01
Total(%)	98.9	100.5	100.6	99.6
FCaO(%)	1.06	0.75	0.83	3.25
IR(%)	-	0.78	1.98	-
Cl (ppm)	-	106	106	-

Table 2. Physical properties of cements

Physical properties	Destination of the cement samples			
	C1	C2	C3	C 4
Relative density	3.05	3.03	3.04	2.99
Specific surface, cm^2/g	3750	3650	4250	3850
consistence, %	25	31	25	33
Initial set, min	170	180	190	315
Final Set, h	3.25	3.75	3.75	6
45 μm residue, %	11.7	0.6	3.9	1.8
90 μm residue %	1.1	0	0.5	0.1
212 μm residue, %	0.2	0	0	0

Table 3. SP characteristics

Characteristics	Destination of super-plasticizers	
	SP1	SP2
Consistency	Liquid	Liquid
Colour	Amber	Brown-green
Density according to ISO 758 (g/cm^3)	1.07	1.05
	± 0.02	± 0.02
Dry content according to EN 480-8 (%)	26	20.3
	± 1.3	± 1
Chlorides soluble in water according to EN 480-10 (%)	< 0.1	≤ 0.1
Alkali content (Na_2O equivalent) according to EN 480-12 (%)	< 2.5	≤ 1

30% and 40% for the fly ash and 30%, 40%, 50%, 60% and 70% for slag, all by mass. After some preliminary investigations, the water–cement ratio (w/c) was selected as 0.45 and the cement content was fixed at 418 kg/m^3. Two different new generation superplasticisers are the following: the first type (SP1) is an admixture with superior performance when compared with traditional naphthalene-sulphonate or melamine-sulphonate based superplasticisers and first generation acrylic admixture in terms of both water reduction and slump retention. The second (SP2), is a new generation polymer based on modified propionates.

Casting, curing and testing

For each mixture, six 100 mm x 100 mm x 100 mm cube moulds were prepared to determine the 7 and 28 day compressive strength. The slump-flow test, T50 test, L-box test and segregation test were conducted to characterise the workability of the fresh concrete and to determine the filling and passing abilities as well as the segregation ratio. During the slump-flow test, the required time for the SCC to reach 500 mm length, slump-flow radius (T50) and the final diameter of the concrete flow circle in two directions were measured. In the L-box test, the test was started by lifting the control gate to allow the flow of SCC through the re-bars into the horizontal part of the L-box. When the flow of fresh SCC stopped, the heights of the concrete at the end (h_2) and the beginning (h_1) of the horizontal section were measured. The blocking ratio was calculated as the ratio ''h_2/h_1''. Specimen cubes were then cast in plastic moulds and were not subjected to any compaction other than their own self-weight. The specimens were kept covered in a controlled chamber at 20 ± 2˚C for 24 hours until demolding. Thereafter, specimens were placed in water pre-saturated with lime at 20˚C. Hardened concrete testing was conducted after 7 and 28 days.

Result and discussion

Figure 1 presents the slump flow and T50 results, which are related to viscosity, for different cements with two different SPs.

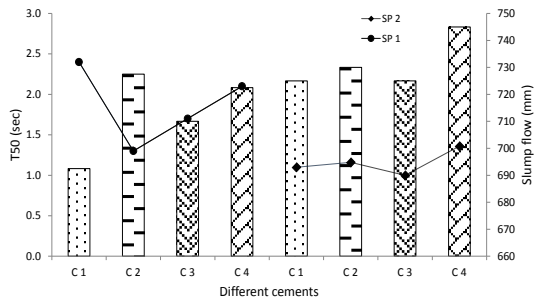

Figure 1. Slump-flow and T50 time of SCC mixes with 4 different cements and two SP's**.**

In terms of slump flow, all optimised SCC mixes exhibited satisfactory slump flows in the range of 640–800 mm, which is an indication of a good flowability. With SP1, C2 and C4 produced higher whilst C1 and C3 produced lower slump-flow values. However with SP2, C2 and C3 produced higher whilst C1 and C2 produced lower slump-flow values.

Figures 2 and 3 show the slump flow and V-funnel results for SP1 and SP2 respectively.

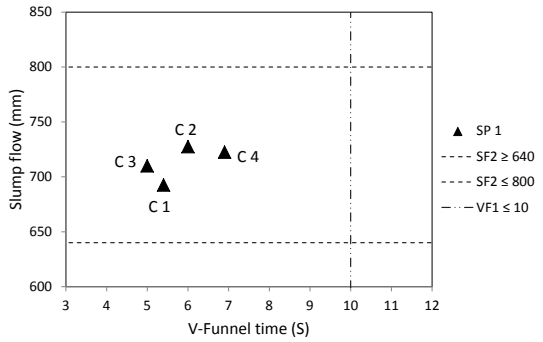

Figure 2. Slump flow results relative to V-funnel results for SP1.

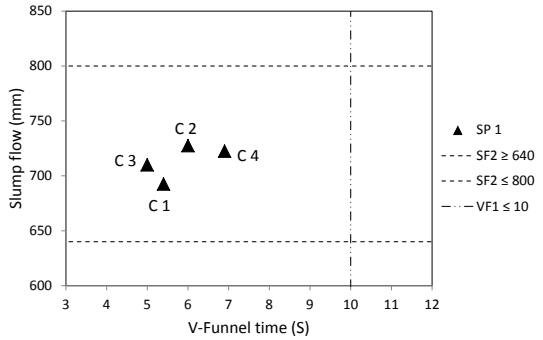

Figure 3. Slump flow results relative to V-funnel results for SP2.

Effect of fly ash 1 on cements with SP1

The effect of the fly ash 1 on different cement base mixes in accordance with the slump flow tests and segregation ratio are illustrated respectively in Figure 4 and Figure 5.

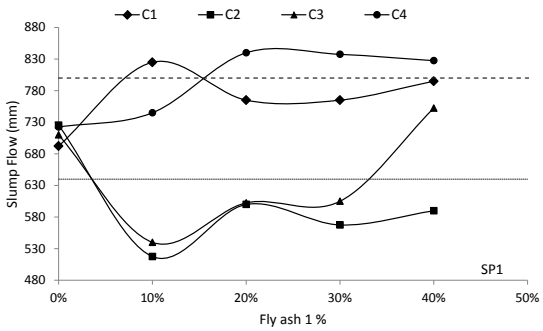

Figure 2. Slump-flow of SCC versus fly ash 1 at different replacement rates for different cements using SP1.

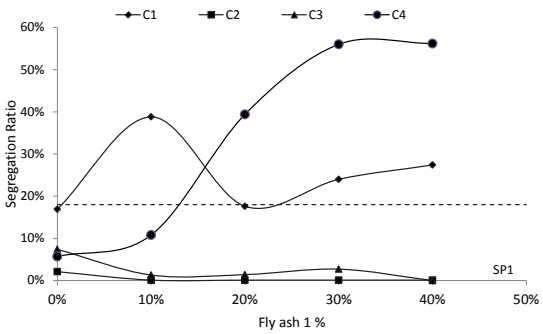

Figure 3. Segregation ratio of SCC versus fly ash 1 at different replacement rates for different cements using SP1.

Effect of fly ash 1 on cements using SP2

The effect of the fly ash 1 on different cements base mixes in accordance with the slump flow tests and segregation ratio are illustrated respectively in Figure 6 and Figure 7.

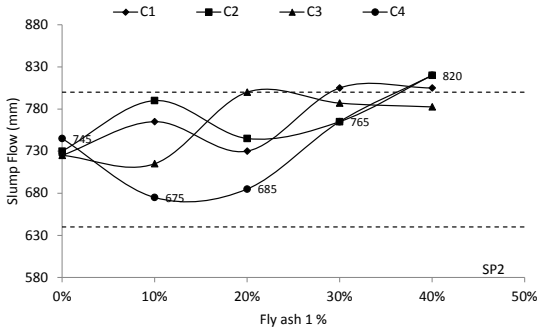

Figure 6. Slump-flow of SCC versus fly ash 1 at different replacement rates for different cements using SP2.

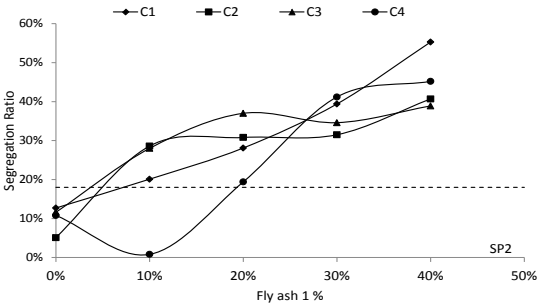

Figure 7. Segregation ratio of SCC versus fly ash 1 at different replacement rates for different cements using SP2.

Effect of fly ash 2 on different cements with SP1

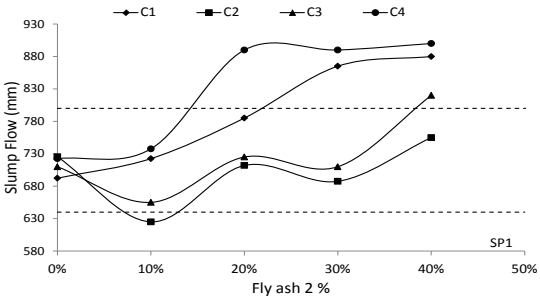

Figure 8. Slump-flow of SCC versus Fly ash 2 at different replacement rates for different cements using SP.

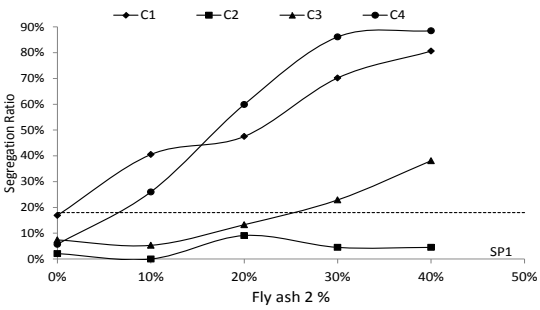

Figure 9 Segregation ratio of SCC versus Fly ash 2 at different replacement rates for different cements using SP.

Effect of fly ash 2 on cements with SP2

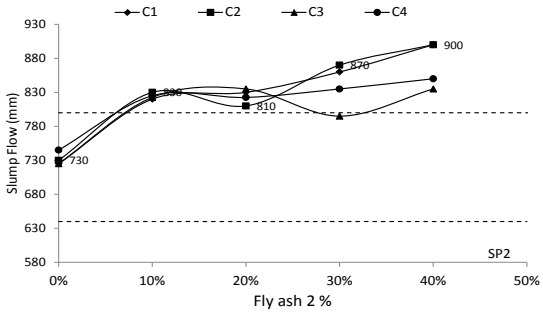

Figure 10. Slump-flow of SCC versus fly ash 2 at different replacement rates for different cements using SP2.

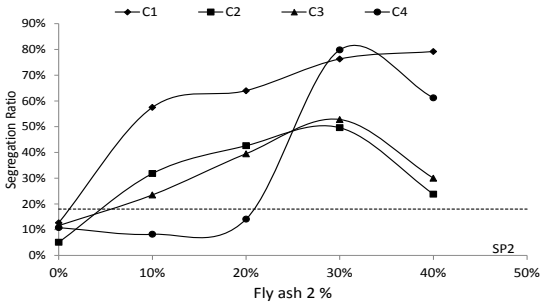

Figure 11. Segregation ratio of SCC versus fly ash 2 at different replacement rates for different cements using SP2.

Effect of Slag on different cements with SP1

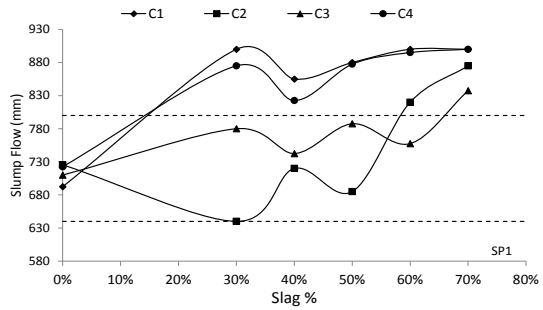

Figure 12. Slump-flow of SCC versus Slag at different replacement rates for different cements using SP1.

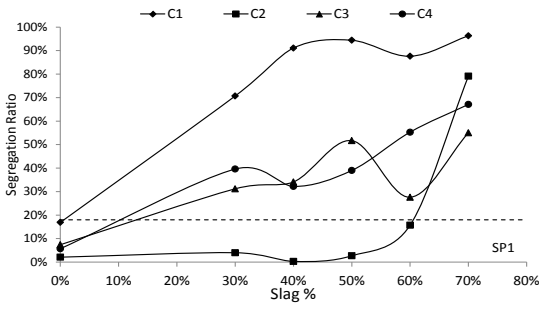

Figure 13. Segregation ratio of SCC versus Slag at different replacement rates for different cements using SP1.

Effect of Slag on different cements with SP2

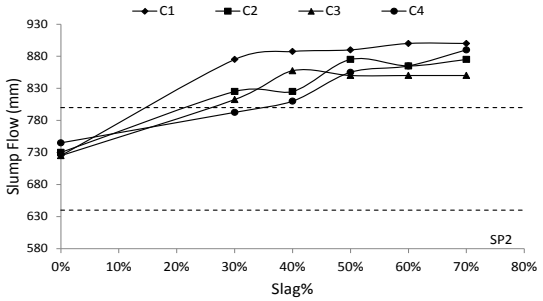

Figure 14. Slump-flow of SCC at different slag replacement rates for different cements using SP2.

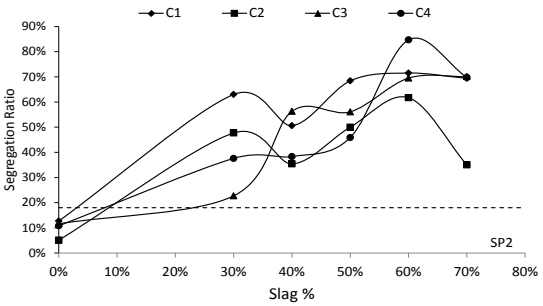

Figure 13. Segregation ratio of SCC at different slag replacement rates for different cements using SP2.

CONCLUSION

The following conclusions can be drawn.

- C2 and C4 have shown higher slump flow while C1 and C3 showed lower slump-flow values with SP1 and SP2.
- An increase in segregation percentage and a reduction in workability was found in C1, when compared with other cements using SP2.
- For both fly ashes there was an increase in passing ratio with C1 and C4 when used with SP1. As the fly ash content was gradually increased from 10% to 40%, mixes moved out of the EFNARC limits
- For fly ash 1, the flowability and viscosity were increased and the segregation and compressive strength increased for C1 and C4.
- For the fly ash 2, the flowability and viscosity were increased and the segregation and compressive strength reduced for C1 and C4.
- For slag, the flowability, viscosity and segregation severely increased to outside the EFNARC limits when used with SP2 for all cements.

REFERENCES

1. Alyamac, K.E., Ince, R. (2009) A preliminary concrete mix design for SCC with marble powders. Construction Build Material. 23: 1201–10.
2. Okamura, H., Ouchi, M. (1999) Self-compacting concrete: development, present use and future. The first international RILEM

symposium on SCC. Bagneux: RILEM Publications SARL. pp. 3–14.

3. Siddique, R. (2011) Properties of self-compacting concrete containing class F fly ash. Mater Design, 32: 1501–1507.
4. Melo, K.A., Carneiro, A.M. (2010) Effect of Metakaolin's finesses and content in self-consolidating concrete. Construction Building Material, 24: 1529–1535.
5. Nishio, A., Tamura, H., Ohashi, M. (1998) Self- compacting concrete with high-volume crushed rock fines. In: Malhotra VM, editor. Fourth CANMET/ACI/JCI international symposium on advances in concrete technology. Tokushima: ACI. pp. 617–30.
6. Topcu, I.B., Uygunoglu T. (2010) Effect of aggregate type on properties of hardened self-consolidating light weight concrete (SCLC). Construction Building Material, 24: 1286–1295.
7. Vengala, J., Sudarshan, M.S., Ranganath, R.V. (2003) Experimental Study for Obtaining Self-Compacting Concrete. The Indian Concrete Journal, 77 (8): 1261 – 1266.
8. Sukumar, B., Nagamani, K., Raghavan, R.S. (2008) Evaluation of strength at early ages of self-compacting concrete with high volume fly ash. Construction Build Material, 22: 1394–1401.
9. Bouzoubaa N, Lachemi M. (2001) Self-compacting concrete incorporating high volumes of class F fly ash preliminary results. Cement and Concrete Research, 31: 413–420.
10. The European Project Group, (May 2005). The European Guidelines for Self-Compacting Concrete Specification, Production and Use.

EFFECT OF DIFFERENT CEMENTS AND SUPERPLASTICISERS ON RHEOLOGY OF CEMENT PASTE

W. Mbasha, R. Haldenwang, I. Masalova

Department of Civil Engineering and Survey, Cape Peninsula University of Technology,
Email: willmbasha@gmail.com

ABSTRACT

The evolution of rheological parameters of four cements from one supplier manufactured at different factories and their interraction with two differents superplasticisers (SPs) were investigated. These were monitored by constructing their flow curves. The experiments were done with an MCR51 rheometer under a controlled temperature. The yield stress evolution over a short time is significant for all cement with and without SP. Even though the different cements are all CEM1 52 type, they react differently to the SPs. Simple flow curves cannot be used to extract rheological parameters such as yield stress and viscosity.

INTRODUCTION.

The main purpose of this research was to study the rheological behaviour and the impact of two different SPs on four different cements.

According to [1] and [2] cement paste can be treated as a colloidal material with non-Newtonian flow properties [3]. TheHerschel Bukley (H.B) model is a general model that is used to characterise the flow properties of cement paste.

$\tau = \tau_y + k\dot{\gamma}^n$.

According to [4] and [5] cement paste is a time and temperature dependent material and under certain conditions it exhibits thixotropic behaviour.

Cement paste microstructure

When cement particles come in contact with water, they are immediately electrically charged, creating an electrical field within the paste [6]. However, the neutrality of the bulk solution is ensured, by the nature of the cement particle double layer that surrounds the outer surface. [5] At rest, as the particles approach each other, there is an interference between the charge of the particle's double layers and when the total energy between neighboring particles reaches its minimum [2, 7] the attraction forces become more relevant and coagulation occurs. In tempting to prevent these inter-particle forces to lead to flocculation, has prompted researchers to use different types of SP that act as dispersing agents [1].

Hydration and setting

It has been proven that at early age, rheological parameters of a fresh cement paste, depends closely on the hydration kinetics within the paste [3]. These reactions are responsable for setting; that is defined as the transformation of cement in the fluid phase to becoming a solid material [8].

The setting has been attributed to the formation of CSH during the hydration process of the most sensitive compounds of cement grain to water such as C_3A, C_3S and C_2S [9].

The impact of these cement compounds on rheological behaviour, can be found elsewhere (e.g. in [10]).

In fact the hydration of C_3S and C_2S yields the same products that control the setting, the early strength and the pH of cement paste. The yield stress evolution is proportional to the development of these product formation during the hydration process [3].

Interaction SP- cement paste

SPs are mainly used in concrete, to enhance properties [11], allowing the material to become more workable at lower W/C ratios, having the advantage of increasing the concrete strength and reducing the concrete price, since the optimization of cement paste can then be acheived [7, 12, 13].

SPs allow the dispersion of particles that makes the material becoming more flowable. This dispersion effect is done by electrostatic repulsion and depletion effect. The compatibility of SP with cement paste depends strongly on the hydration of C_3A and alkali content in the clinker, cement fineness and calcium sulphate [1, 13-15].

MATERIAL AND METHODOLOGY

Matirial

Tables 1-3 give the chemical and physical properties of the 4 cements as well as the characteristics of the 2 SPs used in this research.

Table 1. Chemical Properties of cements

Chemical properties	C1	C2	C3	C4
SiO_2 (%)	20.15	20.7	19.4	21.7
Al_2O_3 (%)	3.82	4.37	3.59	4.95
Fe_2O_3 (%)	3.22	2.45	2.93	2.99
Mn_2O_3 (%)	0.09	0.81	0.75	0.49
TiO_2(%)	0.22	0.33	0.32	0.42
CaO(%)	63.37	63.7	61.7	60.9
MgO(%)	1.13	3.58	4.26	2.17
P_2O_5(%)	0.14	0.08	0.02	0.10
Wet SO_3(%)	2.10	2.27	2.13	3.40
Wet Cl(%)	0.004	0.01	0.01	0.004
K_2O(%)	0.62	0.52	0.29	0.34
Na_2O(%)	0.99	0.16	0.14	0.18
LOI(%)	3.00	1.57	5.13	2.01
Total(%)	98.9	100.5	100.6	99.6
FCaO(%)	1.06	0.75	0.83	3.25
IR(%)	-	0.78	1.98	-
Cl (ppm)	-	106	106	-

Table 2. Physical properties of cements.

Physical properties	C 1	C 2	C3	C 4
Relative Density Pyc	3.05	3.03	3.04	2.99
Reported S/Surface, cm2/g	3750	3650	4250	3850
Std Consistence, %	25.0	31.0	25.0	33.0
Initial Set, min	170	180	190	315
Final Set, h	3.25	3.75	3.75	6.00
45 µm Residue, %	11.7	0.6	3.9	1.8
90 µm Residue %	1.1	0.0	0.5	0.1
212 µm Residue, %	0.2	0.0	0.0	0.0

Table 3. SP characteristics.

Characteristics	SP1	SP2
Consistency	Liquid	Liquid
Color	Amber	Brown-green
Density according to ISO 758 (g/cm3)	1.07 0.02	1.05 0.02
Dry content according to EN 480-8 (%)	26 1.3	20.3 1
Chlorides soluble in water according to EN 480-10 (%)	0.1	0.1
Alkali content (Na2O equivalent) according to EN 480-12 (%)	2.5	1.0

Methodology

The w/c ratio used was 0.45. The mixing was done by hand and lasted 2min. It started immediately after water was added to the solids. The MCR51 rheometer with a serreted parallel plate and gap of 0.6mm was used at a controlled temperature of 25^{0}C. Preshearing at 50/s for 10s was done in all cases before starting the tests. The SPs were optimised at 0.3% (by weight of cement) added to the water and the whole solution to the solids.

The evolution of rheological parameters such as yield stress and viscosity were obtained by constructing the flow curves at different specific times and at a different constant shear rates.

Five different constant shear rates (SR) were considered and the viscosity versus time curves were measured respectively. Thereafter, the viscosity curves were established at a point in time allowing them to have a single value of viscosity. Finally the flow curves were constructed at this given time with different shear stress values calculated from the viscosity cuve.

The rate of rebuilding of cement structure was obtained by evaluating the thixotrophic behaviour (the hysterisis area of up and down curves of the flow curve for a duration of 5min in total). This was done for each cement at different intervals of material resting time.

RESULT AND DISCUSSION

Figures 1 and 2 below give the viscosity vs time curves at only two typical constant shear rates for the four cements without SP.

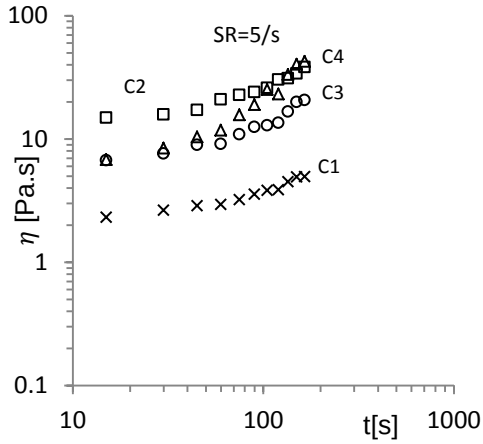

Figure 1. Viscosity vs time at constant SR 5/s for all cements without SP.

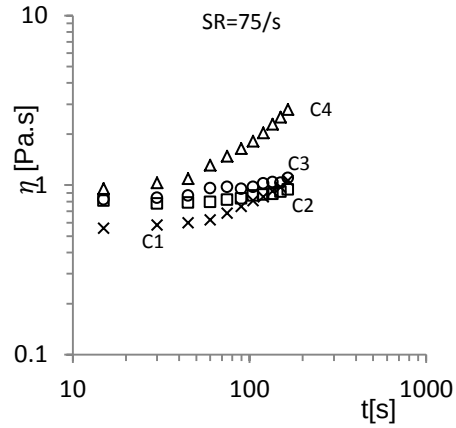

Figure 2. Viscosity vs time at constant SR 75/s for all cements without SP.

It is clearly seen from Figure 1 and 2 that, for cement paste, the viscosity is not a single value or constant over time at a constant shear rate. This puts in question the way previous researchers were estimating rheological parameters especially the yield stress of cement paste.

Figure 3 shows the viscosity curve at 15s on logarithmic scales for all cements without SP.

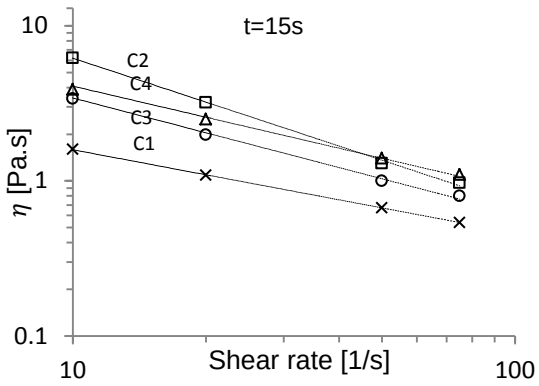

Figure 3. Viscosity curve at 15s of all cements with no SP.

Figure 4 shows the flow curves derived from the viscosity curve (as shown in Figure 3) and fitted by the H.B model.

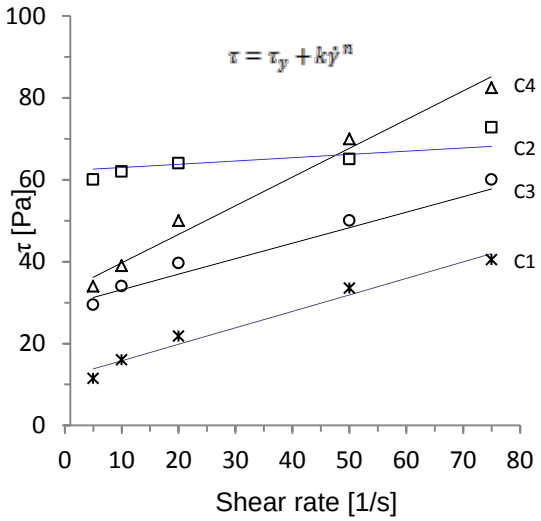

Figure 4. Flow curve at 15s as fitted by H.B for all cements without SP.

The evolution of rheological parameters, yield stress and viscosity, are consequently given in the Figures 5 and 6:

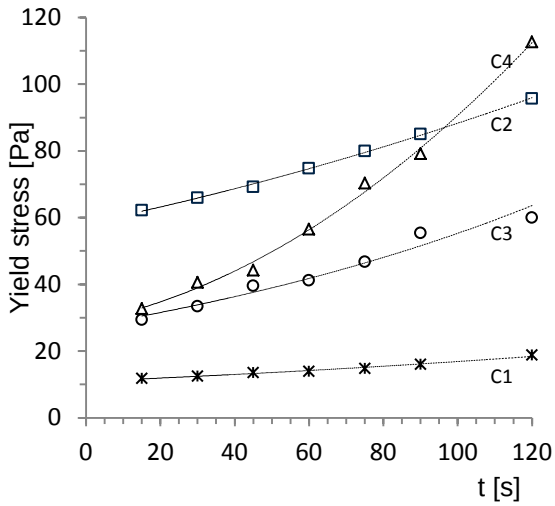

Figure 5. Yield stress evolution of all cements without SP.

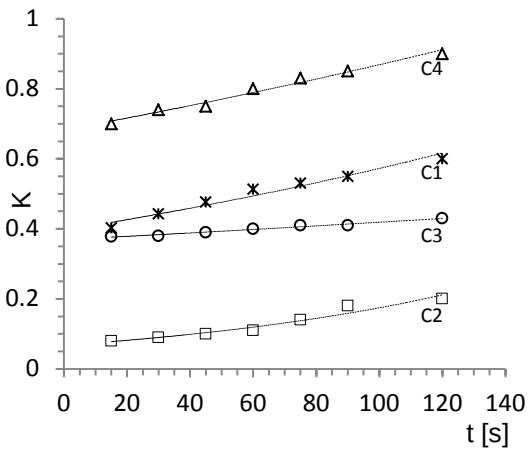

Figure 6. Viscosity evolution of all cements without SP.

Other coefficients of the H.B model that describe the evolution of rheological parameters of cements with SP1 and SP2 are given in tabulated form in Table 4 and 5.

Table 4. Coefficient values as fitted by H.B model for all cements with SP1.

Time (s)	C1		C2		C3		C4	
	τ_y [Pa]	K	τ_y [Pa]	K	τ_y [Pa]	K	τ_y [Pa]	K
15	0.6	0.2	3	0.2	2	0.1	6	0.2
60	0.4	0.2	9	0.2	7	0.1	9	0.2
120	1.5	0.2	26	0.2	24	0.1	23	0.2
180	8.5	0.2	45	0.2	39	0.1	45	0.2
240	21.6	0.2	61	0.2	59	0.1	60	0.2
300	35.0	0.2	85	0.2	105	0.1	91	0.2

Table 5. Coefficient values as fitted by H.B model for all cements with SP2.

Time (s)	C1		C2		C3		C4	
	τ_y [Pa]	K	τ_y [Pa]	K	τ_y [Pa]	K	τ_y [Pa]	K
15	4	0.3	6	0.2	8	0.2	7	0.1
60	6	0.3	8	0.2	9	0.2	11	0.1
120	9	0.3	19	0.2	13	0.2	21	0.2
180	12	0.3	33	0.2	13	0.2	33	0.2
240	20	0.3	48	0.2	20	0.2	43	0.2
300	28	0.3	60	0.2	25	0.2	48	0.2
480	67	0.3	89	0.3	47	0.2	77	0.2
600	96	0.3	114	0.3	68	0.2	106	0.2

In the case where there is no SP as demonstrated in Figures 5 and 6, rheological behaviour of all cements change over time differently, with C1 showing less change in yield stress and only a slight change in viscosity for C2. These change have to be attributed mostly to the physical properties of cements and the reactivity of their C_3A content as cited in the literature [3]. In the first few seconds, the change in yield stress of C2 is very significant, the reason being that it has a great rate of rebuilding as shown in Figure 7.

Figure 7 demonstrates the rate of rebuilding of all cements with no SPs. C2 exhibits a higher rate of rebuilding followed by C4 and C1. C3 has a low rate of restructuring.

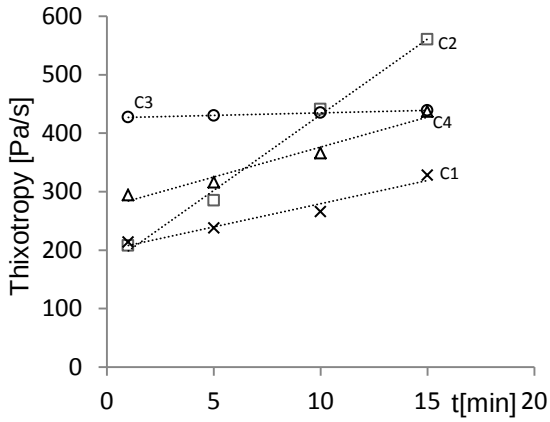

Figure 7. Rate of rebuilding of all cements without SP.

Observing Figure 5 and Table 4 and 5, the yield stress of cements are increasing significantly in a few seconds. In the presence of SPs these changes have to do mostly with the chemical properties of cement, especially the C_3A content in each cement.

Table 4 and 5 shows that the change in viscosity is insignificant for the simple resason that at the saturation dosage of SP, the viscosity is not affected that much.

CONCLUSION

In summary, the observation of these results and the discussion above leads to the following conclusions:

- SPs affect the rheological parameters of the cement by decreasing the yield stress and at the saturation dosage the viscosity will only slightly change over time.
- The Herschel-Bulkley model describes very well the flow behaviour of all cements with or without SP with n=1. (Bingham model)
- The SPs affect the cements differently which could relate to their chemical and mollecular structure.
- Rheological parameters such as yield stress and viscosity cannot be evaluated by measuring the flow curve since the viscosity of the paste is changing and not a single value over time at constant shear rate. Moreover, the measurement of these flow curves takes a few minutes while as demonstrated, the yield stress can change significantly in a few seconds.
- An approach as described in this manuscript has to be formulated in order to evaluate these parameters correctly.

REFERENCES

1. Mikanovic, N., Jolicoeur, C. (2008) *Influence of superplasticizers on the rheology and stability of limestone and cement pastes.* Cement and Concrete Research, 38 (7): 907-919.
2. Wallevik, J.E. (2009) *Rheological properties of cement paste: Thixotropic behavior and structural breakdown.* Cement and Concrete Research, 39 (1): 14-29.
3. Sant, G., Ferraris, C.F., Weiss, J. (2008) *Rheological properties of cement pastes: A discussion of structure formation and mechanical property development.* Cement and Concrete Research, 38 (11): 1286-1296.
4. Wallevik, J.E. (2005) *Thixotropic investigation on cement paste: Experimental and numerical approach.* Journal of Non-Newtonian Fluid Mechanics, 132 (1–3): 86-99.
5. Quanji, Z. (2010) *Thixotropic behaviour of cement-based materials: effect of clay and cement types*, in *Civil and Environmental Engineering*, Iowa State Universisty Iowa. p. 144.
6. Roussel, N., Ovarlez, G., Garrault, S., Brumand, C. (2012) *The origins of thixotropy of fresh cement pastes.* Cement and Concrete Research, 42 (1): 148-157.
7. Hanehara, S., Yamada, K. (1999) *Interaction between cement and chemical admixture from the point of cement hydration, absorption behaviour of admixture, and paste rheology.* Cement and Concrete Research, 29 (8): 1159-1165.
8. Struble, L.J., Lei, W.G. (1995) *Rheological changes associated with setting of cement paste.* Advanced Cement Based Materials, 2 (6): 224-230.
9. Esteves, L.P., Cachim, P.B., Ferreira, V.M. (2010) *Effect of fine aggregate on the rheology properties of high performance cement-silica systems.* Construction and Building Materials, 24 (5): 640-649.
10. Vikan, H., Justnes, H. (2007) *Rheology of cementitious paste with silica fume or limestone.* Cement and Concrete Research, 37 (11): 1512-1517.
11. Anagnostopoulos, C.A. (2014) *Effect of different superplasticisers on the physical and mechanical properties of cement grouts.* Construction and Building Materials, 50 (0): 162-168.
12. Zingg, A., Holzer, L., Kaech, A., Winnefeld, F., Pakusch, J., Becker, S., Gauckler, L. (2008) *The microstructure of dispersed and non-dispersed fresh cement pastes — New insight by cryo-microscopy.* Cement and Concrete Research, 38 (4): 522-529.
13. Zingg, A., Winnefeld, F., Holzer, L., Pakusch, J., Becker, S., Figi, R., Gauckler, L. (2009) *Interaction of polycarboxylate-based superplasticizers with cements containing different C3A amounts.* Cement and Concrete Composites, 31 (3): 153-162.
14. Koehler, E.P. (2007) *aggregates in self compacting concrete*.
15. Chandra, S., Björnström, J. (2002) *Influence of cement and superplasticizers type and dosage on the fluidity of cement mortars—Part I.* Cement and Concrete Research, 32 (10): 1605-1611.

Notes

Notes

Notes